Geodesics in some exact rotating solutions of Einstein's equations

Thesis

UNRESTRICTED

Geodesics in some exact rotating solutions of Einstein's equations

Brian Richard Steadman, BSc (Kent), BA (Open)

A thesis submitted for the degree of Doctor of Philosophy

Applied Mathematics and Mathematical Physics

The Open University

February 2000

~ Abstract ~

In examining some exact solutions of Einstein's field equations, the main approach used here is to study the geodesic motion of light, and sometimes test particles. Difficulties in solving the geodesic equations are avoided by using computer algebra to solve the equations numerically and to plot them in two- or three-dimensional diagrams. Interesting features revealed by these diagrams may then be investigated analytically.

Application of this technique to the van Stockum solution for a rotating dust cylinder and to Bonnor's rotating dust cloud seems to reveal different constraints on the spatial distribution of geodesics with different parameters. Analysis then confirms that, in the highest mass van Stockum case, null geodesics in the vacuum exterior are radially confined according to their initial conditions. Null geodesics plotted in Bonnor's dust cloud seem to be repelled before they can reach the centre. Although there is no event horizon, analysis reveals a central region which cannot be penetrated by light from spatial infinity and from which light cannot escape to spatial infinity.

The gravitomagnetic clock effect is studied in van Stockum spacetime. The effect is found to be frame dependent and can be reduced to zero by a suitable coordinate transformation.

~ Acknowledgements ~

First, my gratitude goes to my internal supervisor, Professor M Crampin of the Open University, without whom I should neither have started nor finished this work. I am especially grateful both for his mathematical insights and for his help with mathematical techniques.

Second, my sincere thanks go to my external supervisor, Professor W B Bonnor of Queen Mary and Westfield College, for his guidance and encouragement concerning the physical aspects of general relativity. One of his papers was the inspiration for this thesis, much of which builds on some of his earlier results.

Finally, I thank my wife Valentine for her unflagging support of many kinds.

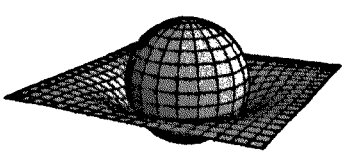

~ Contents ~

~ Chapter 1 ~

Introduction

In December 1915, Karl Schwarzschild found the first exact solution of Einstein's field equations of gravitation. He sent the solution to Einstein who, in acknowledging the manuscript, wrote to Schwarzschild [17]: "I have read your paper with the greatest interest. I had not expected that one could formulate the exact solution of the problem so simply."

In 1997, the Editorial Board of the journal *Classical and Quantum Gravity* augmented its instructions to referees with the warning: "The discovery of a new exact solution does not justify publication *simply for its own sake*. Justification for publishing a new solution would be provided by showing, for example, that it has an interesting physical application or unusual geometrical properties, or that it illustrates an important mathematical point."

Evidently, by 1997, there was no shortage of exact solutions. There are many solutions but not many are well known. In the introduction to a review article on time-independent solutions, Bonnor [39] wrote: "Relativists have not been diligent in interpreting solutions of Einstein's equations. Thus in the book of exact solutions [32] one finds many whose physical meaning is unknown or only partially understood."

It was Bonnor's review article which provided both the stimulus and the starting point for this thesis, which seeks to increase understanding of some rotating solutions largely by examination of the geodesic motion of light and test particles. In Bonnor's estimation "....the essence of interpretation is to understand the *sources* in the exact solutions." A substantial part of this work is devoted to the cylindrically symmetric van Stockum solution [3], a complete solution for a rotating dust interior with a vacuum exterior, and to a related solution for an axially symmetric, rotating dust cloud which was found by Bonnor [40]. Although cylindrical and axial symmetry require precise definition in general relativity (see reference [21], for example), the intuitive definitions, whereby

cylindrical symmetry is a particular case of axial symmetry, the latter describing any shape that is symmetric about the rotation axis, are also applicable in discussing van Stockum's and Bonnor's solutions.

The original proposal for this research project stated the intention of investigating the possible physical relevance of some exact solutions of Einstein's field equations of gravitation. When listing the requirements for starting work, it was stated that 'perhaps computing facilities will be needed'. In the event, computing became the central and indispensable tool for completing the work and algebraic computing was exploited extensively. The software programs used were *Mathematica* [6] and *MathTensor* [7]. The latter, as its name suggests, is designed to do tensor analysis. It works within *Mathematica* which is general purpose mathematical software with good graphics capabilities. The graphical and numerical capabilities of *Mathematica* were as useful as its algebraic ones. Details of some of the computing routines used are shown in Appendix A1.

Such are the graphics capabilities of *Mathematica* that it soon became obvious that a method of plotting geodesics for a given metric would be very useful. Initially, a method was devised for plotting individual geodesics in Schwarzschild spacetime. The method was improved and elaborated with use, and with application to more mathematically complicated metrics. Eventually, it became straightforward to calculate multiple geodesics with finely specified initial conditions and to plot them in a variety of ways.

One of the facilities of *Mathtensor* is to calculate the various tensor components for a given metric and to store them in a file. This file can be used, for example, by the geodesics plotting routine (using *Mathematica*), or to calculate the algebraic and differential invariants (using *MathTensor*). In addition, *Mathematica* was used for all sorts of other mathematical procedures, especially algebraic manipulation and simplification.

The ability to plot both null and timelike geodesics makes it possible to do 'virtual' experimental physics in spacetimes which may be quite awkward to handle analytically. It is necessary only to know the metric coefficients in the coordinate frame of interest and to be able to specify initial conditions in a consistent manner. In this way it was

discovered that there was something odd about the van Stockum case III metric, in that the radial ranges of even null geodesics seemed to be restricted. Thus 'from experiment' it seemed almost certain that there was a maximum radial range for geodesics leaving the dust cylinder. This gave encouragement to the more difficult task of demonstrating the putative phenomenon analytically.

Although experience gained with the van Stockum metric was useful, the first geodesics plotted for Bonnor's rotating dust cloud metric were harder to interpret. The axially symmetric dust cloud had to be investigated in three dimensions, not two as with van Stockum's cylindrical solution. Outwards-going geodesics seemed to have no radial restriction and the central region was a problem. Geodesics could not be plotted from there since the ϕ coordinate is timelike in that region. All inwards-going geodesics seemed to be repelled from the central region. The eventual, analytical, description of the 'central separate zone' helped to explain some characteristics of the geodesics and was a surprising discovery in itself. Here was a region of spacetime which null geodesics cannot penetrate and from which null geodesics cannot escape.

The van Stockum solution of Einstein's gravitational equations represents a rigidly rotating dust cylinder of infinite length together with an associated exterior metric. Although the complete solution was new in 1937, both the interior and exterior metrics were already known as separate solutions. The following three sections give an outline of the three relevant papers to give a setting to the more detailed examination of the solution that follows. An outline of Bonnor's axially symmetric dust cloud solution is given in the last section.

1.1 Lanczos, 1924

The interior metric of van Stockum's solution was originally found by Lanczos [1] in 1924 and was the first exact solution of Einstein's equations with a rotating matter source. Lanczos had been corresponding with Einstein since 1919 and became his assistant, for one year from November 1928, working on unified field theory [23]. He regarded his discovery as a cosmological solution at a time when the universe was thought to consist

solely of the Milky Way galaxy; indeed, he was guided partly by physical intuition, with a view to modelling the galaxy, when finding the solution.

The title of Lanczos's paper is '*On a Stationary Cosmology in the Sense of Einstein's Theory of Gravitation*'. Lanczos's definition of 'stationary' differs from the modern definition to be described later, in Section 2. Lanczos wrote "A world is to be considered stationary in the sense of general relativity if the coefficients of its metric are independent of time in a coordinate system in which the masses are at rest on average." In such a solution, a test particle initially at rest in the coordinate system remains at rest. He went on to say "...there are no stationary solutions which are also spherically symmetric for the original field equations." This is what led Einstein to introduce the cosmological constant λ into the field equations [22]. The matter density and the overall mass in Einstein's cosmological solution are determined by λ. Lanczos had been uneasy because the value of λ required to account for the observed universe, which at the time was thought to be 'static', seemed to arise by coincidence. His cosmological solution, for the equations with $\lambda = 0$, needed no such coincidence.

The choice of a stationary metric leads to a general form for the line element,

$$ds^2 = d\sigma^2 + 2\, g_{14}\, dx^1\, dt + 2\, g_{24}\, dx^2\, dt + 2\, g_{34}\, dx^3\, dt - dt^2, \qquad (1)$$

where $d\sigma^2$ is the quadratic form of the space variables and the g_{i4} are independent of the time-like coordinate t. Lanczos first took the field equations with zero cosmological constant,

$$R_{ik} = T_{ik} - \tfrac{1}{2} g_{ik} T, \qquad (2)$$

and considered the individual stars to be so far apart as to have no influence on each other, enabling him to use the energy-momentum tensor for non-interacting dust,

$$T^{ik} = \rho u^i u^k, \qquad (3)$$

where ρ is the proper mass density and u^i is the dust four-velocity. Since the matter is at rest in the coordinate frame, the only non-zero component is T^{44}.

Lanczos then showed that the matter density in a stationary world must be positive so that the mutual gravitational interaction of matter is attractive, not repulsive, an indication that his solution might have physical relevance. Observing that the Milky Way

galaxy, although not spherically symmetric, had approximate rotational symmetry, Lanczos then chose one of the coordinates to be an angular variable $x^3 = \phi$, so that the metric coefficients become functions of x^1 and x^2 only. By suitable transformations of ϕ and t, $g_{13} = g_{14} = 0$. Further simplification comes from setting $g_{23} = g_{24} = 0$ and from choosing isotropic coordinates for x^1 and x^2 whereby $g_{11} = g_{22}$ and $g_{12} = 0$.

After all these simplifications, the line element becomes

$$ds^2 = H(r)(dz^2 + dr^2) + L(r)\,d\phi^2 + 2\,M(r)\,d\phi dt - dt^2, \tag{4}$$

r being the radial coordinate and ϕ the angular coordinate, such that $0 \le \phi \le 2\pi$. The notation is that of van Stockum, for consistency with the remainder of the thesis. Four field equations remain to be solved with three unknown functions to be found, but only three of the equations are independent.

By solving the field equations, and by setting the only parameter equal to one, Lanczos defined a 'natural unit of length' and obtained the line element for his cylindrical cosmological solution,

$$ds^2 = \exp(-r^2)(dz^2 + dr^2) + r^2(1 - r^2)\,d\phi^2 + 2\,r^2\,d\phi dt - dt^2, \tag{5}$$

noting the coordinate condition $L + M^2 = r^2$ and the mass density $\rho = 4\exp r^2$.

The radial distance s, to any given r, is given by

$$s = \int_0^r \exp\left(-\frac{r^2}{2}\right) dr = \sqrt{\frac{\pi}{2}}\,\mathrm{erf}\left(\frac{r}{\sqrt{2}}\right), \tag{6}$$

and a plot of s, for $0 \le r \le 10$, is given in Figure 1.1,

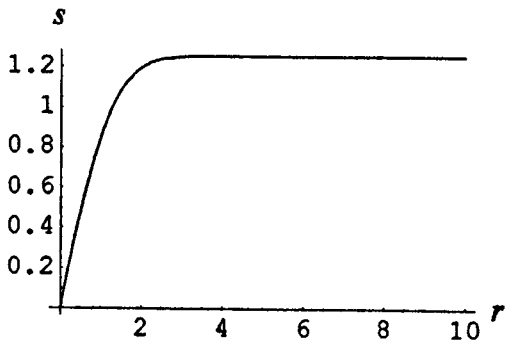

Figure 1.1 Radial distance s in the Lanczos metric.

Since erf $(\infty) = 1$, then as $r \to \infty$, $s \to \sqrt{\pi/2}$, so the metric is finite in the r direction. Since the mass density $\rho = 4 \exp r^2 \to \infty$ as $r \to \infty$, s is also limited for physical reasons.

Lanczos noted that the determinant of the spatial part of the metric is zero at $r = 1$ and negative for $r > 1$ but implied that this was not necessarily of physical significance. When considering the van Stockum solution, we shall find reasons to restrict attention to metrics with $ar < 1$ which is equivalent to $r < 1$ in Lanczos's solution.

Exploring the physical relevance of his solution, Lanczos investigated the null geodesics and found that any geodesic starting from the axis of symmetry had a limited radial range. This phenomenon was rediscovered and elaborated by Opher, Santos and Wang [2] in 1996. Introducing a cosmological constant, Lanczos repeated his calculations and, in one case, reproduced Einstein's cosmological solution [22]. In the remainder of the paper, he explored the physical attributes of the solution with an eye to their relevance to the galaxy and even discussed the possibility of astronomical verification.

1.2 Lewis, 1932

Lanczos had come to an axially symmetric metric in his attempt to model the Milky Way galaxy, specialising to cylindrical symmetry for simplicity. Lewis's paper deals with axial symmetry from the start, generalising already-existing work on static axially symmetric solutions to include rotating situations. To quote Lewis [4], "The problem of axially symmetric fields was first treated by Weyl ..." [24], then slightly differently by Levi-Civita [25] who "...discussed fully the case in which the field is produced by an infinite cylinder." Those papers dealt with exact static solutions. Lewis also mentioned Lanczos's cosmological solution and then went on to present his own exact solutions for stationary, vacuum, axially symmetric spacetimes. (From this section onwards, the term 'stationary' has its modern meaning). Lewis's solutions contain the Weyl and Levi-Civita solutions as special cases.

Lewis obtained his field equations for the vacuum using the variational principle on an action function derived from the general form of the axisymmetric line element,

$$ds^2 = \exp\mu\,(dx^1)^2 + \exp\nu\,(dx^2)^2 + L\,(dx^3)^2 + 2M\,dx^3\,dx^4 - F\,(dx^4)^2, \qquad (7)$$

where $x^1 = 0$ is the axis of symmetry, x^3 is a periodic coordinate varying from 0 to 2π and x^4 is the time coordinate. The metric coefficients are functions of x^1 and x^2. The determinant of the metric is given by

$$g = -r^2 \exp(\mu+\nu), \text{ where } r^2 = FL + M^2\,. \qquad (8)$$

Note that r is simply being used as a symbol at this stage.

After finding five field equations, which he simplified by setting $\nu = \mu$, Lewis noticed that three of them are invariant under a transformation of the type

$$x^1 + ix^2 = f(x'^1 + ix'^2). \qquad (9)$$

Also, subtracting the other two equations gave a simple equation in r,

$$r_{,11} + r_{,22} = 0, \qquad (10)$$

where the suffix 1 denotes differentiation with respect to x^1 etc. Hence if z is the conjugate of r, the following identification can be made,

$$r + iz = x^1 + ix^2, \qquad (11)$$

and the usual r and z cylindrical coordinates may thereby be defined.

Several special solutions of the vacuum field equations $R_{ik} = 0$ were investigated. In one case, Lewis found the vacuum field later discovered by van Stockum to be generated by an infinite rotating cylinder,

$$F = \kappa^2(\beta_1{}^2 r^{\epsilon} - \omega^2 \beta_2{}^2 r^{2-\epsilon}),\ L = \kappa^2(\beta_1{}^{-2} r^{2-\epsilon} - \omega^2 \beta_2{}^{-2} r^{\epsilon}),$$

$$M = \kappa^2 \omega(\beta_2{}^2 r^{2-\epsilon} - \beta_1{}^2 r^{\epsilon})\,\beta_1{}^{-1}\beta_2{}^{-1},\ \exp\mu = \left(\frac{r}{r_0}\right)^{(k^2-1)/2}, \qquad (12)$$

$$\text{where } \nu = \mu,\ \kappa = (1-\omega^2)^{-1/2},\ \epsilon = 1-k$$

$$\text{and } \kappa,\ \omega,\ \epsilon,\ k,\ \beta_1,\ \beta_2 \text{ and } r_0 \text{ are all constants.}$$

The constant r_0 is inessential and could be absorbed into β_1 and β_2. The constant k is arbitrary and although real here, can be imaginary. When $\omega = 0$, the solutions reduce to those of Levi-Civita for the field of the infinite, static cylinder, so ω, which is dimensionless, is a measure of rotational angular velocity. The constant ϵ is also

dimensionless and is proportional to the mass per unit length of the source cylinder. Constants β_1 and β_2 seem not to have such direct physical relevance. In fact, β_1 is dimensionless and almost equal to unity, whereas β_2 has units of reciprocal length and "Newtonian theory gives no indication of its magnitude".

Another of Lewis's cylindrical solutions, also used by van Stockum, has the form

$$\begin{aligned} F &= (a_1^2 - b_1^2)\, r\cos\psi - 2\, a_1\, b_1\, r\sin\psi, \\ L &= -(a_2^2 - b_2^2)\, r\cos\psi + 2\, a_2\, b_2\, r\sin\psi, \\ M &= -(a_1\, a_2 - b_1\, b_2)\, r\cos\psi + (a_1\, b_2 + b_1\, a_2)\, r\sin\psi, \\ \exp\mu &= \left(\frac{r}{r_0}\right)^{(k'^2-1)/2}, \end{aligned} \tag{13}$$

$$\text{where } \nu = \mu \text{ and } \psi = -k' \log(r/r_0).$$

The choice of constants a_i and b_i, where i = 1,2, is arbitrary except for the condition $a_1\, b_2 - a_2\, b_1 = 1$. There is no correspondence to a static solution, i.e. $M = 0$ everywhere, for any choice of a_i and b_i.

Both of the above cases appear, in different forms, in van Stockum's paper and the parameters of Lewis's solutions are still a topic of interest to researchers, with recent papers by de Silva et al [26], [27] and by MacCallum and Santos [28].

1.3 van Stockum, 1937

In 1937, van Stockum [3] re-discovered the infinite rotating cylinder metric as a particular case of a more general class of axially symmetric rotating dust solutions. Although it had been found previously by Lanczos, van Stockum went further by matching it to stationary, cylindrically symmetric vacuum metrics obtained by Lewis. He found that there are 'two essentially different types of external field' according to the characteristics of the cylinder. In more recent years, a number of papers dealing with the peculiarities of the van Stockum solution have been published, the most comprehensive being that of Bonnor [5] in 1980. Bonnor called the two types of vacuum exterior 'case I' and 'case III', with 'case II' being the intermediate situation, and a limiting case of either

of the other two.

Although van Stockum acknowledged the work of Lewis in finding the exterior metrics, he made no mention of Lanczos. Like Lewis, van Stockum was examining stationary, axially symmetric solutions themselves, not modelling a particular physical situation. Starting with a long geometrical definition of axial symmetry and by using suitable coordinate transformations, van Stockum arrived at a general form for the axially symmetric line element,

$$ds^2 = \exp[2\Psi(x^1, x^2)]\left[(dx^1)^2 + (dx^2)^2\right] + L(x^1, x^2)\,(dx^3)^2 + 2\,M(x^1, x^2)\,dx^3\,dx^4 - F(x^1, x^2)\,(dx^4)^2, \tag{14}$$

where x^3 and x^4 are the angular (azimuth), and time coordinates respectively. From this metric, he calculated the non-zero components of the Ricci tensor.

For the energy tensor, van Stockum considered a distribution of dust particles rotating around the axis of symmetry on circular (x_1 = constant, x_2 = constant) paths in space. The particles were assumed to be non-interacting so that the circular paths are geodesics in spacetime. The energy tensor is thus

$$T^{ik} = \rho(x_1, x_2)\,u^i\,u^k, \tag{15}$$

where ρ is the proper mass density and u^i is the non-interacting particle four-velocity. Having calculated the non-zero components of the T^{ik}, van Stockum simplified their form by transforming to a coordinate frame in which the particles are at rest.

Like Lewis, van Stockum then transformed to r, z cylindrical coordinates as shown in equation (11), above. Thus he solved the field equations

$$R_{ik} = T_{ik} - \frac{1}{2}\,g_{ik}\,T, \tag{16}$$

giving, in cylindrical polar coordinates,

$$ds^2 = \exp[2\Psi(r, z)]\,(dz^2 + dr^2) + (r^2 - M(r, z)^2)\,d\phi^2 + 2\,M(r, z)\,d\phi dt - dt^2, \tag{17}$$

where $-\infty < z < \infty$, $0 \le r < \infty$, $0 \le \phi \le 2\pi$ (the hypersurfaces $\phi = 0$ and $\phi = 2\pi$ being identified), $-\infty < t < \infty$ and where M is any solution of

$$M_{,rr} + M_{,zz} - \frac{M_{,r}}{r} = 0, \tag{18}$$

which is one of the field equations. The function Ψ may be found from two more of the field equations

$$\Psi_{,r} = -\frac{(M_{,r})^2 - (M_{,z})^2}{4r}, \quad \Psi_{,z} = -\frac{M_{,r}\, M_{,z}}{2r}. \tag{19}$$

In light of equation (18), the integrability condition for equations (19) is satisfied, so that M may be found just from (18). Note that in solving the field equations, L became dependent on M due to the coordinate condition $r^2 = FL + M^2$.

To consider the particular case of a cylindrical solution, van Stockum supposed M to be a function of r only, which results in $M = a\,r^2$, a being the integration constant. Hence the line element for the infinite dust cylinder, in the rest frame of the dust,

$$\begin{aligned} ds^2 = \exp(-a^2 r^2)(dz^2 + dr^2) + r^2(1 - a^2 r^2)\,d\phi^2 + \\ 2a r^2\, d\phi dt - dt^2. \end{aligned} \tag{20}$$

This is like Lanczos's line element except that Lanczos set the rotation parameter $a = 1$, thus defining the unit of length. Although van Stockum left a unspecified, he wanted to keep the coefficient of $d\phi^2 > 0$. Thus a and r can have any values provided that the product $ar < 1$.

Using Lewis's vacuum solution, but obtaining it by a method more convenient for finding constants, by using boundary conditions, van Stockum obtained his cylindrical vacuum solution by putting $\rho = 0$ in the field equations and proceeding with the requirement that the vacuum metric should match the interior metric at the surface of the dust cylinder. His method was to solve the field equations by equating the known boundary conditions and their first differentials for the interior with their unknown equivalents for the exterior, then solving for the metric coefficients. The exterior thus obtained has two parameters, a as before and R, the radial coordinate of the boundary between the interior and the exterior, and its form differs from that found by Lewis.

The line element may be written in several ways, making it more or less convenient for different purposes. The following has the advantage of encapsulating cases I, II and III in one expression,

$$ds^2 = H(r)\,(dz^2 + dr^2) + L(r)\,d\phi^2 + 2\,M(r)\,d\phi dt - F(r)\,dt^2, \tag{21}$$

where $-\infty < z < \infty$, $0 \le r < \infty$, $0 \le \phi \le 2\pi$ and $-\infty < t < \infty$, with

$$\begin{aligned} H(r) &= \exp\left(n^2 - \frac{1}{4}\right)\left(\frac{r}{R}\right)^{\frac{1}{2}(4n^2-1)}, \\ L(r) &= \frac{(4n^2+3)\,r\,R\cosh A}{4} + \frac{(12n^2+1)\,r\,R\sinh A}{8n} \\ M(r) &= \frac{\sqrt{1-4n^2}\,r\cosh A}{2} + \frac{\sqrt{1-4n^2}\,r\sinh A}{4n}, \\ F(r) &= \frac{r\sinh A}{2nR} - \frac{r\cosh A}{R}, \end{aligned} \tag{22}$$

where

$$A = 2n\log\left(\frac{r}{R}\right), \quad n^2 = \frac{1}{4} - a^2R^2. \tag{23}$$

In case I, $1/4 > n^2 > 0$ and in case III, $-3/4 < n^2 < 0$. Thus in terms of the metric parameters, case I has $0 < aR < 1/2$ and case III has $1/2 < aR < 1$. Case II is obtained by taking the limit of either case I or case III as $n \to 0$, whereby $aR \to 1/2$. Although n is imaginary in case III, the metric functions are nevertheless real. Both the interior and the exterior solutions are examined in subsequent chapters.

Lewis's equations (12) and (13) give the case I and case III versions of equations (22) when the appropriate choice of constants is made. For example, putting the (real) constants

$$a_1 = \frac{\sqrt{m\left(2m+\sqrt{4m^2+1}\right)R}}{2mR}, \quad a_2 = \frac{\left(1-2m\left(2m+\sqrt{4m^2+1}\right)\right)R}{4\sqrt{m\left(2m+\sqrt{4m^2+1}\right)R}} \tag{24}$$

$$b_1 = \frac{1}{2\sqrt{m\left(2m+\sqrt{4m^2+1}\right)R}},\quad b_2 = \frac{\left(4m+\sqrt{4m^2+1}\right)R}{4\sqrt{m\left(2m+\sqrt{4m^2+1}\right)R}},$$

$$k' = -2m,\ r_0 = R,$$

where $m = i\,n$, into equations (13), when $-3/4 < n^2 < 0$, gives the case III version of equations (22).

1.4 Bonnor, 1977

By supposing M in equation (17) to be a function only of r, van Stockum obtained his solution for an infinite cylinder of dust. Bonnor [40], in finding an axially symmetric rotating dust cloud solution, made M, a solution of equation (18), a function of both r and z with

$$M = \frac{2hr^2}{R^3}, \qquad R^2 = z^2 + r^2, \tag{25}$$

so that

$$\Psi = \frac{h^2 r^2 (r^2 - 8z^2)}{2R^8}, \tag{26}$$

where h is the rotation parameter. The density of the dust is given by

$$\rho = \frac{\exp(-\Psi) h^2 (r^2 + 4z^2)}{2\pi R^8}. \tag{27}$$

Note that R here is different from the R in the van Stockum solution.

This is one of a family of dust cloud solutions and it has the properties that, as $R \to \infty$, the density of the dust tends to zero and the metric tends to Minkowski values. There is, however, a singularity at the origin. An intriguing feature of Bonnor's dust cloud is that it has no Newtonian equivalent, since that would collapse due to the density gradient parallel to the axis of rotation.

~ Chapter 2 ~

Mathematical preliminaries

2.1 Killing vectors and conserved quantities

In simple terms, both the dust cylinder and dust cloud metrics are 'stationary' in the sense that their rotations are unvarying. A metric is stationary if, in some coordinate system(s), the metric functions are independent of time, so that if x^4 is the time coordinate,

$$\frac{\partial g_{ik}}{\partial x^4} \doteq 0, \tag{1}$$

where the symbol $\doteq$ means that the equation holds only in a particular coordinate system.

Defining the vector field $X^i = \delta^i_4$ and taking the Lie derivative of g_{ik} with respect to X^i gives

$$\pounds_X g_{ik} = X^m g_{ik,m} + g_{im} X^m{}_{,k} + g_{km} X^m{}_{,i} \doteq \delta^m_4 g_{ik,m} = g_{ik,4} = 0, \tag{2}$$

where commas indicate partial derivatives, and the Einstein summation convention is used. Since $\pounds_X g_{ik} = 0$ are Killing's equations,

$$\pounds_X g_{ik} = X_{i;k} + X_{k;i} = 0, \tag{3}$$

then X^i must be a Killing vector field. Thus a coordinate-independent definition of a stationary metric is a metric that admits a timelike Killing vector field.

In addition, if

$$X_{[l,k} X_{m]} = 0, \tag{4}$$

where the square brackets indicate skew symmetrization, then the Killing vector field is hypersurface-orthogonal and the spacetime is known as 'static'. In coordinate notation, if x^4 is the time coordinate, then the spacetime is static if the metric functions are independent of time and in some coordinate system(s) there are no cross terms in $dx^4 dx^i$, where $i = 1,2,3$.

Closely connected with Killing vectors are the conserved quantities associated with null and timelike geodesics, the constants of the motion. This connection may be seen by contracting the Killing vector Y with the tangent vector, u, to a geodesic, and taking the directional derivative along the geodesic,

$$\nabla_u (u \cdot Y) = (\nabla_u u) \cdot Y + u \cdot (\nabla_u Y). \tag{5}$$

Since $\nabla_u u = 0$ is the geodesic equation, and using the Killing equations (3),

$$(\nabla_u u) \cdot Y + u \cdot (\nabla_u Y) = u^i u^k Y_{i;k} = u^i u^k Y_{(i;k)} = 0, \tag{6}$$

the brackets in the subscript denoting symmetrisation. Thus $\nabla_u (u \cdot Y) = 0$ so that $u \cdot Y$ is a constant along the geodesic.

2.2 The geodesic equations and null geodesics

The geodesic equations for a spacetime whose line element is given by

$$ds^2 = g_{ik}\, dx^i\, dx^k \tag{7}$$

may be obtained from the Lagrangian $\mathcal{L}$, where

$$\mathcal{L} = \frac{1}{2} g_{ik} \frac{dx^i}{d\tau} \frac{dx^k}{d\tau}, \tag{8}$$

and τ is an affine parameter. This is demonstrated, for example, by Chandrasekhar [17].

Using the van Stockum line element, equation (21), from Section 1.3,

$$ds^2 = H(r)(dz^2 + dr^2) + L(r)\, d\phi^2 + 2\, M(r)\, d\phi\, dt - F(r)\, dt^2, \tag{9}$$

and the coordinate condition

$$FL + M^2 = r^2, \tag{10}$$

the Euler-Lagrange equations

$$\frac{d}{ds}\left(\frac{\partial \mathcal{L}}{\partial \dot{x}^i}\right) - \frac{\partial \mathcal{L}}{\partial x^i} = 0, \quad \text{where } \dot{x}^i = \frac{dx^i}{ds}, \tag{11}$$

give, since the metric coefficients are functions only of r, the geodesic equations

$$
\begin{aligned}
\ddot{z} &= -\frac{\dot{r}\dot{z}H'}{H}, \\
\ddot{r} &= \frac{-\dot{t}^2F' - \dot{r}^2H' + \dot{z}^2H' + \dot{\phi}^2L' + 2\dot{t}\dot{\phi}M'}{2H}, \\
\ddot{\phi} &= \frac{\dot{r}(\dot{t}(MF' - FM') - \dot{\phi}(FL' + MM'))}{r^2}, \\
\ddot{t} &= -\frac{\dot{r}(\dot{\phi}(ML' - LM') + \dot{t}(LF' + MM'))}{r^2},
\end{aligned}
\tag{12}
$$

where the dashes indicate differentiation with respect to r and superior dots indicate differentiation with respect to an affine parameter.

The corresponding constants of the motion along any geodesic, which were described in the context of Killing vectors in the previous section, may be easily calculated as first integrals of the geodesic equations, using *Mathematica*. They are

$$
P_z = H\dot{z}, \quad P_\phi = M\dot{t} + L\dot{\phi}, \quad E = F\dot{t} - M\dot{\phi}, \tag{13}
$$

where P_z, P_ϕ and E may be interpreted (at least, when $F > 0$) as linear momentum in the z direction, angular momentum and energy, respectively, of photons or test particles. In consequence of equations (13) and the coordinate condition (10), it follows that

$$
\begin{pmatrix} P_\phi \\ -E \end{pmatrix} = \begin{pmatrix} L & M \\ M & -F \end{pmatrix}\begin{pmatrix} \dot{\phi} \\ \dot{t} \end{pmatrix} \Rightarrow (\dot{\phi}\ \ \dot{t}) = \frac{1}{r^2}(P_\phi\ \ -E)\begin{pmatrix} F & M \\ M & -L \end{pmatrix}. \tag{14}
$$

Since null geodesics have $ds^2 = 0$, the line element (9) for null geodesics may be written

$$
H(\dot{z}^2 + \dot{r}^2) = -(\dot{\phi}\ \ \dot{t})\begin{pmatrix} L & M \\ M & -F \end{pmatrix}\begin{pmatrix} \dot{\phi} \\ \dot{t} \end{pmatrix} = -(\dot{\phi}\ \ \dot{t})\begin{pmatrix} P_\phi \\ -E \end{pmatrix}. \tag{15}
$$

Since H is always positive, and using (14),

$$
-(\dot{\phi}\ \ \dot{t})\begin{pmatrix} P_\phi \\ -E \end{pmatrix} = -\frac{1}{r^2}(P_\phi\ \ -E)\begin{pmatrix} F & M \\ M & -L \end{pmatrix}\begin{pmatrix} P_\phi \\ -E \end{pmatrix} \geq 0. \tag{16}
$$

It follows that everywhere on a given null geodesic,

$$
E^2L + 2EMP_\phi - FP_\phi^2 \geq 0. \tag{17}
$$

To have the equality condition in (17) requires $\dot{z} = \dot{r} = 0$ since $H \neq 0$.

2.3 The nature of the van Stockum t and ϕ coordinates

Much of the analysis and all of the numerical work (see Appendix 1) of this thesis requires orthonormal bases composed of three spacelike coordinate vectors and one timelike coordinate vector. In the co-rotating coordinate frame (the rest frame of the dust particles), the interior metric has three spacelike and one timelike coordinates where $ar < 1$, although the ϕ coordinate is timelike where $ar > 1$. The exterior metric usually seen in the literature is in a reference frame in which the cylinder is at rest. In this frame, when $aR \leq 1/2$ (cases I and II), the t coordinate is timelike close to the cylinder but is spacelike above a certain value of r. When $aR > 1/2$ (case III), the t and ϕ coordinates are timelike in some regions and spacelike in others, in all combinations.

Taking Ω to be a constant, van Stockum made use of coordinate transformations of the form

$$z \to z,\ r \to r,\ \phi \to \phi + \Omega t,\ t \to t, \tag{18}$$

which produce changes of angular velocity of the reference frame and result in new metric functions such that

$$H \to H,\ L \to L,\ M \to M + \Omega L,\ F \to F - 2\Omega M - \Omega^2 L. \tag{19}$$

Such transformations are used in several places in the thesis.

2.3.1 The astronomical rest frame

Van Stockum found the transformation to what he called the 'astronomical rest frame for the observer on the axis of symmetry', which gives a version of the case I exterior metric in which t remains timelike throughout. For this observer, the angular velocities of test particles in circular geodesic orbits (z = constant and r = constant, in either direction) tend to become equal and opposite, and tend to zero, as $r \to \infty$. The case I circular geodesics are studied in Chapter 5.

Using the metric equations (22) in Section 1.3, the case I metric functions in the co-rotating frame may be written

$$H(r) = \exp(-a^2 R^2)\left(\frac{r}{R}\right)^{-2a^2R^2}, \quad L(r) = \frac{rR\sinh(3\epsilon+\theta)}{2\sinh(2\epsilon)\cosh\epsilon},$$
$$M(r) = \frac{r\sinh(\epsilon+\theta)}{\sinh(2\epsilon)}, \quad F(r) = \frac{r\sinh(\epsilon-\theta)}{R\sinh\epsilon}, \tag{20}$$

where $\theta = \sqrt{1-4a^2R^2}\,\log(\frac{r}{R})$, $\epsilon = \tanh^{-1}\left(\sqrt{1-4a^2R^2}\right)$ and $0 < aR < 1/2$. Using coordinate transformation (18), with Ω given by (simplifying van Stockum's expression),

$$\Omega = -\frac{2\,\mathrm{sech}\epsilon}{R(\tanh\epsilon+1)^2} \equiv -\frac{4a}{\left(\sqrt{1-4a^2R^2}+1\right)^2}, \tag{21}$$

gives the new metric functions, according to (19), whereby

$$H(r) = \exp(-a^2 R^2)\left(\frac{r}{R}\right)^{-2a^2R^2}, \quad L(r) = \frac{rR\sinh(3\epsilon+\theta)}{2\sinh(2\epsilon)\cosh\epsilon},$$
$$M(r) = \frac{-r}{\exp(3\epsilon-\theta)}, \quad F(r) = \frac{8\,r\cosh^2\epsilon\,\sinh\epsilon}{R\exp(3\epsilon-\theta)}. \tag{22}$$

Clearly, $F(r) > 0$ for all r in (22) and the t coordinate is timelike everywhere, whereas $F(r)$ in (20) changes sign where $\epsilon = \theta$.

Taking case II to be the limit, as $aR \to 1/2$, of case I in the astronomical rest frame, results in a null t coordinate.

2.3.2 The orbiting coordinate frame

Transformation to the astronomical rest frame results in a timelike t coordinate at all r only in case I. However, in case III only, it turns out that in the reference frame of an observer in circular orbit (z = constant, r = constant) outside the cylinder, the metric functions L and F alternate in sign but are always positive or negative together. Thus t is timelike when ϕ is spacelike and vice versa as r increases. This enables the construction of two orthonormal frames to specify initial conditions for case III geodesics throughout the whole of the van Stockum exterior except where, in the transformed coordinates, $L = F = 0$.

Although transformation (18) can be used directly to find a form of the metric in which $F \propto L$, so that t is timelike when ϕ is spacelike and vice versa, the Ω that results is r-dependent. Also, the resulting metric functions don't have the particularly simple form found in the orbiting frame, which is necessary for the calculations in Chapter 5.

Using the metric equations (22) from Section 1.3, the case III metric functions in the co-rotating frame may be written

$$H(r) = \exp(-a^2 R^2)\left(\frac{r}{R}\right)^{-2a^2R^2}, \quad L(r) = \frac{r R \sin(3\epsilon+\theta)}{2\sin(2\epsilon)\cos\epsilon},$$
$$M(r) = \frac{r\sin(\epsilon+\theta)}{\sin(2\epsilon)}, \quad F(r) = \frac{r\sin(\epsilon-\theta)}{R\sin\epsilon}, \tag{23}$$

where $\theta = \sqrt{4a^2R^2-1}\,\log(\frac{r}{R})$, $\epsilon = \tan^{-1}\left(\sqrt{4a^2R^2-1}\right)$ and $1/2 < aR < 1$. To find the transformation to the orbiting frame requires the expression for the angular velocity of case III circular timelike geodesics. This will be derived in Chapter 5, and is

$$\frac{d\phi}{dt} = \frac{2a}{(2a^2R^2 - \cot(\theta/2)\,\tan\epsilon - 1)}. \tag{24}$$

Putting $dz = dr = 0$ into the line element (9) gives, for circular geodesics,

$$ds^2 = L(r)\,d\phi^2 + 2\,M(r)\,d\phi\,dt - F(r)\,dt^2. \tag{25}$$

For timelike geodesics, $ds^2 = -d\tau^2 < 0$, where τ is proper time. Thus for an observer in a circular orbit, we may write

$$\frac{d\phi}{d\tau} = \left(\left(\frac{dt}{d\phi}\right)^2 - 2\,M(r)\left(\frac{dt}{d\phi}\right) - L(r)\right)^{-1/2}. \tag{26}$$

Substituting from (23) and (24) gives the expression for circular timelike orbits in the co-rotating frame, in terms of proper time:

$$\frac{d\phi}{d\tau} = -\frac{2\,a\,\sin(\theta/2)\,\cot\epsilon}{\sqrt{r/R}}. \tag{27}$$

Equations (24) and (27) describe the same orbital angular velocities in terms of coordinate time and proper time respectively. Equation (24) may be re-written as

$$\begin{aligned} dt &= \frac{(2\,a^2\,R^2-1)}{2\,a}\,d\phi - \frac{\cot(\frac{\theta}{2})\tan\epsilon}{2\,a}\,d\phi \\ &\equiv \frac{(2\,a^2\,R^2-1)}{2\,a}\,d\phi - \frac{\cos(\frac{\theta}{2})}{2\,a\sin(\frac{\theta}{2})\cot\epsilon}\,d\phi\cdot \end{aligned} \tag{28}$$

Since, from (27), $d\phi/d\tau = -2\,a\sin(\frac{\theta}{2})\cot\epsilon\,\sqrt{R/r}$, this leads to the transformation to the orbiting frame, in which the proper time of the orbiting observer is also the coordinate time of the transformed metric,

$$\begin{aligned} dz \to dz,\quad dr \to dr,\quad d\phi \to d\phi, \\ dt \to \frac{(2\,a^2\,R^2-1)}{2\,a}\,d\phi + \frac{\cos(\theta_{orb}/2)}{\sqrt{r_{orb}/R}}\,d\tau, \end{aligned} \tag{29}$$

where $\theta_{orb} = \tan\epsilon\,\log(r_{orb}/R)$ and r_{orb} is the r coordinate of the orbiting observer. Re-writing τ as t, and writing the line element as

$$ds^2 = \hat{H}(r)\,(dr^2 + dz^2) + \hat{L}(r)\,d\phi^2 + 2\,\hat{M}(r)\,d\phi dt - \hat{F}(r)\,dt^2, \tag{30}$$

to distinguish it from the line element in co-rotating coordinates, the case III metric functions in the orbiting frame are

$$\begin{aligned} \hat{H}(r) &= \exp(-a^2\,R^2)\left(\frac{r}{R}\right)^{-2\,a^2\,R^2},\quad \hat{L}(r) = r\,R\,\sin\epsilon\,\sin(\epsilon-\theta), \\ \hat{M}(r) &= r\,\sqrt{\chi}\,\cos(\epsilon-\theta),\quad \hat{F}(r) = \frac{r\,\chi\,\sin(\epsilon-\theta)}{R\,\sin\epsilon}, \end{aligned} \tag{31}$$

where $\chi = R\cos^2(\theta_{orb}/2)/r_{orb}$. The coordinate condition becomes $\hat{L}\,\hat{F} + \hat{M}^2 = r^2\,\chi$.

The nature of the t and ϕ coordinates changes at r values where $\hat{L} = \hat{F} = 0$ and this happens where $(\epsilon - \theta) = k\,\pi$, where k is an integer. From the metric equation (30) with definitions (31), $d\phi/dt$ for light with $\dot{z} = \dot{r} = 0$ is given by

$$\frac{d\phi}{dt} = \frac{\sqrt{\chi}\,\tan(\frac{\epsilon-\theta}{2})}{R\,\sin\epsilon} \text{ and } \frac{d\phi}{dt} = -\frac{\sqrt{\chi}\,\cot(\frac{\epsilon-\theta}{2})}{R\,\sin\epsilon}\cdot \tag{32}$$

Thus $d\phi/dt$ for light with $\dot{z} = \dot{r} = 0$ tends to zero or infinity as $\theta \to \epsilon - k\,\pi$. Where $\theta = \epsilon - k\,\pi$, both ϕ and t are null coordinates.

Taking case II to be the limit, as $aR \to 1/2$, of case III in the orbiting frame, results in a null ϕ coordinate.

2.4 Orthonormal bases

Both for the analytical treatment of geodesics that follows and in the numerical solution of the geodesic equations, it is useful to set up tetrad bases of four orthonormal vector fields in regions where there are three spacelike and one timelike coordinates in some coordinate frame. Two bases are required, one for geodesics originating in regions where t is the timelike coordinate and another for those originating in regions where ϕ is the timelike coordinate. The examples below use the general form of the van Stockum metric (9).

2.4.1 t timelike, ϕ spacelike

Let X_z, X_r, X_ϕ and X_t denote the coordinate vector fields in a region where t is timelike. Then, provided that $L > 0$, so that ϕ is a spacelike coordinate, an orthonormal basis is given by

$$\xi_z = \frac{X_z}{\sqrt{H}}, \quad \xi_r = \frac{X_r}{\sqrt{H}}, \quad \xi_\phi = \frac{X_\phi}{\sqrt{L}}, \quad \xi_t = \frac{(L\,X_t - M\,X_\phi)}{r\sqrt{L}}. \tag{33}$$

Since $F > 0$, any null vector N can be written as

$$N = x\,(\sin\beta\,\xi_z + \cos\alpha\,\cos\beta\,\xi_r + \sin\alpha\,\cos\beta\,\xi_\phi + \xi_t), \tag{34}$$

where x is a scale factor. Any timelike vector T can be written as

$$T = \lambda\,(v\sin\beta\,\xi_z + v\cos\alpha\,\cos\beta\,\xi_r + v\sin\alpha\,\cos\beta\,\xi_\phi + \xi_t), \tag{35}$$

where $\lambda^2 = (1 - v^2)^{-1}$ and v is the speed (i.e. the modulus of the 3-velocity) of a test particle such that $0 \le v < 1$. As shown in Figure 2.1, the angle that the perpendicular projection of N and T on to the r, ϕ plane makes with ξ_r is α and the angle between the vector and the plane is β, so $-\pi \le \alpha \le \pi$ and $-\pi/2 \le \beta \le \pi/2$.

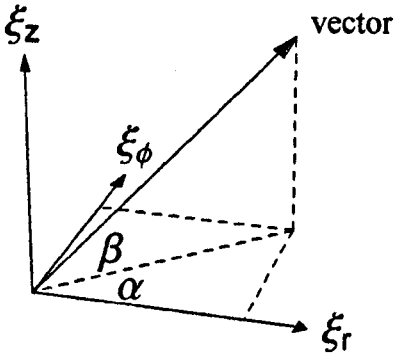

Figure 2.1 The angles α and β where t is timelike and ϕ is spacelike.

Applying this construction to geodesics gives functions $\alpha(\tau)$, $\beta(\tau)$ and $x(\tau)$ or $\lambda(\tau)$ along the geodesics. Their relationship to $\dot{z}$, $\dot{r}$, $\dot{\phi}$ and $\dot{t}$ is shown by expressing N and T in terms of the coordinate vectors:

$$N = x\left(\frac{\sin\beta\, X_z}{\sqrt{H}} + \frac{\cos\alpha\cos\beta\, X_r}{\sqrt{H}} + \frac{(\sin\alpha\cos\beta - \frac{M}{r})\, X_\phi}{\sqrt{L}} + \frac{\sqrt{L}\, X_t}{r}\right), \tag{36}$$

$$T = \lambda\left(\frac{v\sin\beta\, X_z}{\sqrt{H}} + \frac{v\cos\alpha\cos\beta\, X_r}{\sqrt{H}} + \frac{(v\sin\alpha\cos\beta - \frac{M}{r})\, X_\phi}{\sqrt{L}} + \frac{\sqrt{L}\, X_t}{r}\right). \tag{37}$$

Thus for null and timelike geodesics respectively,

$$\dot{z} = x\frac{\sin\beta}{\sqrt{H}},\ \dot{r} = x\frac{\cos\alpha\cos\beta}{\sqrt{H}},$$
$$\dot{\phi} = x\frac{(\sin\alpha\cos\beta - \frac{M}{r})}{\sqrt{L}},\ \dot{t} = x\frac{\sqrt{L}}{r}, \quad \text{and} \tag{38}$$

$$\dot{z} = \lambda\frac{v\sin\beta}{\sqrt{H}},\ \dot{r} = \lambda\frac{v\cos\alpha\cos\beta}{\sqrt{H}},$$
$$\dot{\phi} = \lambda\frac{(v\sin\alpha\cos\beta - \frac{M}{r})}{\sqrt{L}},\ \dot{t} = \lambda\frac{\sqrt{L}}{r}. \tag{39}$$

2.4.2 ϕ timelike, t spacelike

In regions where ϕ is timelike (and t is spacelike) an orthonormal basis is given by

$$\xi_z = \frac{X_z}{\sqrt{H}}, \ \xi_r = \frac{X_r}{\sqrt{H}}, \ \xi_\phi = \frac{-(F\,X_\phi + M\,X_t)}{r\sqrt{-F}}, \ \xi_t = \frac{X_t}{\sqrt{-F}}. \tag{40}$$

Any null vector N can be written as

$$N = x\,(\sin\beta\,\xi_z + \cos\alpha\,\cos\beta\,\xi_r - \sin\alpha\,\cos\beta\,\xi_t + \xi_\phi), \tag{41}$$

where x is a scale factor. Any timelike vector T can be written as

$$T = \lambda\,(v\sin\beta\,\xi_z + v\cos\alpha\,\cos\beta\,\xi_r - v\sin\alpha\,\cos\beta\,\xi_t + \xi_\phi), \tag{42}$$

where $\lambda = (1 - v^2)^{-1/2}$ and v is the speed of a test particle such that $0 \le v < 1$. As shown in Figure 2.2, the angle that the perpendicular projection of N and T on to the r, t plane makes with ξ_r is α and the angle between the vector and the plane is β, so $-\pi \le \alpha \le \pi$ and $-\pi/2 \le \beta \le \pi/2$ as before.

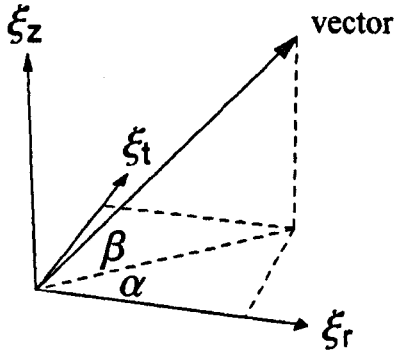

Figure 2.2 The angles α and β where ϕ is timelike and t is spacelike.

Thus the vectors N and T may be expressed in terms of the coordinate vectors:

$$N = x\left(\frac{\sin\beta\,X_z}{\sqrt{H}} + \frac{\cos\alpha\,\cos\beta\,X_r}{\sqrt{H}} - \frac{(\frac{M}{r} - \sin\alpha\,\cos\beta)\,X_t}{\sqrt{-F}} + \frac{\sqrt{-F}\,X_\phi}{r}\right), \tag{43}$$

$$T = \lambda\left(\frac{v\sin\beta X_z}{\sqrt{H}} + \frac{v\cos\alpha\cos\beta X_r}{\sqrt{H}} - \frac{(\frac{M}{r} - v\sin\alpha\cos\beta)X_t}{\sqrt{-F}} + \frac{\sqrt{-F}X_\phi}{r}\right), \tag{44}$$

and for null and timelike geodesics respectively,

$$\dot{z} = x\frac{\sin\beta}{\sqrt{H}},\ \dot{r} = x\frac{\cos\alpha\cos\beta}{\sqrt{H}},$$
$$\dot{t} = x\frac{(\sin\alpha\cos\beta - \frac{M}{r})}{\sqrt{-F}},\ \dot{\phi} = x\frac{\sqrt{-F}}{r},\quad \text{and} \tag{45}$$

$$\dot{z} = \lambda\frac{v\sin\beta}{\sqrt{H}},\ \dot{r} = \lambda\frac{v\cos\alpha\cos\beta}{\sqrt{H}},$$
$$\dot{t} = \lambda\frac{(v\sin\alpha\cos\beta - \frac{M}{r})}{\sqrt{-F}},\ \dot{t} = \lambda\frac{\sqrt{-F}}{r}. \tag{46}$$

2.5 The signature of the van Stockum metric

The matrix of metric coefficients is

$$g = \begin{pmatrix} H & 0 & 0 & 0 \\ 0 & H & 0 & 0 \\ 0 & 0 & L & M \\ 0 & 0 & M & -F \end{pmatrix}, \tag{47}$$

so the eigenvalues of g are,

$$\lambda_1 = H,\ \lambda_2 = H,\ \lambda_3 = \frac{1}{2}\left(L - F - \sqrt{F^2 + 2LF + L^2 + 4M^2}\right),$$
$$\lambda_4 = \frac{1}{2}\left(L - F + \sqrt{F^2 + 2LF + L^2 + 4M^2}\right). \tag{48}$$

Since, using the coordinate condition (10),

$$\lambda_3\lambda_4 = -(LF + M^2) = -r^2, \tag{49}$$

then λ_3 and λ_4 are always of opposite sign. As the signature of a metric is the number of positive eigenvalues minus the number of negative eigenvalues at any point (see [18], for example), the signature of the van Stockum metric must be the same everywhere.

~ Chapter 3 ~

The geodesics plotting routine

Much of this thesis involves the investigation of various exact solutions of Einstein's gravitational equations, and especially van Stockum spacetime, by examining null and timelike geodesics. The geodesic equations may be solved numerically and plotted in a variety of ways using *Mathematica* software [6]. At the beginning of this work, it was hoped that studying the plots of geodesics would give clues to the nature of spacetimes which could then be investigated and described analytically. This hope turned out not to be ill-founded.

The routine for plotting geodesics in four dimensional spacetime, which is described here, grew from a *Mathematica* method in the book by Gray [20] which shows how to calculate and plot geodesics on 2-D surfaces in Euclidean space. Once the geodesic equations are solved numerically, a geodesic is represented as a file of numbers giving coordinate values over the range of affine parameter specified. There are then several ways of representing the geodesic. For example, as well as straightforward plotting, an impression of speeds of geodesics can be obtained by plotting with dots at equal intervals of the affine parameter or at equal intervals of the coordinate time. Animated displays can be made of cartoon-like sequences of geodesics plotted for progressively longer times.

3.1 Schwarzschild geodesics

For the sake of familiarity, this section uses Schwarzschild spacetime in the first example of the numerical solution of geodesic equations using *Mathematica*. The metric in spherical polar coordinates may be written

$$ds^2 = \left(1 - \frac{2M}{r}\right)^{-1} dr^2 + r^2 d\theta^2 + r^2 \sin^2\theta \, d\phi^2 - \left(1 - \frac{2M}{r}\right) dt^2 . \qquad (1)$$

The geodesic equations are calculated from the metric using *Mathematica*'s variational calculus package, hence

$$\begin{aligned}
\ddot{t} &= \frac{2M\dot{r}\dot{t}}{r(2M-r)}, \\
\ddot{r} &= -\frac{(r-2M)^2\left(M\dot{t}^2 + r^3\left[\dot{\theta}^2 + \sin^2\theta\,\dot{\phi}^2\right]\right) + Mr^2\dot{r}^2}{r^3(2M-r)}, \\
\ddot{\theta} &= -\frac{2\dot{r}\dot{\theta}}{r} + \cos\theta\,\sin\theta\,\dot{\phi}^2, \\
\ddot{\phi} &= -\frac{2(\dot{r} + r\cot\theta\,\dot{\theta})\,\dot{\phi}}{r},
\end{aligned} \tag{2}$$

superior dots indicating differentiation with respect to an affine parameter. If we choose $\theta = \pi/2$ when $\dot{\theta} = 0$, then $\ddot{\theta} = 0$ and $\theta = \pi/2$ always. Thus, without loss of generality, we restrict attention to the hypersurface $\theta = \pi/2$, using units such that $c = G = 1$. The geodesic equations are then put into a file in a form more suitable for *Mathematica* to handle (see Appendix A.1.1).

To solve the three geodesic equations numerically, initial values t_0, r_0 and ϕ_0 must be specified together with $\dot{t}_0$, $\dot{r}_0$ and $\dot{\phi}_0$. The former three are straightforward choices but the latter three are not so obvious. A useful way of specifying a geodesic, once the initial position is chosen, is to give its initial direction, together with its initial velocity if it is a timelike geodesic. To find $\dot{t}_0$, $\dot{r}_0$ and $\dot{\phi}_0$ in terms of initial direction (and velocity), first let X_r, X_ϕ and X_t denote the coordinate vector fields in the hypersurface $\theta = \pi/2$, so that

$$\begin{gathered}
g(X_r, X_r) = \left(1 - \frac{2M}{r}\right)^{-1},\ g(X_\phi, X_\phi) = r^2,\ g(X_t, X_t) = -\left(1 - \frac{2M}{r}\right), \\
g(X_r, X_\phi) = g(X_r, X_t) = g(X_\phi, X_t) = 0,
\end{gathered} \tag{3}$$

where g is the metric tensor. An orthonormal basis, for $r > 2M$, is given by

$$\xi_r = \sqrt{1 - \frac{2M}{r}}\,X_r,\quad \xi_\phi = \frac{X_\phi}{r},\quad \xi_t = \frac{X_t}{\sqrt{1 - \frac{2M}{r}}}, \tag{4}$$

so that

$$\begin{gathered}
g(\xi_r, \xi_r) = g(\xi_\phi, \xi_\phi) = 1,\ g(\xi_t, \xi_t) = -1, \\
g(\xi_r, \xi_\phi) = g(\xi_r, \xi_t) = g(\xi_\phi, \xi_t) = 0.
\end{gathered} \tag{5}$$

Consider a tangent vector to a geodesic and its perpendicular projection on to the r, ϕ plane. If α is the angle that the perpendicular projection makes with ξ_r, then any null vector N can be written as

$$N = x(\cos\alpha\,\xi_r + \sin\alpha\,\xi_\phi + \xi_t), \tag{6}$$

where $-\pi \le \alpha \le \pi$, and x is a scale factor, and any timelike vector T can be written as

$$T = \lambda(v\cos\alpha\,\xi_r + v\sin\alpha\,\xi_\phi + \xi_t), \tag{7}$$

where $-\pi \le \alpha \le \pi$, $0 \le v < 1$ and $\lambda = (1-v^2)^{-1/2}$ and v is the modulus of the 3-velocity. Applying this construction to geodesics gives functions $x(\tau)$, $\lambda(\tau)$ and $\alpha(\tau)$, of the affine parameter, along the geodesic. The relationships of x, λ and α to $\dot{r}$, $\dot{\phi}$ and $\dot{t}$ may be shown by first expressing N and T in terms of the coordinate vectors,

$$N = x\left(\cos\alpha\sqrt{1-\frac{2M}{r}}\,X_r + \sin\alpha\,\frac{X_\phi}{r} + \frac{X_t}{\sqrt{1-\frac{2M}{r}}}\right), \tag{8}$$

$$T = \lambda\left(v\cos\alpha\sqrt{1-\frac{2M}{r}}\,X_r + v\sin\alpha\,\frac{X_\phi}{r} + \frac{X_t}{\sqrt{1-\frac{2M}{r}}}\right). \tag{9}$$

Then $\dot{r}$, $\dot{\phi}$ and $\dot{t}$ can be expressed in terms of the position and direction of the tangent vector. Thus for null geodesics,

$$\dot{r} = x\cos\alpha\sqrt{1-\frac{2M}{r}},\quad \dot{\phi} = \frac{x\sin\alpha}{r},\quad \dot{t} = \frac{x}{\sqrt{1-\frac{2M}{r}}}, \tag{10}$$

and for timelike geodesics, where speed also must be specified,

$$\dot{r} = \lambda v\cos\alpha\sqrt{1-\frac{2M}{r}},\quad \dot{\phi} = \frac{\lambda v\sin\alpha}{r},\quad \dot{t} = \frac{\lambda}{\sqrt{1-\frac{2M}{r}}}. \tag{11}$$

In this way, initial conditions for solving the geodesic equations may be more intuitively specified by the direction in the coordinate frame, and the speed v for timelike geodesics.

Once the choice of initial conditions and the specification of null or timelike geodesic are made, *Mathematica* can calculate a list of data points of $t(\tau)$, $r(\tau)$ and $\phi(\tau)$ for the range of parameter τ that is specified. The list may then be used for plotting the geodesic

in various ways.

Although radial distances between r_1 and r_2, for $r > 2M$, in the Schwarzschild metric above are given by

$$d = \int_{r_1}^{r_2} g_{rr}^{1/2}\, dr = \int_{r_1}^{r_2} \left(1 - \frac{2M}{r}\right)^{-1/2} dr, \tag{12}$$

the geodesics are often plotted, for convenience, using the usual Cartesian coordinates given by $x = r \sin\theta \cos\phi$, $y = r \sin\theta \cos\phi$ and $z = r \cos\theta$. For $r < 2M$, the r coordinate is timelike. Putting $M = 1$, Figure 3.1 shows a timelike geodesic projected on to the equatorial plane with $r_0 = 10$, $\alpha_0 \simeq 2.62$ and $v_0 = 0.89$, remembering that r is not radial distance. The geodesic spirals into the event horizon at $r = 2$, where the coordinate singularity prevents further numerical solution of the equations.

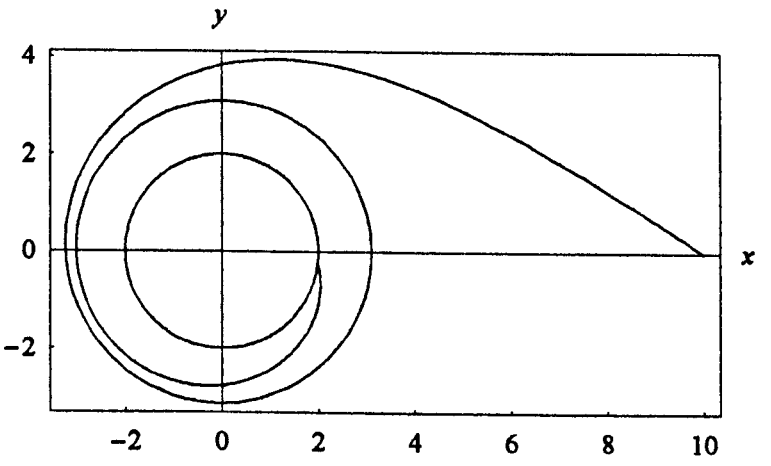

Figure 3.1 A geodesic in the plane of $\theta = \pi/2$.

The second example, Figure 3.2, shows the same timelike geodesic but this time plotted with radial distances from the horizon calculated according to (12) above. Calling the radial coordinate for this plot ρ and putting $M = 1$, the horizon is shown, rather arbitrarily, at $\rho = 2$ and the relationship between r and ρ, is

$$\rho = 2 + \sqrt{r^2 - 2r} + \log\left(\frac{r}{2}\right) + 2\log\left(\sqrt{1 - \frac{2}{r}} + 1\right). \tag{13}$$

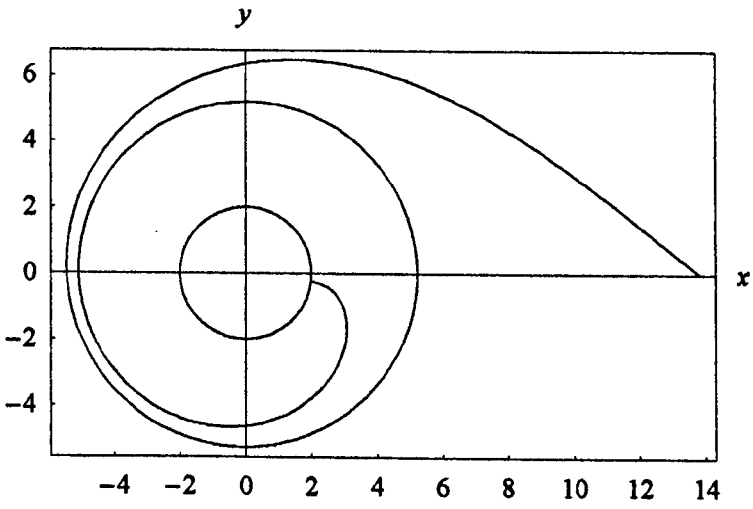

Figure 3.2 A geodesic in the plane of $\theta = \pi/2$.

Both plotting methods are compromise attempts to illustrate geodesics in curved spacetime, the former having the advantage of simplicity.

Any coordinate along the geodesic may be plotted against any other or against the affine parameter, proper time here, as in Figure 3.3. The left hand plot has an approximately horizontal portion corresponding with the part of the geodesic which is almost circular. The right hand plot shows the observed slowing of the test particle's proper time as the event horizon is approached.

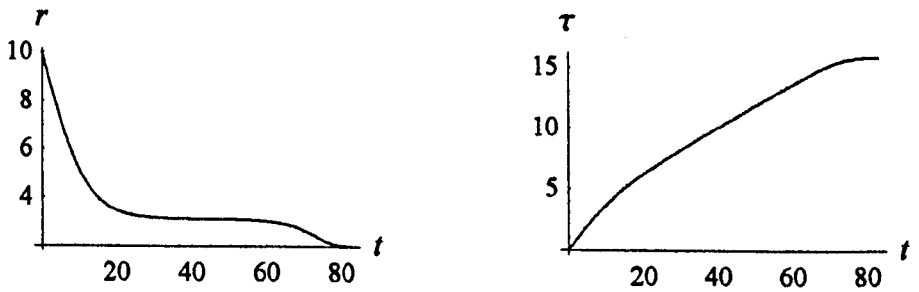

Figure 3.3 Test particle r coordinate and proper time plotted against t.

By using an additional dimension, coordinate time t may be shown in the plot of the geodesic and the event horizon is seen as a cylinder. Figure 3.4 is thus the spacetime version of Figure 3.1.

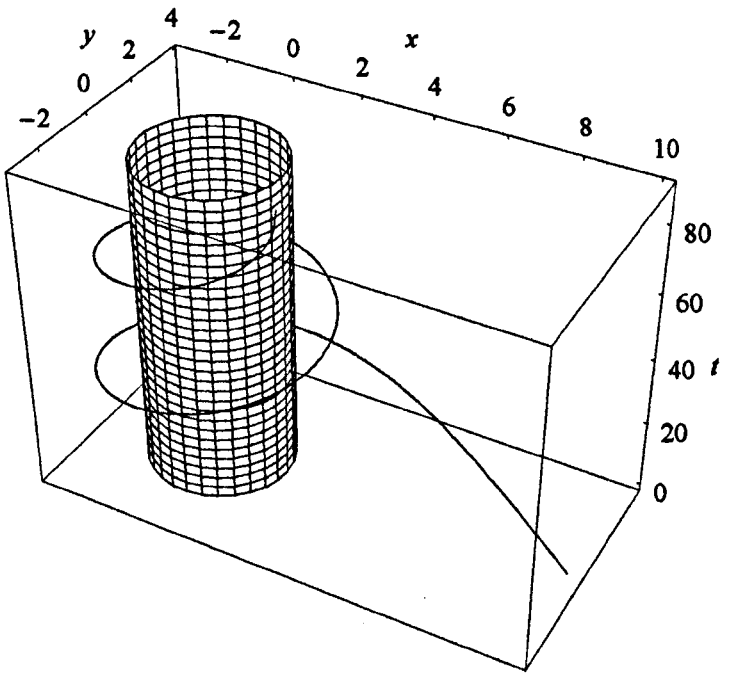

Figure 3.4 The geodesic in the plane of $\theta = \pi/2$ plotted against t.

3.2 Kerr geodesics

In Section 3.1, the method for finding and plotting Schwarzschild geodesics showed mathematical expressions explicitly. This was done for transparency but was only practical due to the relatively simple metric functions. The more complicated Kerr metric functions are better represented symbolically, the *Mathematica* routines calling up a file containing the actual metric functions as required. Thus we use, for the Kerr line element in spherical polar coordinates,

$$\begin{aligned} ds^2 = A(r,\theta)\,dr^2 + B(r,\theta)\,d\theta^2 + F(r,\theta)\,d\phi^2 + \\ 2\,J(r,\theta)\,d\phi\,dt + K(r,\theta)\,dt^2, \end{aligned} \tag{14}$$

where A, B, F, J and K are defined in a *Mathematica* file as the Kerr metric functions. The file containing the geodesic equations in terms of A, B, F, J and K is shown in Appendix A.1.2 and the explicit forms of the functions are called up when the file is used.

The initial conditions $\dot{r}_0$, $\dot{\theta}_0$, $\dot{\phi}_0$ and $\dot{t}_0$ for timelike geodesics may be found as follows.

Let X_r, X_θ, X_ϕ and X_t denote the coordinate vector fields, then an orthonormal basis is given by

$$\xi_r = \frac{X_r}{\sqrt{A}},\ \xi_\theta = \frac{X_\theta}{\sqrt{B}},\ \xi_\phi = \frac{X_\phi}{\sqrt{F}},\ \xi_t = \frac{F\,X_t - J\,X_\phi}{\sqrt{F}\,\sqrt{J^2 - F\,K}}. \tag{15}$$

Consider a test particle with speed v, where $0 \le v < 1$, following a geodesic in Kerr spacetime. Any tangent vector to the geodesic can be written as

$$T = \lambda\,(v\cos\alpha\,\cos\beta\,\xi_r - v\,\sin\beta\,\xi_\theta + v\sin\alpha\,\cos\beta\,\xi_\phi + \xi_t), \tag{16}$$

where $\lambda = (1 - v^2)^{-1/2}$. The angle that the perpendicular projection of T on to the r, ϕ plane makes with ξ_r is α, and β is the angle between the vector and the plane, as shown in Figure 3.5, so $-\pi \le \alpha \le \pi$ and $-\pi/2 \le \beta \le \pi/2$.

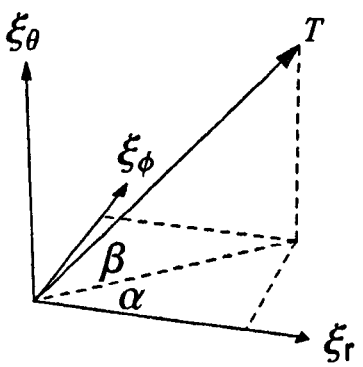

Figure 3.5 The angles α and β.

The relationship of $\dot{r}$, $\dot{\theta}$, $\dot{\phi}$ and $\dot{t}$, where $\dot{r} = dr/d\tau$ etc. and τ is proper time, to the functions $\lambda(\tau)$, $\alpha(\tau)$, and $\beta(\tau)$ may be shown by expressing T in terms of the coordinate vectors:

$$T = \lambda\left(\frac{v\cos\alpha\cos\beta\,X_r}{\sqrt{A}} - \frac{v\sin\beta\,X_\theta}{\sqrt{B}} + \left(v\sin\alpha\cos\beta - \frac{J}{\sqrt{J^2 - F\,K}}\right)\frac{X_\phi}{\sqrt{F}} + \frac{\sqrt{F}\,X_t}{\sqrt{J^2 - F\,K}}\right). \tag{17}$$

Hence:

$$\dot{r} = \lambda v \frac{\cos\alpha \cos\beta}{\sqrt{A}}, \quad \dot{\theta} = -\lambda v \frac{\sin\beta}{\sqrt{B}},$$
$$\dot{\phi} = \frac{\lambda}{\sqrt{F}} \left(v \sin\alpha \cos\beta - \frac{J}{\sqrt{J^2 - FK}} \right), \quad \dot{t} = \frac{\lambda \sqrt{F}}{\sqrt{J^2 - FK}}. \tag{18}$$

For null geodesics, a similar calculation, with a suitable affine parameter, gives

$$\dot{r} = x \frac{\cos\alpha \cos\beta}{\sqrt{A}}, \quad \dot{\theta} = -x \frac{\sin\beta}{\sqrt{B}}, \dot{\phi} = \frac{x}{\sqrt{F}} \left(\sin\alpha \cos\beta - \frac{J}{\sqrt{J^2 - FK}} \right),$$
$$\dot{t} = \frac{x \sqrt{F}}{\sqrt{J^2 - FK}}, \tag{19}$$

where x is a scale factor.

Using similar *Mathematica* techniques to those used for the Schwarzschild metric, the more complicated Kerr geodesic equations, with two parameters a and M, may be readily solved numerically. When the mass parameter M is zero, the Kerr metric reduces to the Minkowski metric in Cartesian coordinates given by [21]

$$x = (r^2 + a^2)^{1/2} \sin\theta \cos\phi, \; y = (r^2 + a^2)^{1/2} \sin\theta \sin\phi, \; z = r \cos\theta, \tag{20}$$

and not $x = r \sin\theta \cos\phi$, $y = r \sin\theta \sin\phi$ and $z = r \cos\theta$ as might be expected. Kerr geodesics are therefore plotted in Cartesian coordinates according to equations (20).

As an example, we examine a timelike geodesic close to the Kerr outer event horizon which is at $r = M + (M^2 - a^2)^{1/2}$. First, the geodesic is shown as a continuous line starting at the top right hand corner of Figure 3.6. The initial conditions include $r_0 = 10$, $\theta_0 = \pi/4$, $\alpha_0 = 1/2$, $\beta_0 = \pi/4$ and $v = -0.4862$. The spheroid represents the outer event horizon. Then, by plotting with dots at equal intervals of proper time, in Figure 3.7, the test particle is observed to speed up when looping around the horizon since the dots are spaced further apart there.

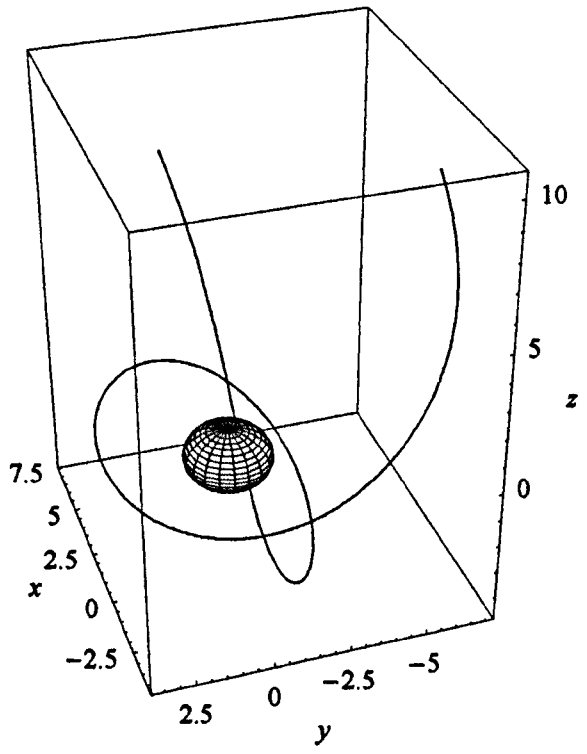

Figure 3.6 A timelike geodesic. Parameters, $a = 1, M = 1$.

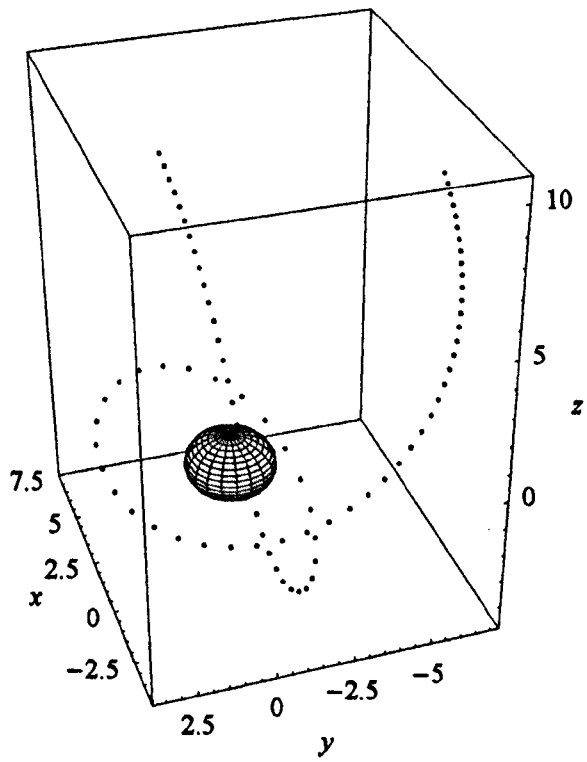

Figure 3.7 The same geodesic, plotted at intervals of proper time.

3.3 Van Stockum geodesics

To find and plot van Stockum interior and exterior geodesics, we use the general form of the line element in cylindrical polar coordinates,

$$ds^2 = H(r)(dz^2 + dr^2) + L(r)\,d\phi^2 + 2\,M(r)\,d\phi dt - F(r)\,dt^2, \qquad (21)$$

where H, L, M and F have the definitions, in a *Mathematica* file, that are shown in Chapters 4 and 5. These files contain the metric functions of either the interior or exterior region of the solution and may be in one of several coordinate frames. The file containing the geodesic equations in terms of H, L, M and F and their derivatives is shown in Appendix A.1.3. This file, when used, calls up the required form of the metric. In the example shown in the appendix, this is the interior metric in comoving coordinates "vsintout.m".

The initial conditions $\dot{z}_0$, $\dot{r}_0$, $\dot{\phi}_0$ and $\dot{t}_0$ were derived in Section 2.4 on orthonormal bases, since they are also used in analytical work on the geodesics. Once the initial conditions are supplied, the *Mathematica* routine 'solve3', for example, can numerically solve the geodesic equations in a z = constant hypersurface and store the results as a list of data points as already described for the Schwarzschild and Kerr metrics.

An added feature with the van Stockum solution is that it has both interior and exterior regions. Consider a null geodesic which originates within the dust cylinder and then passes out into the vacuum exterior region. It is straightforward, using *Mathematica*, to plot the interior part of the geodesic and then to find $\dot{z}_0$, $\dot{r}_0$, $\dot{\phi}_0$ and $\dot{t}_0$ at R, the boundary of the interior, from the data file for the geodesic. In fact, *Mathematica* can perform differentiation on the data directly. These values may then be used as initial conditions to plot the geodesic starting at R and going into the exterior. Examples of this are shown in Section 4.4.

As with the Schwarzschild metric, when plotting geodesics, r is a coordinate, not a distance. As the mass per unit length of the source cylinder increases, r departs more and more from radial distance, especially near the cylinder, but this does not reduce the usefulness of plotting in exploring the behaviour of geodesics.

3.4 Dust cloud geodesics

The general form of the line element for Bonnor's rotating dust cloud in cylindrical polar coordinates is

$$ds^2 = H(z, r)(dz^2 + dr^2) + L(z, r)\,d\phi^2 + 2\,M(z, r)\,d\phi dt - F(z, r)\,dt^2. \qquad (22)$$

The details of H, L, M and F are shown in Chapter 6 and defined in a *Mathematica* file for plotting geodesics. This file is shown in Appendix A.1.4. and geodesics are calculated and plotted in a similar manner to that described in Section 3.3 for the van Stockum solution. Away from the central region, the z and r coordinates are very closely approximated by Cartesian coordinates and r, z and ϕ are plotted in the diagrams in Chapter 6.

~ Chapter 4 ~

The van Stockum dust cylinder

Although unrealisable in nature due to the infinite length of the source cylinder, the van Stockum solution is nevertheless of great importance to classical general relativity being a complete (interior plus matching exterior) rotating solution whose source is composed of physically reasonable matter. The interior metric is characterised by a single parameter a.

4.1 Range of the rotation parameter a

The metric for the interior in co-rotating coordinates is

$$ds^2 = \exp(-a^2 r^2)(dz^2 + dr^2) + r^2(1 - a^2 r^2)\,d\phi^2 + 2\,a\,r^2\,d\phi dt - dt^2, \tag{1}$$

and the parameter a is related to the rotation of the cylinder. It has the dimension of inverse distance. The energy momentum tensor for non-interacting dust is defined by

$$T^{ik} = \rho\, u^i u^k, \tag{2}$$

where ρ is the proper mass density and u^i is the dust four-velocity. The density in the rest frame of the dust, in customary units, is

$$\rho = \frac{a^2 c^2 \exp(a^2 r^2)}{2\pi G}. \tag{3}$$

Lanczos chose to set the parameter a equal to one and considered the dust cylinder through the range $0 \le r \le \infty$, finding singular behaviour only at $r = \infty$. He noted, however, that at $r = 1$, the determinant of the spatial part of the line element is zero and is negative where $r > 1$.

In his treatment, van Stockum denoted the boundary of the cylinder by $r = R$ then restricted the value of the rotation parameter so that $aR < 1$ to prevent the coefficient of

$d\phi^2$ in the interior of the cylinder becoming negative.

In 1973, Tipler [9] pointed out that, since the ϕ coordinate is timelike for $ar > 1$, there are closed timelike lines of r = constant, z = constant and t = constant connecting any two events within such a van Stockum dust cylinder. Although causality violation in the cylinder may be avoided by restriction to cylinders with $aR < 1$, he also showed that, in the vacuum exterior, there are closed timelike lines when $aR > 1/2$ (i.e. case III). In his argument, Tipler invoked Carter's causality theorem [10], which states the necessary and sufficient conditions for closed timelike lines. The theorem is summarised in the reference section of Tipler's paper.

Bonnor [5] made a purely local coordinate transformation, to the locally non-rotating 'Bardeen' frame [8], by using the transformation $z \to z$, $r \to r$, $\phi \to \phi - \omega t$ and $t \to t$. The constant ω is the angular velocity of the locally non-rotating frame, with respect to the rest frame of the dust, at the coordinate distance $r = r_1$. Using expressions (19) from Section 2.3 (the transformed metric functions), for the transformed metric to be diagonal at $r = r_1$ requires

$$\omega = -\frac{M(r_1)}{L(r_1)} = \frac{-a}{1 - a^2 r_1^2}, \tag{4}$$

so that as $r_1 \to 0$, $\omega \to -a$. Thus Bonnor found a to be the angular velocity of the dust on the axis, in agreement with what van Stockum found by a different method. The dust is rotating rigidly, i.e. with zero shear, and the individual dust particles are moving on circular geodesics.

The metric in the locally non-rotating frame is

$$ds^2 = \exp(-a^2 r^2)(dz^2 + dr^2) + r^2(1 - a^2 r^2)\,d\phi^2 + \frac{a^3 r^2 (r_1^2 - r^2)}{a^2 r_1^2 - 1}\,d\phi dt - \frac{a^4 r^4 + a^2 r^2 + a^4 r_1^4 - 2(r^2 a^4 + a^2) r_1^2 + 1}{(a^2 r_1^2 - 1)^2}\,dt^2. \tag{5}$$

Thus, in the locally non-rotating frame, as $ar_1 \to 1$, the coefficient of $dt^2 \to \infty$. Also, from equation (4), $\omega \to -\infty$ as $ar_1 \to 1$.

In light of the above findings, restriction to cylinders having $aR < 1$, would seem to

give the best hope of physical relevance to any results obtained in the analysis. However, some of the above results were found in particular coordinate systems, so it would be interesting to examine some of the invariants of the Riemann curvature tensor to see if these reveal any peculiar behaviour at $ar = 1$.

Looking first at algebraic invariants A1 = $R_{ijkl}R^{ijkl}$, A2 = $C_{ijkl}C^{ijkl}$ and differential invariants D1 = $R_{ijkl;m}R^{ijkl;m}$, D2 = $C_{ijkl;m}C^{ijkl;m}$ formed from the Riemann tensor R_{ijkl} and the Weyl tensor C_{ijkl} for the interior, the following were calculated using *MathTensor* software (see Appendix 2 for some discussion of the Weyl tensor):

$$\begin{aligned} \text{A1} &= 16a^4 \exp(2a^2 r^2)(2 - a^2 r^2), \\ \text{A2} &= \frac{16}{3} a^4 \exp(2a^2 r^2)(1 - 3a^2 r^2), \\ \text{D1} &= -16a^6 \exp(3a^2 r^2)(16 - 11a^2 r^2 + 8a^4 r^4), \\ \text{D2} &= -\frac{16}{3} a^6 \exp(3a^2 r^2)(24 - 13a^2 r^2 + 24a^4 r^4). \end{aligned} \tag{6}$$

Plots of these invariants from $ar = 0$ to beyond $ar = 1$ are shown in Figures 4.1 and 4.2.

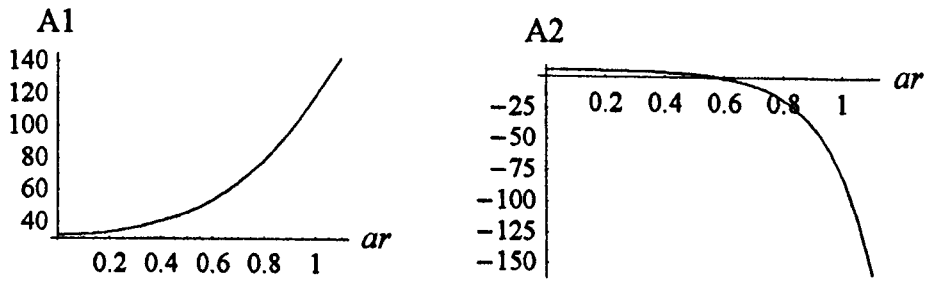

Figure 4.1 The algebraic invariants with $a = 1$.

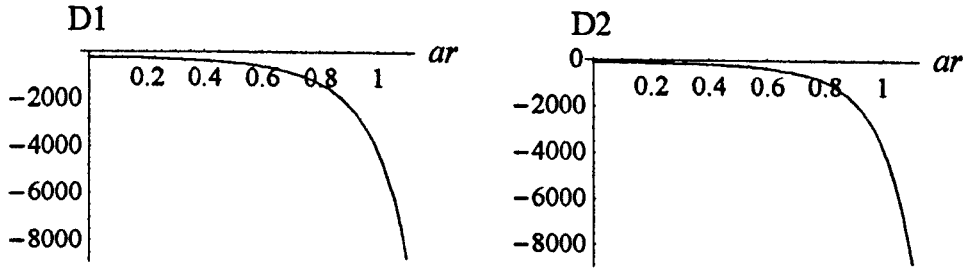

Figure 4.2 The differential invariants with $a = 1$.

$R_{ijkl}R^{ijkl}$ is positive in the plotted range and increasing through $ar = 1$, whereas $C_{ijkl}C^{ijkl}$ has a maximum value of $16a^4/3$ at $r = 0$ and is strictly decreasing,

reaching zero at $ar = 1/\sqrt{3}$ before going negative. The differential invariants are strictly decreasing and always negative.

None of the above invariants shows any remarkable behaviour at $ar = 1$, however, we end this section by turning to a scheme which brings the Newtonian concept of forces into general relativity and which does pick out $ar = 1$ and $ar = 1/\sqrt{3}$ as being special.

In recent years, Abramowicz and co-workers [35]-[37] have developed a covariant definition of the inertial forces in general relativity. The gravitational, centrifugal, Coriolis and Euler accelerations are defined in the co-moving frame of a test particle which may or may not be in geodesic motion. Fundamental to the scheme is the choice of the reference frame in which the test particle's velocity in space is measured. In axially symmetric spacetimes, this reference frame corresponds to the locally non-rotating frame described above and it makes sense to consider test particles in circular orbits of constant angular velocity around the axis of symmetry.

Interestingly, $r = \left(a\sqrt{3}\right)^{-1}$, (where $C_{ijkl}C^{ijkl} = 0$), turns out to be the radial coordinate of the orbit of zero centrifugal acceleration (regardless of test particle speed) obtained by using the analysis of Abramowicz et al. (In static spacetimes, this orbit coincides with a circular null geodesic). Using the same analysis, and considering the cylinder's constituent dust particles as test particles, the gravitational, Coriolis and centrifugal accelerations on the dust particles are finite for $ar < 1$ but become infinite at $ar = 1$. For the van Stockum interior,

$$\text{gravitational acceleration} = \frac{a^2 r}{1 - a^2 r^2}, \tag{7}$$

$$\text{Coriolis acceleration} = \frac{-2a^4 r^3}{(1 - a^2 r^2)^2}, \tag{8}$$

$$\text{centrifugal acceleration} = \frac{a^2 r(3a^2 r^2 - 1)}{(1 - a^2 r^2)^2}. \tag{9}$$

Since the cylinder's dust particles are moving in geodesic orbits, the sum of the three accelerations is zero. More details of this scheme are given in Appendix 3.

To summarise, there seems to be no need to restrict the range of the parameter a, but there are several reasons to restrict the product ar in the dust cylinder to $ar < 1$. This is

equivalent, in the global solution, to requiring $aR < 1$. Bonnor [5] showed that aR is related, rather surprisingly, more to the mass per unit length of the dust cylinder than to its angular momentum. With the simplifying assumption $a^2 R^2 << 1$, he found the following expressions for the dust cylinder,

$$\begin{aligned} \text{mass per unit length} &= \frac{1}{2} a^2 R^2, \\ \text{angular momentum} &= \frac{1}{4} a^3 R^4. \end{aligned} \tag{10}$$

Thus two cylinders with the same mass per unit length can be rotating at quite different angular velocities. A particular value of a sets both the angular velocity of a dust cylinder and its central density (equations (4) and (3) above).

4.2 The physics of the dust cylinder

To give an impression of the physics of the dust cylinder, van Stockum calculated that if the cylinder's density on the axis is the same as that of water, the period of rotation is about 2 hours 42 minutes. Suppose $aR = 1/4$, then for this density, the radius of the cylinder is about 165 times the equatorial radius of the sun. If $aR = 1/2$, the radius is 320 times that of the sun and if $aR = 3/4$, the radius is 455 times that of the sun. For comparison, white dwarf star density would require $a \approx 2\times10^{-9}$ and such a cylinder, with $aR = 1/2$, would have a radius of about one third that of the sun and a period of about 10 seconds.

Calling the density on the axis ρ_0 and the density at the surface ρ_R, then the density at the surface, using equation (3), is

$$\rho_R = \rho_0 \exp(a^2 R^2), \tag{11}$$

and is thus always comparable to ρ_0 within a small factor. The central density of the dust is the same as that of water when $a \approx 2\times10^{-12}$. If the radius of the cylinder is sufficiently large, even the highest mass, case III, cylinder can have this central density. However, there are obvious relativistic effects on the radius, and especially the circumference, of

such a cylinder.

The radius is given by

$$\int_0^R \sqrt{g_{22}}\, dr = \frac{\sqrt{\frac{\pi}{2}}\,\mathrm{erf}\left(\frac{aR}{\sqrt{2}}\right)}{a}, \tag{12}$$

and a plot of radius against R is shown in Figure 4.3.

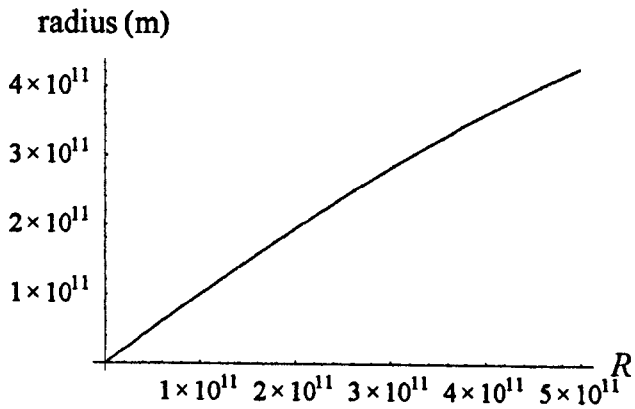

Figure 4.3 Variation of radius with R for $a = 2 \times 10^{-12}$.

The circumference is given by

$$\int_0^{2\pi} \sqrt{g_{33}}\, d\phi = 2\pi R\sqrt{1 - a^2 R^2}\,. \tag{13}$$

For a given value of a, the circumference increases with R until it reaches a maximum value of πa^{-1} when $R = \left(a\sqrt{2}\right)^{-1}$, Figure 4.4 showing an example. Thereafter, the circumference decreases with increasing R, tending to zero as $aR \to 1$. However, note that from equation (3), the proper density of the dust remains finite as $aR \to 1$.

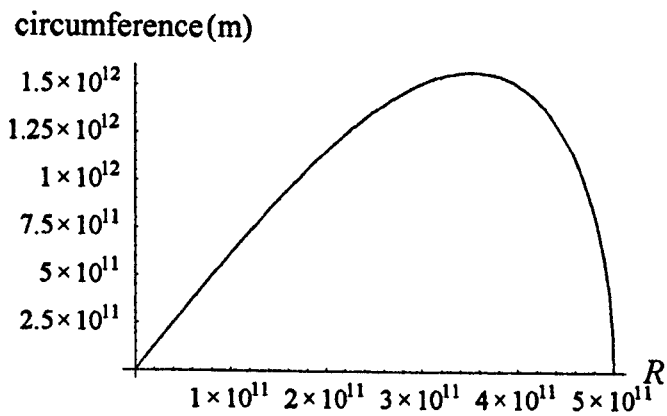

Figure 4.4 Variation of circumference with R for $a = 2 \times 10^{-12}$.

The ratio of circumference to diameter of the cylinder for $0 \leq aR \leq 1$ is plotted in Figure 4.5 and clearly shows the increasing departure from Euclidean conditions as aR increases.

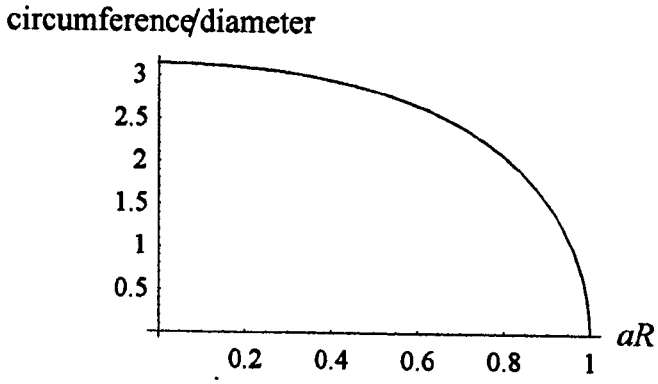

Figure 4.5 The ratio of circumference to diameter for $0 \leq aR \leq 1$.

In light of the infinite Newtonian accelerations when $aR = 1$, and observations of the circumference as $aR \to 1$, it makes physical sense to consider van Stockum spacetime only when $aR < 1$.

4.3 Geodesics within the dust cylinder

4.3.1 Circular geodesics

Circular geodesics are defined as geodesics with z = constant and r = constant, so that $\dot{z} = \dot{r} = \ddot{z} = \ddot{r} = 0$, where the superior dot indicates differentiation with respect to the affine parameter. They are analysed here both for intrinsic interest and for their relevance to the clock effect of Chapter 7. When $\dot{r} = \dot{z} = 0$, the geodesic equations from Section 2.1 become

$$\ddot{z} = 0, \quad \ddot{r} = \frac{-\dot{t}^2 F' + \dot{\phi}^2 L' + 2\dot{t}\dot{\phi} M'}{2H}, \quad \ddot{\phi} = 0, \quad \ddot{t} = 0. \tag{14}$$

Putting $\ddot{r} = 0$, solving for $\dot{\phi}$ and dividing through by $\dot{t}$ gives the conditions for circular geodesics, whether null, time-like or space-like:

$$\frac{d\phi}{dt} = \frac{-M' \pm \sqrt{F'L' + M'^2}}{L'}. \tag{15}$$

There are solutions for geodesics at $r = r_0$ provided that $F'(r_0)\,L'(r_0) + [M'(r_0)]^2 \geq 0$. Substituting the derivatives of the metric functions

$$M' = 2a\,r, \quad L' = 2r(1 - 2a^2 r^2), \quad F' = 0, \tag{16}$$

gives $F'\,L' + M'^2 = 4\,a^2 r^2$. Thus there are circular geodesics at all r and (15) becomes

$$\begin{aligned} \frac{d\phi}{dt} &= 0 \text{ (using the plus sign)}, \\ \frac{d\phi}{dt} &= \frac{2a}{2a^2 r^2 - 1} \quad \text{(using the minus sign)}. \end{aligned} \tag{17}$$

Since the dust particles are at rest in the coordinate system, the first solution describes their geodesics. The second solution shows circular geodesics of some kind. To find the nature of these, put $dr = dz = 0$ in the metric equation and divide through by dt^2 to get

$$\left(\frac{ds}{dt}\right)^2 = L(r)\left(\frac{d\phi}{dt}\right)^2 + 2\,M(r)\,\frac{d\phi}{dt} - F(r). \tag{18}$$

Then $(ds/dt)^2 < 0 \Rightarrow$ time-like geodesics, $(ds/dt)^2 = 0 \Rightarrow$ null geodesics and $(ds/dt)^2 > 0 \Rightarrow$ space-like geodesics. Substituting $d\phi/dt$ from (17) into (18) gives

$$\left(\frac{ds}{dt}\right)^2 = -1, \left(\frac{ds}{dt}\right)^2 = \frac{4a^2 r^2 - 1}{(1 - 2a^2 r^2)^2}. \tag{19}$$

The first equation confirms that the dust particles follow timelike geodesics. In the second equation, since $(ds/dt)^2 = 0$ where $r = (2a)^{-1}$, there is a circular null geodesic at $r = (2a)^{-1}$ only. Clearly, there are circular time-like geodesics where $r < (2a)^{-1}$, but when $r > (2a)^{-1}$ then $(ds/dt)^2 > 0$ and the circular geodesics are space-like.

4.3.2 Radial ranges of null geodesics

Lanczos found that null geodesics passing through the axis of rotation could not exceed a radial coordinate value of $r = 1$. In the van Stockum solution, this corresponds to light escaping the surface of any source cylinder with $aR < 1$, but Lanczos's solution had no vacuum exterior, being a cosmological solution with dust out to spatial infinity.

Opher, Santos and Wang [2] recently found that certain geodesics cannot reach the surface of the dust cylinder, depending on the geodesic parameters. Since this amounted to a degree of radial confinement, they speculated on the applicability of the van Stockum solution to the modelling of extragalactic jets. To quote their paper, "Ubiquitous extragalactic jets appear in active galaxies and various models have been suggested for their origin." Figure 4.6 shows a Hubble Space Telescope image [46] of the giant elliptical galaxy M87, with the jet emanating from its nucleus.

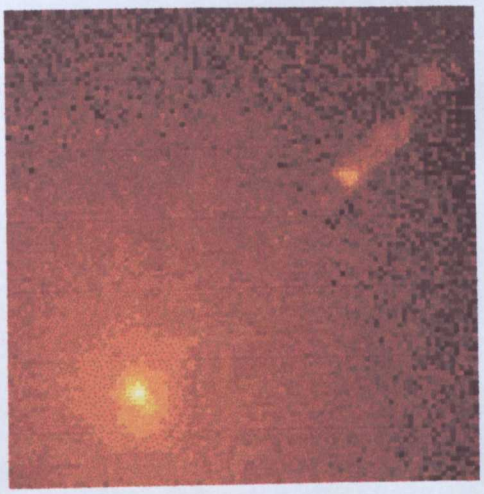

Figure 4.6 Galaxy M87 in the Virgo cluster of galaxies.

By using the rotating dust cylinder as a simple model for a rotating galaxy, perhaps radial confinement of geodesics can be invoked as an explanation for the formation of jets.

In this section, we shall be investigating which null geodesics can escape from a dust cylinder with $aR < 1$ and the highest value of r coordinate attainable by those that are confined. This will clarify the work on null geodesics by Opher, Santos and Wang and enable some of their results for light to be quantified more simply.

We saw from Section 2.2 that in terms of the metric coefficients and the constants of the motion, the general form of the line element for van Stockum null geodesics, whether in the interior or the exterior, may be written

$$H(\dot{z}^2 + \dot{r}^2) = E^2 L + 2EMP_\phi - FP_\phi^2 \tag{20}$$

$$\text{where } P_\phi = M\dot{t} + L\dot{\phi} \text{ and } E = F\dot{t} - M\dot{\phi}, \tag{21}$$

and consequently, everywhere along a given null geodesic,

$$2EMP_\phi + E^2L - FP_\phi^2 \geq 0. \tag{22}$$

In this, and in subsequent chapters, we shall examine null geodesics of given P_ϕ/E, and find what values of r satisfy equation (22). This will determine the allowed radial disposition of the geodesics.

The metric functions for the interior in co-rotating coordinates are

$$H = \exp(-a^2r^2),\ L = r^2(1-a^2r^2),\ M = ar^2,\ F = 1, \tag{23}$$

so that (22) becomes

$$2EMP_\phi + E^2L - FP_\phi^2 = r^2 - \left(\frac{P_\phi}{E} - ar^2\right)^2 \geq 0, \tag{24}$$

and everywhere along a null geodesic of given P_ϕ/E, the r coordinate must satisfy

$$r(ar-1) \leq \frac{P_\phi}{E} \leq r(ar+1). \tag{25}$$

Since $0 \leq ar < 1$ then $r(ar-1) \leq 0$ and $r(ar+1) \geq 0$. Several conclusions about null geodesics may now be drawn from equation (25):

(i) If $P_\phi/E = 0$, conditions (25) are satisfied for all r so a null geodesic with $P_\phi = 0$ is allowed anywhere within the dust cylinder.

(ii) A null geodesic at $r = 0$ must have $P_\phi = 0$.

(iii) Null geodesics with $P_\phi/E < 0$ must have $r < a^{-1}$, and thus may be confined within the cylinder, depending on the value of a. The highest and lowest r coordinates attainable by these geodesics are given by solving $P_\phi/E = r(ar-1)$:

$$r_{\text{lowest}} = \frac{1-\sqrt{4aP_\phi/E+1}}{2a},\quad r_{\text{highest}} = \frac{1+\sqrt{4aP_\phi/E+1}}{2a}. \tag{26}$$

(iv) Null geodesics with $P_\phi/E > 0$ may reach the surface of any cylinder. The lowest r coordinate attainable is given by solving $P_\phi/E = r(ar+1)$ and taking the positive result:

$$r_{\text{lowest}} = \frac{\sqrt{4aP_\phi/E+1}-1}{2a}. \tag{27}$$

Figure 4.7 illustrates these points for a cylinder with $a = 1$. The minimum value of P_ϕ/E, from the equation $P_\phi/E = r\,(ar-1)$, occurs at $r = (2a)^{-1}$ and the dashed vertical line passes through $r = 1/2$.

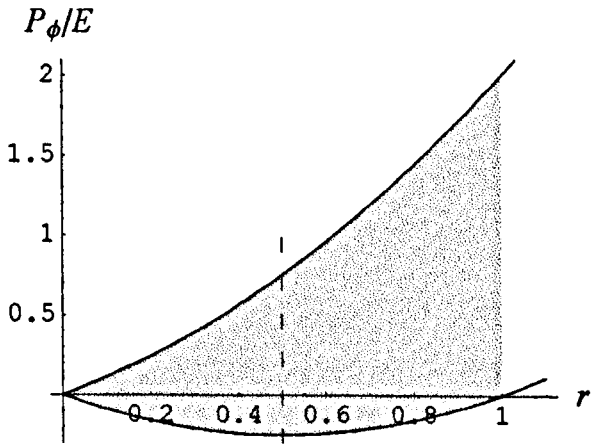

Figure 4.7 The shaded region between $P_\phi/E = r\,(ar+1)$ and $P_\phi/E = r\,(ar-1)$ shows the allowed radial distribution for null geodesics with a given value of P_ϕ/E.

A convenient way of analysing the results is to consider dust cylinders which give rise to the three different cases of exterior, again putting $a = 1$ without loss of generality. A case I interior thereby has $0 < R < 1/2$, case II has $R = 1/2$ and case III has $1/2 < R < 1$. Thus the radial ranges of null geodesics are as follows :

- Case I interior : Since $R < 1/2$, the case I cylinder lies to the left of the dashed line so no null geodesics are confined to the cylinder.
- Case II interior : Since $R = 1/2$, the case II cylinder extends to the dashed line. No null geodesics are confined except the circular one at the surface.
- Case III interior : Since $1/2 < R < 1$, the case III cylinder extends to the right of the dashed line at $r = 1/2$ and geodesics with $P_\phi/E < 0$ may be confined. Specifically, since the lower bound of the shaded area is defined by $P_\phi/E = r(ar-1)$, it is only null geodesics with $P_\phi/E < R\,(aR-1)$ that are confined within the cylinder.

Results (i) to (iv) above reproduce the results for null geodesics found, in a somewhat similar way, by Opher et al [2]. Since the geodesic plotting routines use initial conditions, it is useful to repeat some of the above calculations for confined null geodesics in terms of initial positions and directions.

From Section 2.4 we may put, (setting the scale factor $x = 1$),

$$\dot{\phi} = \frac{(\sin\alpha\cos\beta - \frac{M}{r})}{\sqrt{L}} \text{ and } \dot{t} = \frac{\sqrt{L}}{r}, \tag{28}$$

then using (21) and (23) gives the constants of the motion in terms of initial conditions,

$$P_\phi = \sqrt{1 - a^2 r_0^2}\, r_0 \sin\alpha_0 \cos\beta_0, \quad E = \frac{(1 - a\, r_0 \sin\alpha_0 \cos\beta_0)}{\sqrt{1 - a^2 r_0^2}}. \tag{29}$$

Subsituting these versions of P_ϕ and E into the second of equations (26), for example, gives the highest r coordinate attainable, r_{peak}, for any null geodesic that is confined within the dust cylinder,

$$r_{peak} = \frac{1}{2a} + \frac{\sqrt{(1 - a r_0 \sin\alpha_0 \cos\beta_0)\,(1 - (4a^2 r_0^2 - 3)\, a r_0 \sin\alpha_0 \cos\beta_0)}}{2a(1 - a r_0 \sin\alpha_0 \cos\beta_0)}. \tag{30}$$

From conclusion (iii) above, it is null geodesics with $P_\phi/E < 0$ that may be confined within the dust cylinder and using equations (29),

$$P_\phi / E = \frac{r_0 (a^2 r_0^2 - 1) \sin\alpha_0 \cos\beta_0}{a r_0 \sin\alpha_0 \cos\beta_0 - 1}. \tag{31}$$

Since $a r_0 < 1$, $-\pi \le \alpha_0 \le \pi$ and $-\pi/2 \le \beta_0 \le \pi/2$, then $P_\phi/E < 0 \Rightarrow -\pi \le \alpha_0 < 0$. Thus it is case III geodesics with $-\pi \le \alpha_0 < 0$ that may be confined, irrespective of the value of r_0. (Figure 2.1 showed the definitions of the angle α and β).

Note that, since $\cos\beta_0 \ge 0$, only the magnitude of P_ϕ/E is affected by the value of $\dot{z}_0$, not the sign. Thus whether or not a geodesic is confined is not influenced by the value of $\dot{z}_0$, although radial range is affected.

4.4 Null geodesics passing out of the dust cylinder

The final part of this chapter will serve to illustrate the plotting of geodesics from the numerical solution of the geodesic equations in two different coordinate frames, the co-rotating frame and the astronomical rest frame. The exterior metric in the astronomical rest-frame was described in Section 2.3, and the transformation shown there may also be used to get the corresponding metric for the interior,

$$ds^2 = \exp(-a^2 r^2)(dz^2 + dr^2) +$$

$$r^2(1 - a^2 r^2)\,d\phi^2 + \frac{\exp(-3\epsilon)\, r^2 (\exp(2\epsilon)(r^2 - 2R^2) - R^2)}{[1 + \exp(2\epsilon)]\, R^3}\, d\phi dt - \tag{32}$$

$$\frac{\exp(-6\epsilon)[1 + \exp(2\epsilon)]^2 (a^2 [r^2 + 2\exp(2\epsilon) R^2] - 1) r^2 + R^2}{R^2}\, dt^2,$$

where $\epsilon = \tanh^{-1}\left(\sqrt{1 - 4a^2 R^2}\right)$.

Figure 4.8 shows null geodesics passing from the dust cylinder out into the vacuum exterior. For comparison, the same thirty-two null geodesics are plotted in a hypersurface of z = constant in the two coordinate frames. They originate just below the surface of a dust cylinder with $a = 0.49$ and $R = 1$ so that the solution is at the upper end of the case I mass range and no geodesics are confined to the interior. The dotted geodesics have initial angles $\alpha_0 = 0$, $\alpha_0 = \pm\pi/2$ and $\alpha_0 = \pi$. In solving the geodesic equations, the final conditions of the geodesics as they reach $r = R$ become the initial conditions as the geodesics enter the vacuum region.

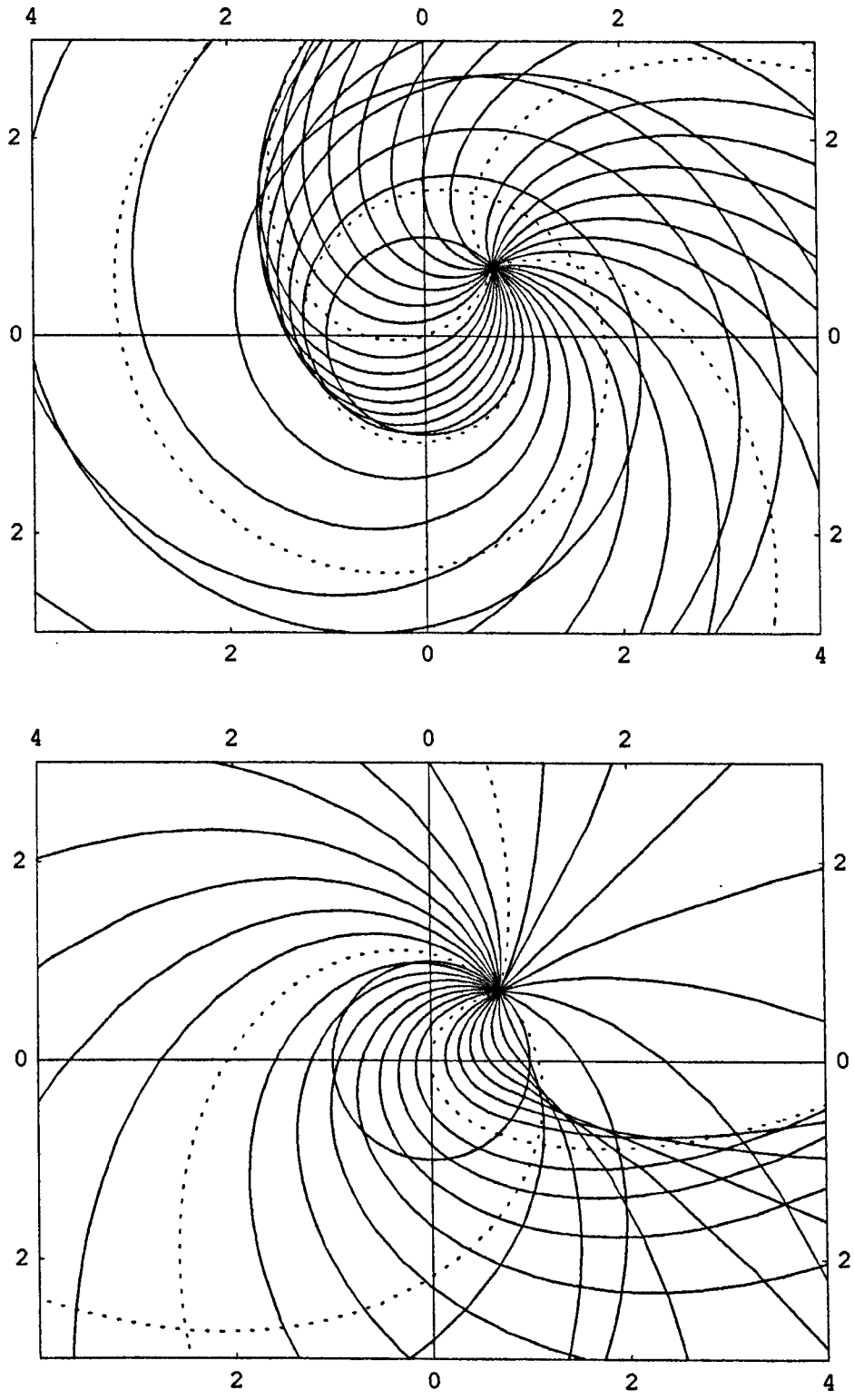

Figure 4.8 Upper: null geodesics in the co-rotating frame.

Lower: the same geodesics in the astronomical rest-frame.

$a = 0.49, R = 1.$

~ Chapter 5 ~

The van Stockum vacuum exterior

In Chapter 1, the metric for the van Stockum exterior was given in the form

$$ds^2 = H(r)\,(dz^2 + dr^2) + L(r)\,d\phi^2 + 2\,M(r)\,d\phi dt - F(r)\,dt^2, \tag{1}$$

where $-\infty < z < \infty$, $0 \le r < \infty$, $0 \le \phi \le 2\pi$ and $-\infty < t < \infty$, with

$$\begin{aligned} H(r) &= \exp\left(n^2 - \frac{1}{4}\right)\left(\frac{r}{R}\right)^{\frac{1}{2}(4n^2-1)}, \\ L(r) &= \frac{(4n^2+3)\,r\,R\cosh A}{4} + \frac{(12n^2+1)\,r\,R\sinh A}{8n}, \\ M(r) &= \frac{\sqrt{1-4n^2}\,r\cosh A}{2} + \frac{\sqrt{1-4n^2}\,r\sinh A}{4n}, \\ F(r) &= \frac{r\sinh A}{2nR} - \frac{r\cosh A}{R}, \end{aligned} \tag{2}$$

where

$$A = 2n\log\left(\frac{r}{R}\right), \quad n^2 = \frac{1}{4} - a^2R^2. \tag{3}$$

In this form, case I has $1/4 > n^2 > 0$ and case III has $-3/4 < n^2 < 0$. Although n is imaginary in case III, the metric functions are always real. Case II metric functions may be obtained from either case I or case III by taking the limit as $n \to 0$. In the following sections, it is more convenient to write the metric in the form given by van Stockum and to analyse the three cases of the vacuum exterior separately.

In 1962, Ehlers and Kundt [11] reported that the dust cylinder can be regularly joined to the Levi-Civita static vacuum metric. In 1971, Frehland [12] stated that the exterior metric (in all three cases) is static. It was remarked by Tipler [9] that the case I field is static, in that there is a coordinate transformation which leaves the metric in a diagonal form, but that a periodic time coordinate is required for the transformation. Tipler also

gave a proof that the van Stockum exterior is the only possible exterior for the infinite rotating dust cylinder.

More recently, Bonnor [5] proved Ehlers, Kundt and Frehland wrong by showing that only the case I metric had a hypersurface orthogonal timelike Killing vector, although stressing the requirement for a periodic time coordinate in the diagonalised metric. He thus described case I spacetime as 'locally static'. Returning to the problem in 1995 [13], he found that the Weyl tensor for case I can be classified as 'electric', whereas rotation is expected to generate 'magnetic' spacetimes. However, the correspondence between this classification scheme and physical characteristics is uncertain, Bonnor himself pointing out that there are spacetimes with vorticity whose Weyl tensors are not magnetic [14], [15]. Appendix A2 gives more details of the electric and magnetic Weyl tensors.

In view of Tipler's demonstration of the uniqueness of the van Stockum exterior, there is no chance of finding a case I exterior metric that cannot be diagonalised. However, the periodic time coordinate required for diagonalisation of the case I metric implies that the more physically reasonable interpretation is that the van Stockum solution, in all three cases, indeed represents an infinite rotating cylinder and its associated vacuum exterior.

5.1 Geodesics in the case I exterior, $0 < aR < 1/2$

The exterior metric has two parameters a and R. The metric functions for $0 < aR < 1/2$, as given by van Stockum, in a reference frame co-rotating with the dust, are

$$H = \exp(-a^2 R^2)\left(\frac{r}{R}\right)^{-2a^2R^2}, \quad L = \frac{rR\sinh(3\epsilon+\theta)}{2\sinh(2\epsilon)\cosh\epsilon},$$
$$M = \frac{r\sinh(\epsilon+\theta)}{\sinh(2\epsilon)}, \quad F = \frac{r\sinh(\epsilon-\theta)}{R\sinh\epsilon}, \tag{4}$$

with $\theta = \tanh\epsilon \log(r/R)$, $\tanh\epsilon = (1-4a^2R^2)^{1/2}$, $0 < aR < 1/2$.

The metric functions H, L and M are positive for all r but F is negative where $\theta > \epsilon$ so the t coordinate is spacelike in the region where $r > R\exp(\epsilon\coth\epsilon)$. However, van Stockum found the 'astronomical rest frame' in which t remains timelike everywhere, as described in Section 2.3.1.

5.1.1 Circular geodesics in case I

Following the method of Section 4.3.1, for the general form of the metric (1), provided that $F' L' + M'^2 \geq 0$, the circular geodesics are given by

$$\frac{d\phi}{dt} = \frac{-M' \pm \sqrt{F' L' + M'^2}}{L'}, \tag{5}$$

where the dashes indicate differentiation with respect to r, and for circular geodesics,

$$\left(\frac{ds}{dt}\right)^2 = L\left(\frac{d\phi}{dt}\right)^2 + 2M\frac{d\phi}{dt} - F. \tag{6}$$

Substituting the differentials of the metric functions (4) into (5) gives the angular velocities of circular geodesics,

$$\begin{aligned}\left(\frac{d\phi}{dt}\right)_1 &= -\frac{2\cosh\epsilon \sinh(\frac{\theta}{2})}{R\sinh(2\epsilon + \frac{\theta}{2})},\\ \left(\frac{d\phi}{dt}\right)_2 &= -\frac{2\cosh\epsilon \cosh(\frac{\theta}{2})}{R\cosh(2\epsilon + \frac{\theta}{2})},\end{aligned} \tag{7}$$

where $\theta = \tanh\epsilon \log(r/R)$ and $\tanh\epsilon = (1 - 4a^2R^2)^{1/2}$. Substituting equations (7) and the metric functions (4) into equation (6) gives

$$\begin{aligned}\left(\frac{ds}{dt}\right)_1^2 &= -\frac{r\sinh^2(2\epsilon)}{R\sinh^2(2\epsilon + \frac{\theta}{2})},\\ \left(\frac{ds}{dt}\right)_2^2 &= -\frac{r\sinh^2(2\epsilon)}{R\cosh^2(2\epsilon + \frac{\theta}{2})}.\end{aligned} \tag{8}$$

Since both $(ds/dt)^2$ are always less than zero, there must be circular timelike geodesics in both directions at all distances from the cylinder in case I. Consequently, there are no circular null geodesics in case I. The angular velocities for the timelike geodesics are given by equations (7). Note that in some coordinate frames, the circular geodesics could both appear to have the same direction but the term 'both directions' is used here and elsewhere for brevity.

5.1.2 Ranges of null geodesics in case I

Consider null geodesics going outwards from the cylinder (ie. from $r_0 = R$), denoting initial values by a subscript R, putting $L_R \equiv L(R)$ etc. Then using equations (13), from Section 2.2, for P_ϕ and E with equations (38), from Section 2.4.1, for $\dot{\phi}$ and $\dot{t}$ with $x = 1$, gives P_ϕ and E in terms of the initial conditions,

$$P_\phi = \sqrt{L_R}\,\sin\alpha_R \cos\beta_R, \quad E = \frac{(R - M_R \sin\alpha_R \cos\beta_R)}{\sqrt{L_R}}, \tag{9}$$

where $-\pi/2 \le \alpha_R \le \pi/2$ and $-\pi/2 \le \beta_R \le \pi/2$. (Section 2.4.1 has the definitions of the angles α and β).

From Section 2.2, everywhere on a null geodesic, we have

$$2EMP_\phi + E^2 L - F P_\phi^2 \ge 0, \tag{10}$$

the equality condition requiring $\dot{z} = \dot{r} = 0$. Using (4) and (9), this becomes

$$\begin{aligned} r R\,\mathrm{csch}(3\epsilon)\,\{&\cos\beta_R \sin\alpha_R\,[2\sinh\theta - \cos\beta_R \sin\alpha_R \sinh(3\epsilon - \theta)] + \\ &\sinh(3\epsilon + \theta)\} \ge 0. \end{aligned} \tag{11}$$

Expression (11) may be more easily interpreted when the hyperbolic terms are written in exponential form, i.e. by putting $\sinh\theta \to \frac{1}{2}[\exp\theta - \exp(-\theta)]$ etc. It then becomes,

$$\frac{r R\,\{\exp(2\theta)\,[\exp(3\epsilon) + \sin\alpha_R \cos\beta_R]^2 - [1 + \exp(3\epsilon)\sin\alpha_R \cos\beta_R]^2\}}{\exp\theta\,[\exp(6\epsilon) - 1]} \ge 0. \tag{12}$$

The equality condition in (12) requires $\dot{z}_R = \dot{r}_R = 0 \Rightarrow \alpha_R = \pm\,\pi/2$ and $\beta_R = 0$, but the equality is then obtained only when $\theta = 0 \Rightarrow r = R$.

Since, provided $\alpha_R \neq \pm\,\pi/2$ and $\beta_R \neq 0$,

$$\begin{aligned} &(\exp(3\epsilon) + \sin\alpha_R \cos\beta_R)^2 - (1 + \exp(3\epsilon)\sin\alpha_R \cos\beta_R)^2 \; = \\ &\qquad (\exp(6\epsilon) - 1)(1 - \sin^2\alpha_R \cos^2\beta_R) > 0, \end{aligned} \tag{13}$$

then the left hand side of (12) is greater than zero for all r and any α_R, β_R except when $r = R$, $\alpha_R = \pm\,\pi/2$ and $\beta_R = 0$, as we have just seen. Therefore for all $r > R$, the left hand side of (12) is greater than zero for any α_R and β_R. Thus all null geodesics leaving the cylinder's surface may reach any r coordinate and hence extend outwards indefinitely. Checking with the geodesic equations shows that when $\alpha_R = \pm\,\pi/2$ and $\beta_R = 0$ then $\ddot{r}_R >$

0, showing that these geodesics go outwards from the cylinder's surface. Thus there is no confinement of case I null geodesics.

Figure 5.1 shows a range of null geodesics leaving the cylinder, in a plane of z = constant, with $-\pi/2 \leq \alpha_R \leq \pi/2$. The dotted geodesics have $\alpha_R = -\pi/2$, $\alpha_R = 0$ and $\alpha_R = \pi/2$. All were plotted over the same proper time.

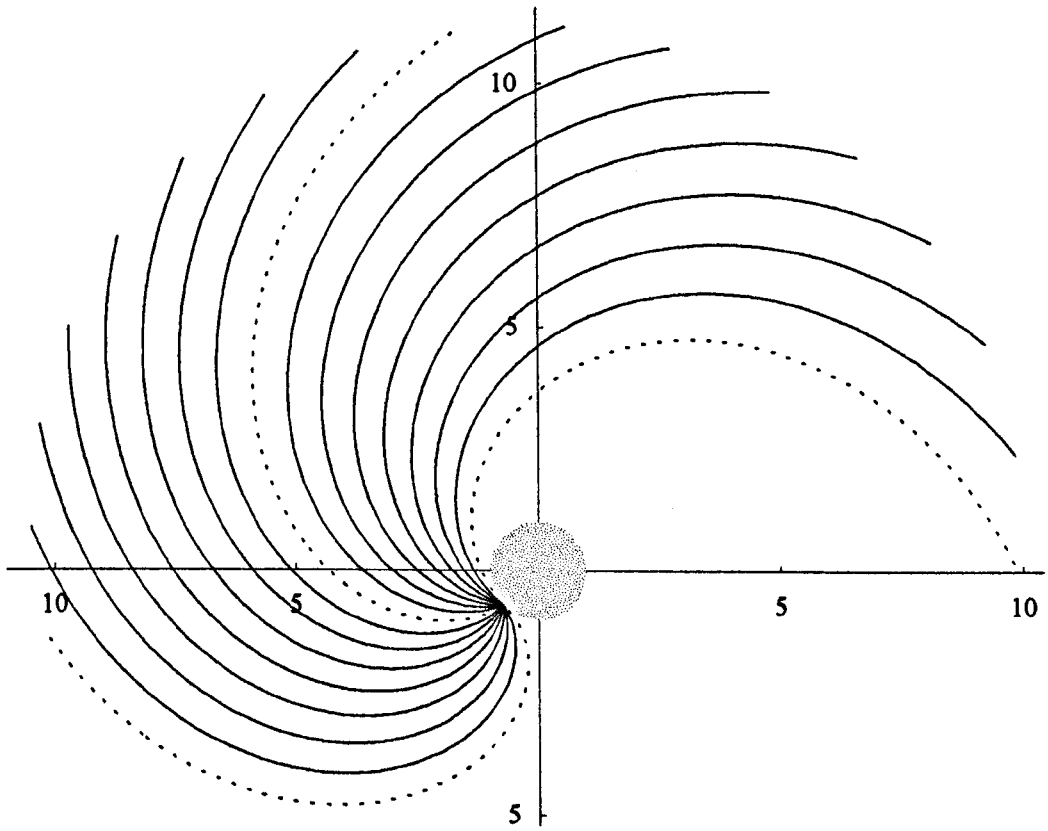

Figure 5.1 Null geodesics leaving the dust cylinder with $\dot{z} = 0$.

$a = 1/4, R = 1.$

5.1.3 Summary of case I geodesics

(1) There are circular, timelike geodesics at all r and in both directions.

(2) There are no circular null geodesics.

(3) All null geodesics leaving the dust cylinder may extend to radial infinity.

5.2 Geodesics in the case II exterior, $aR = 1/2$

The case II metric may be found from equations (4) in the limit as $aR \to 1/2$. The metric functions are

$$H = \exp(-\tfrac{1}{4})\sqrt{\frac{R}{r}}, \quad L = \tfrac{1}{4} r R\left(\log\left(\frac{r}{R}\right) + 3\right),$$
$$M = \tfrac{1}{2} r\left(\log\left(\frac{r}{R}\right) + 1\right), \quad F = \frac{r(1 - \log(\frac{r}{R}))}{R}. \tag{14}$$

As in case I, the metric functions H, L and M are positive for all r, but where $r > eR$, F is negative and the t coordinate is spacelike.

5.2.1 Circular geodesics in case II

Proceeding as in Section 5.1.1, the angular velocities of the circular geodesics are

$$\left(\frac{d\phi}{dt}\right)_1 = -\frac{2\log(\frac{r}{R})}{R(\log(\frac{r}{R}) + 4)},$$
$$\left(\frac{d\phi}{dt}\right)_2 = -\frac{2}{R}. \tag{15}$$

The associated expressions using the metric (14) are

$$\left(\frac{ds}{dt}\right)_1^2 = -\frac{16r}{R(4 + \mathrm{Log}[\frac{r}{R}])^2}, \quad \left(\frac{ds}{dt}\right)_2^2 = 0. \tag{16}$$

Since $(ds/dt)_1^2 < 0$ at all r, there are circular timelike geodesics with angular velocity $(d\phi/dt)_1$ at all distances from the cylinder. Since $(ds/dt)_2^2 = 0$, there are null geodesics with the (constant) angular velocity of $(d\phi/dt)_2 = -2/R$ at all r.

5.2.2 Ranges of null geodesics in case II

With the case II metric functions (14), expression (10) becomes

$$\frac{rR(1 + \sin\alpha_R \cos\beta_R)(\log(\frac{r}{R})(1 + \sin\alpha_R \cos\beta_R) + 3(1 - \sin\alpha_R \cos\beta_R))}{3} \geq 0. \tag{17}$$

When $\alpha_R = -\pi/2$ and $\beta_R = 0$, the equality condition in (17) prevails for all r. When $\alpha_R = \pi/2$ and $\beta_R = 0$, the equality condition holds only at $r = R$. Otherwise, the left hand side of (17) is greater than zero for all r. When $\alpha_R = -\pi/2$ and $\beta_R = 0$, $\ddot{r}_R = 0$ and the geodesic describes a circle at the cylinder's periphery. This coincides with the interior circular null geodesic at $r = (2a)^{-1}$, described in Section 4.3.1. When $\alpha_R = \pi/2$ and $\beta_R = 0$, $\ddot{r}_R > 0$ and the geodesic goes outwards. Thus all null geodesics, except the circular one at $r = R$, can extend outwards indefinitely.

5.2.3 Summary of case II geodesics

(1) There are circular timelike geodesics at all r, but in one direction only.

(2) There are circular null geodesics at all r, and they have angular velocity $-2/R$.

(3) All null geodesics leaving the dust cylinder may extend outwards indefinitely.

5.3 Geodesics in the case III exterior, $1/2 < aR < 1$

The metric functions for case III, as given by van Stockum, are

$$H = \exp(-a^2 R^2)\left(\frac{r}{R}\right)^{-2a^2R^2}, \quad L = \frac{rR\sin(3\epsilon+\theta)}{2\sin(2\epsilon)\cos\epsilon},$$
$$M = \frac{r\sin(\epsilon+\theta)}{\sin(2\epsilon)}, \quad F = \frac{r\sin(\epsilon-\theta)}{R\sin\epsilon}, \tag{18}$$

with $\theta = \tan\epsilon \log(r/R)$, $\tan\epsilon = (4a^2R^2 - 1)^{1/2}$, $1/2 < aR < 1$. Since L, M and F are now composed of trigonometric functions, they change sign periodically. Although at the cylinder's surface and nearby, ϕ is spacelike and t is timelike, as r increases, the ϕ and t coordinates occur in all spacelike/timelike combinations. Van Stockum thought that the signature of the metric changes when L changes sign, but this is not the case, as was shown in Section 2.5.

5.3.1 Circular geodesics in case III

Proceeding as in Section 5.1.1, the angular velocities of the circular geodesics are

$$\left(\frac{d\phi}{dt}\right)_1 = \frac{2a}{(2a^2R^2 - \cot(\theta/2)\tan\epsilon - 1)},$$
$$\left(\frac{d\phi}{dt}\right)_2 = \frac{2a}{(2a^2R^2 + \tan(\theta/2)\tan\epsilon - 1)}. \qquad (19)$$

We also have the associated expressions,

$$\left(\frac{ds}{dt}\right)_1^2 = -\frac{r\sin^2(2\epsilon)}{R\sin^2(2\epsilon + \frac{\theta}{2})},$$
$$\left(\frac{ds}{dt}\right)_2^2 = \frac{r\sin^2(2\epsilon)}{R\cos^2(2\epsilon + \frac{\theta}{2})}. \qquad (20)$$

Examination of $(ds/dt)_1^2$ and $(ds/dt)_2^2$ reveals that the former is always less than zero and the latter is always greater than zero. Thus there are circular timelike geodesics with angular velocity $(d\phi/dt)_1$ at all distances from the cylinder, but the geodesics with angular velocity $(d\phi/dt)_2$ are spacelike. Since $(ds/dt)^2 \neq 0$, there are no circular null geodesics.

5.3.2 Ranges of case III null geodesics leaving the dust cylinder

Whereas case I and case II null geodesics may extend from the dust cylinder towards radial infinity, from plotting geodesics it seems that those leaving the cylinder in case III are radially confined. The radial range of geodesics appears to be greatest for geodesics with $\alpha_R = \pi/2$ and $\beta_R = 0$. The following analysis confirms these impressions and proves that all case III null geodesics are indeed radially confined. Calculations are far simpler when carried out in the orbiting coordinate frame described in Section 2.3.2. If we put $r_{orb} = R$, then $\chi = 1$ and the metric has its simplest form,

$$\hat{H}(r) = \exp(-a^2R^2)\left(\frac{r}{R}\right)^{-2a^2R^2}, \quad \hat{L}(r) = rR\sin\epsilon\sin(\epsilon - \theta),$$
$$\hat{M}(r) = r\cos(\epsilon - \theta), \quad \hat{F}(r) = \frac{r\sin(\epsilon - \theta)}{R\sin\epsilon}, \qquad (21)$$

with $\theta = \tan\epsilon\log(r/R)$, $\tan\epsilon = (4a^2R^2 - 1)^{1/2}$.

After substituting the metric functions (21) and division throughout by E^2, expression (10) becomes

$$\frac{r\left(2\frac{P_\phi}{E}R\cos(\epsilon-\theta)+\left(R^2\sin\epsilon-\left(\frac{P_\phi}{E}\right)^2\csc\epsilon\right)\sin(\epsilon-\theta)\right)}{R}\geq 0. \tag{22}$$

If null geodesics with a given value of P_ϕ/E are restricted to a particular region, then at the boundary of the region the equality condition must hold and solving for P_ϕ/E gives

$$\left(\frac{P_\phi}{E}\right)_1 = R\sin\epsilon\cot\left(\frac{\epsilon-\theta}{2}\right),\ \left(\frac{P_\phi}{E}\right)_2 = -R\sin\epsilon\tan\left(\frac{\epsilon-\theta}{2}\right). \tag{23}$$

Equations (9) show the general expressions for P_ϕ and E in terms of initial conditions when $r_0 = R$ and t is timelike. In the orbiting coordinate frame (21), the ratio P_ϕ/E in terms of initial conditions becomes

$$\frac{P_\phi}{E} = \frac{R\sin\alpha_R\cos\beta_R\sin^2\epsilon}{1-\sin\alpha_R\cos\beta_R\cos\epsilon}, \tag{24}$$

where $-\pi/2\leq\alpha_R\leq\pi/2$ and $-\pi/2\leq\beta_R\leq\pi/2$. Equating $(P_\phi/E)_1$ and $(P_\phi/E)_2$ in turn with P_ϕ/E and solving for θ gives the values, θ_1 and θ_2, at which the equality condition in (22) holds for null geodesics leaving the cylinder with any given α_R and β_R,

$$\begin{aligned}\theta_1 &= 2k\pi+\epsilon-2\cot^{-1}\left(\frac{\cos\beta_R\sin\alpha_R\sin\epsilon}{1-\cos\beta_R\sin\alpha_R\cos\epsilon}\right),\\ \theta_2 &= 2k\pi+\epsilon+2\tan^{-1}\left(\frac{\cos\beta_R\sin\alpha_R\sin\epsilon}{1-\cos\beta_R\sin\alpha_R\cos\epsilon}\right),\end{aligned} \tag{25}$$

where k is an integer.

Both θ_1 and θ_2 have maximum values where $\alpha_R = \pi/2$ and $\beta_R = 0$ and minimum values where $\alpha_R = -\pi/2$ and $\beta_R = 0$, as it is straightforward to show. Hence, substituting these values of α_R and β_R into (25),

$$(1+2k)\pi\leq\theta_1\leq 2k\pi,\ 2k\pi\leq\theta_2\leq(1+2k)\pi. \tag{26}$$

Clearly, there can be no such θ_1. By putting $\theta_2 = \tan\epsilon\log(r/R)$ in (26), we obtain

$$R\exp[2k\pi\cot\epsilon]\leq r\leq R\exp[(2k+1)\pi\cot\epsilon]. \tag{27}$$

Since $r\geq R$, the only physically relevant result is obtained by putting $k = 0$ to get

$$R\leq r\leq R\exp(\pi\cot\epsilon). \tag{28}$$

Therefore, although case I and case II geodesics leaving the dust cylinder are unconfined, all such case III null geodesics are confined within the region of space enclosed by a cylindrical surface with radial coordinate r_{max}, where

$$r_{max} = R\exp(\pi\cot\epsilon). \tag{29}$$

Conceivably, geodesics leaving the dust cylinder could be confined within a smaller range of r. However, at least the geodesic with $\alpha_R = \pi/2$ and $\beta_R = 0$ reaches r_{max}. Using the initial conditions, from Section 2.4.1, and the geodesic equations, from Section 2.2, the geodesic has $\dot{r}_R = 0$ and $\ddot{r}_R > 0$ and so must leave the cylinder's surface. From equations (25) - (28), it does not achieve $\dot{r} = 0$ again until it reaches r_{max}. At $r = r_{max}$, $\ddot{r} < 0$ and the geodesic turns inwards.

For null geodesics with $\dot{z}_R \neq 0 \Rightarrow \beta_R \neq 0$, the equality condition in (22) is never attained because $P_z = H\dot{z}$, so that $\dot{z}_R \neq 0 \Rightarrow \dot{z} \neq 0$ everywhere along the geodesic. Thus geodesics with $\dot{z}_R \neq 0$ are confined within a smaller region than those with $\dot{z}_R = 0$, since the boundary of the allowed region is never reached.

By solving $\theta_2 = \tan\epsilon \log(r/R)$ for r (with θ_2 from (25), putting $\beta_R = 0$ and $k = 0$), we obtain an expression which gives the highest r coordinate attainable, r_{peak}, by a null geodesic leaving the dust cylinder in any given direction in a hypersurface of z = constant,

$$r_{peak} = R\exp(\,[\epsilon - 2\cot^{-1}(\cot\epsilon - \csc\alpha_R\,\csc\epsilon)]\cot\epsilon). \tag{30}$$

A plot of r_{peak} is shown in Figure 5.2.

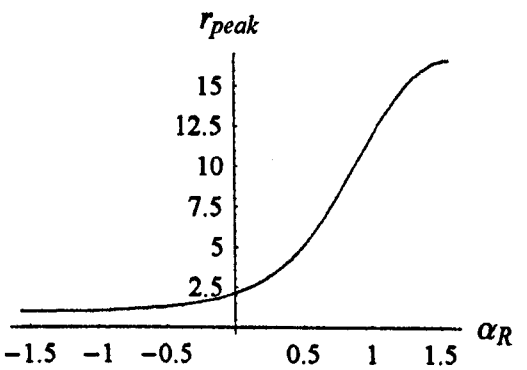

Figure 5.2 The plot of r_{peak} when $a = 3/4$, $R = 1$ and $-\pi/2 \leq \alpha_R \leq \pi/2$.

Figure 5.3 shows a range of null geodesics leaving the surface of the cylinder in the lower left-hand quadrant of the diagram (with $-\pi/2 \leq \alpha_R \leq \pi/2$ and $\beta_R = 0$), and returning to the surface. The dotted geodesics have $\alpha_R = 0$ and $\alpha_R = \pi/2$, only the latter reaching r_{max}. The calculated value (29) with $a = 3/4$ and $R = 1$, is $r_{max} \simeq 16.6$.

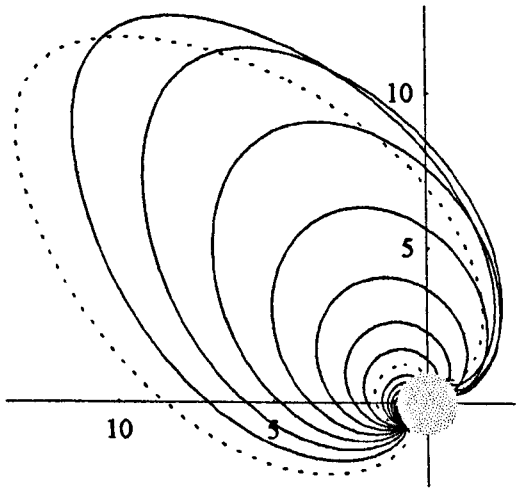

Figure 5.3 Confinement of null geodesics leaving the dust cylinder with $\dot{z} = 0$.

The parameters are $a = 3/4$, $R = 1$.

When the source cylinder is of lower mass per unit length, case III geodesics may orbit the cylinder more than once before returning. Figure 5.4 shows a single null geodesic leaving the cylinder, reaching $r_{peak} \simeq 33.2$ and then turning inwards. This value of r_{peak} can be calculated using equation (30).

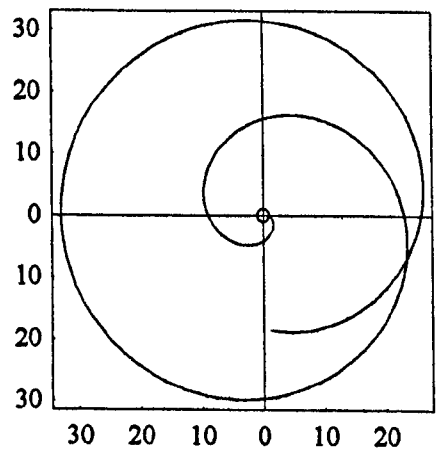

Figure 5.4 Null geodesic with $r_0 = R$, $\alpha_0 = \beta_0 = 0$.

The parameters are $a = \sqrt{5}/4$, $R = 1$.

5.3.3 Ranges of arbitrary case III null geodesics

It was shown in the previous sections that no case I or case II null geodesics leaving the cylinder are radially confined (although there is a circular null orbit at the surface of the case II cylinder) but that all case III null geodesics leaving the cylinder are confined. It remains to investigate what happens to case III null geodesics with initial positions $r_0 > R$.

So far, the analysis has covered both the whole of the interior, and the exterior for geodesics starting from $r = R$, where t is timelike and ϕ spacelike. In the case III exterior in van Stockum's coordinates, t and ϕ are sometimes timelike, sometimes spacelike, in all combinations, hence the requirement for the transformation in Section 2.3.2 to the metric where t is timelike when ϕ is spacelike and vice versa. The resulting metric functions are shown in equations (21), wherein the simplifying choice of $r_{orb} = R$ was made.

Where $\hat{L} = \hat{F} = 0$, it is clear from equations (21) that we must have $\epsilon - \theta = m\pi$, where m is an integer. Hence, since $\theta = \tan \epsilon \log(r/R)$, the r coordinates of these t, ϕ 'crossover' points are found at

$$r = R\exp[(\epsilon - m\pi)\cot\epsilon], \tag{31}$$

with $m \leq 0$. Equation (31) delineates the concentric regions for $R \leq r < \infty$ within which either t is timelike and ϕ is spacelike (which is the case for the region closest to the cylinder) or ϕ is timelike and t is spacelike. Orthonormal bases for both kinds of region were calculated in Section 2.4.

The analysis now follows that of Section 5.3.2, but with initial values denoted by a subscript zero, putting $L_0 \equiv L(r_0)$ etc. By analogy to equations (9), the constants of the motion for null geodesics with initial conditions r_0, α_0 and β_0, with r_0 in a region where t is timelike, are

$$P_\phi = \sqrt{\hat{L}_0}\,\sin\alpha_0\cos\beta_0, \quad E = \frac{(r_0 - \hat{M}_0\sin\alpha_0\cos\beta_0)}{\sqrt{\hat{L}_0}}. \tag{32}$$

As before, if null geodesics originating at r_0 with a given value of P_ϕ/E are restricted to a particular region, then for null geodesics at the boundary of the region, we must have

$$\left(\frac{P_\phi}{E}\right)_1 = R\sin\epsilon\cot\left(\frac{\epsilon-\theta}{2}\right),\ \left(\frac{P_\phi}{E}\right)_2 = -R\sin\epsilon\tan\left(\frac{\epsilon-\theta}{2}\right). \tag{33}$$

Using (21), the ratio P_ϕ/E in terms of initial conditions is now

$$\frac{P_\phi}{E} = \frac{R\cos\beta_0\sin\alpha_0\sin\epsilon\sin(\epsilon-\theta_0)}{1-\cos\beta_0\sin\alpha_0\cos(\epsilon-\theta_0)}, \tag{34}$$

where $-\pi \le \alpha_0 \le \pi$ and $-\pi/2 \le \beta_0 \le \pi/2$. Equating $(P_\phi/E)_1$ and $(P_\phi/E)_2$ in turn with P_ϕ/E and solving for θ gives the values, θ_1 and θ_2, at which the equality condition in (22) holds for null geodesics leaving r_0 with any given α_0 and β_0,

$$\begin{aligned}\theta_1 &= 2k\pi + \epsilon - 2\cot^{-1}\left(\frac{\cos\beta_0\sin\alpha_0\sin(\epsilon-\theta_0)}{1-\cos\beta_0\sin\alpha_0\cos(\epsilon-\theta_0)}\right),\\ \theta_2 &= 2k\pi + \epsilon + 2\tan^{-1}\left(\frac{\cos\beta_0\sin\alpha_0\sin(\epsilon-\theta_0)}{1-\cos\beta_0\sin\alpha_0\cos(\epsilon-\theta_0)}\right),\end{aligned} \tag{35}$$

where k is an integer. Both θ_1 and θ_2 have maximum values where $\alpha_0 = \pi/2$ and $\beta_0 = 0$ and minimum values where $\alpha_R = -\pi/2$ and $\beta_R = 0$. These deductions rely on the fact that in regions where t is timelike, $\sin(\epsilon-\theta_0) > 0$. Substituting these values of α_0 and β_0 into (35) gives,

$$\begin{aligned}(1+2k)\pi+\theta_0 \le\ \theta_1 \le\ 2k\pi+\theta_0,\\ 2k\pi+\theta_0 \le\ \theta_2 \le\ (1+2k)\pi+\theta_0.\end{aligned} \tag{36}$$

There is no such θ_1, and solving $\theta_2 = \tan\epsilon\log(r/R)$, for r, we obtain

$$r_0\exp[2k\pi\cot\epsilon] \le\ r\ \le\ r_0\exp[(2k+1)\pi\cot\epsilon]. \tag{37}$$

Since we are interested in geodesics with $r \ge r_0$, the physically relevant result is again obtained by putting $k = 0$, to get

$$r_0 \le\ r \le\ r_0\exp(\pi\cot\epsilon). \tag{38}$$

Thus all null geodesics originating from r_0 in a region where t is a timelike coordinate in this metric are confined within the region of space enclosed by a cylindrical surface with radial coordinate r_{max} where

$$r_{max} = r_0\exp(\pi\cot\epsilon), \tag{39}$$

and geodesics with $\alpha_0 = \pi/2$ and $\beta_0 = 0$ are the only ones that can reach r_{max}.

The procedure when r_0 is in a region where t is spacelike and ϕ is timelike is much the same as before, so just an outline follows. However, in such regions, to maintain the connection with classical angular momentum and energy, the definitions of P_ϕ and E are different. Putting the relevant expressions for $\dot{\phi}$ and $\dot{t}$ (see Section 2.4.2) into the new expressions for the constants of the motion, gives

$$P_\phi = \sqrt{-\hat{F}_0}\,\cos\beta_0 \sin\alpha_0, \quad E = \frac{r_0 - \hat{M}_0 \cos\beta_0 \sin\alpha_0}{\sqrt{-\hat{F}_0}}, \tag{40}$$

where P_ϕ and E can be interpreted as angular momentum and energy in regions where ϕ is the timelike coordinate. With the new P_ϕ and E, the equality condition in (10) now gives

$$\left(\frac{P_\phi}{E}\right)_1 = \frac{\tan(\frac{\epsilon-\theta}{2})}{R\sin\epsilon}, \left(\frac{P_\phi}{E}\right)_2 = -\frac{\cot(\frac{\epsilon-\theta}{2})}{R\sin\epsilon}. \tag{41}$$

The ratio P_ϕ/E in terms of initial conditions is

$$\frac{P_\phi}{E} = \frac{\cos\beta_0 \sin\alpha_0 \csc\epsilon \sin(\epsilon - \theta_0)}{R(\cos\beta_0 \sin\alpha_0 \cos(\epsilon - \theta_0) - 1)}, \tag{42}$$

where $-\pi \le \alpha_0 \le \pi$ and $-\pi/2 \le \beta_0 \le \pi/2$. Equating $(P_\phi/E)_1$ and $(P_\phi/E)_2$ with P_ϕ/E and solving for θ gives the same values of θ_1 and θ_2 as in equations (35), but with the suffixes reversed. Thus using the same analysis as before, but with θ_1 now giving the relevant result, all null geodesics originating from r_0 in a region where ϕ is a timelike coordinate in this metric are confined within the region of space enclosed by a cylindrical surface with radial coordinate r_{max} where

$$r_{max} = r_0 \exp(\pi \cot\epsilon), \tag{43}$$

and geodesics with $\alpha_0 = \pi/2$ and $\beta_0 = 0$ are the only ones that can reach r_{max}.

To illustrate the confinement of null geodesics originating at r_0, the upper diagram in Figure 5.5 shows 32 geodesics, with $r_0 = 40$, $-\pi \le \alpha_0 \le \pi$ and $\beta_0 = 0$. The dotted

geodesics have $\alpha_0 = 0$, $\alpha_0 = \pm \pi/2$ and $\alpha_0 = \pi$. The geodesic with $\alpha_0 = \pi/2$ is the only one to reach $r_{max} \simeq 664$. The lower diagram shows the region around the dust cylinder.

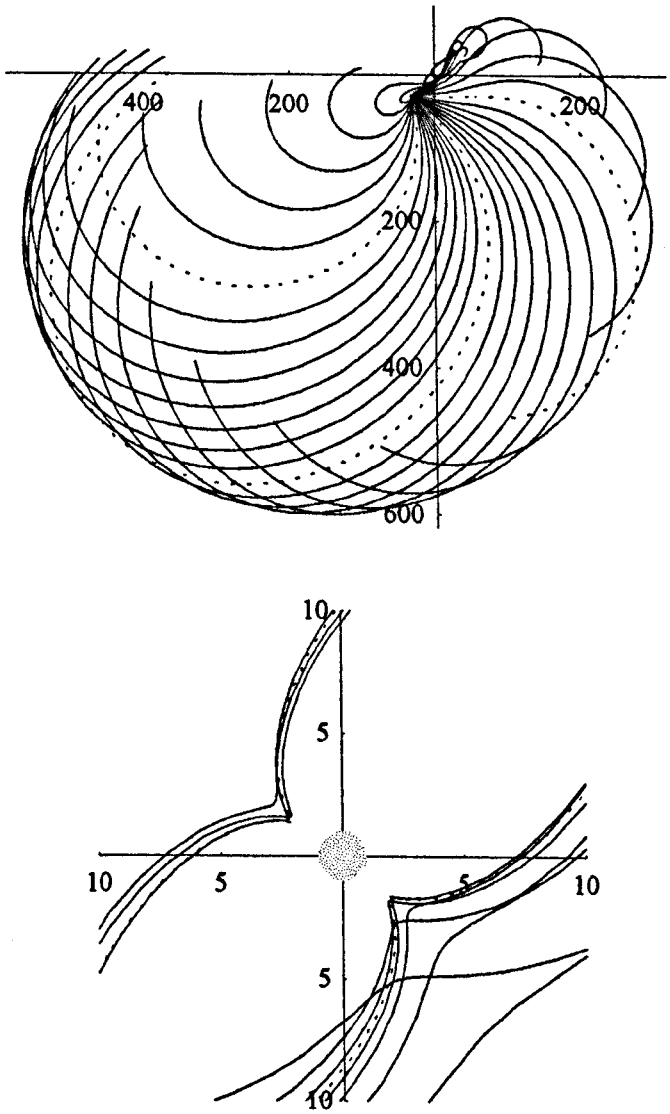

Figure 5.5 Confinement of null geodesics leaving $r_0 = 40$ with $\dot{z} = 0$.

The parameters are $a = 3/4$, $R = 1$.

The only omission in the analysis is the behaviour of null geodesics having r_0 such that the metric functions $\hat{L}(r_0) = \hat{F}(r_0) = 0$ (see equation (31) above). Since, in these cases, the orthonormal bases of Section 2.4 are not defined, the preceding analysis does not apply so the following procedure is applied.

Consider a null geodesic with r_0 such that $\hat{L}(r_0) = \hat{F}(r_0) = 0$. Since there are no circular null geodesics in case III, the geodesic from r_0 must either go outwards or inwards. In the former case, it must pass through the radial coordinate $r_1 = r_0 + \delta$, for some sufficiently small $\delta > 0$. Since $\hat{L}(r_1) \neq 0$ and $\hat{F}(r_1) \neq 0$,

$$r_{max}(r_0) \leq r_1 \exp(\pi \cot \epsilon) \equiv (r_0 + \delta) \exp(\pi \cot \epsilon). \tag{44}$$

This expression must also be true for geodesics which go inwards from r_0. Thus, since in the limit as $\delta \to 0$, $r_1 = r_0$, all null geodesics from r_0 must have $r_{max} \leq r_0 \exp(\pi \cot \epsilon)$.

Suppose $r_{max}(r_0) < r_0 \exp(\pi \cot \epsilon)$, then there is some $r_2 < r_0$ such that $r_{max}(r_2) > r_{max}(r_0)$. If a geodesic has $\alpha_{r_2} = \pi/2$ and $\beta_{r_2} = 0$, then it must reach $r = r_{max}(r_2)$, crossing $r = r_0$ on the way. However, a geodesic through r_0 cannot pass through a point with $r > r_{max}(r_0)$, and this contradiction means that $r_{max}(r_0) \not< r_0 \exp(\pi \cot \epsilon)$. Thus we must have the result that for null geodesics with r_0 such that $\hat{L}(r_0) = \hat{F}(r_0) = 0$,

$$r_{max} = r_0 \exp(\pi \cot \epsilon), \tag{45}$$

and this has now been shown to hold for all $r_0 \geq R$.

5.3.4 Summary of case III geodesics

(1) There are circular, timelike geodesics at all r but in one direction only.

(2) There are no circular null geodesics.

(3) Whether null geodesics originate in a region where t is the timelike coordinate or ϕ is the timelike coordinate, all are confined within the region of space enclosed by a cylindrical surface of radial coordinate $r_{max} = r_0 \exp(\pi \cot \epsilon)$. Geodesics with $\alpha_0 = \pi/2$ and $\beta_0 = 0$ are the only ones that can reach r_{max}, all others falling short.

(4) Where r_0 is such that $\hat{L}(r_0) = \hat{F}(r_0) = 0$, $r_{max} = r_0 \exp(\pi \cot \epsilon)$.

5.4 The exterior in the astronomical rest frame

The astronomical rest frame turns out to have several interesting features. One of these, which is surprising in a rotating metric, is the presence of radial geodesics.

Consider the constants of the motion for the general form of the metric,

$$P_z = H\dot{z}, \quad P_\phi = M\dot{t} + L\dot{\phi}, \quad E = F\dot{t} - M\dot{\phi}. \tag{46}$$

Defining a radial tangent vector as one having $\dot{\phi} = 0$, then the (constant) ratio P_ϕ/E for a geodesic that has a radial tangent vector at any point p is defined by

$$\frac{P_\phi}{E} = \frac{M(p)}{F(p)} = k, \text{ where } k \text{ is a constant.} \tag{47}$$

Thus anywhere on a geodesic that has a radial tangent vector somewhere,

$$\frac{P_\phi}{E} = \frac{M(r)\dot{t} + L(r)\dot{\phi}}{F(r)\dot{t} - M(r)\dot{\phi}} = k, \tag{48}$$

so that

$$\dot{\phi} = \frac{\dot{t}[F(r)k - M(r)]}{L(r) + kM(r)}. \tag{49}$$

Suppose there is a transformation that leaves the metric coefficients in a form such that $M \propto F$. Then using equation (47), for all r we must have

$$k = \frac{M(r)}{F(r)}. \tag{50}$$

Using the condition $LF + M^2 = r^2$, the denominator of equation (49) then becomes

$$L(r) + kM(r) = L(r) + \frac{M(r)^2}{F(r)} = \frac{r^2}{F(r)} \neq 0, \tag{51}$$

and the numerator is identically zero. If a geodesic in this frame has $\dot{\phi} = 0$ anywhere, it must have $\dot{\phi} = 0$ everywhere. Thus in a coordinate frame where the ratio M/F is constant, a geodesic that has a radial tangent vector anywhere must be a radial geodesic and, conversely, no non-radial geodesic can have a radial tangent vector anywhere. This can also be seen from the geodesic equations (Section 2.2), wherein if $\dot{\phi} = 0$ and $M = kF$, then $\ddot{\phi} = 0$.

In the astronomical rest frame of case I, in which the preceding analysis applies, the metric functions M and F (from Section 2.3.1) may be written

$$M(r) = -\frac{(1-2n)^{3/2} r (\frac{r}{R})^{-2n}}{(2n+1)^{3/2}}, \quad F(r) = \frac{16n(\frac{r}{R})^{1-2n}}{(2n+1)^3}, \qquad \text{where } n = \frac{1}{2}\sqrt{1-4a^2R^2}\,. \tag{52}$$

Hence

$$\frac{M(r)}{F(r)} = -\frac{(1-4n^2)^{3/2} R}{16n} = \text{constant}, \tag{53}$$

and so there must be radial geodesics in the astronomical rest frame. In the co-moving frame, this is not the case, the ratio M/F being r-dependent.

Note that $\dot{\phi} = 0 \Rightarrow P_\phi = M(r)\dot{t} \neq 0$, so particles on radial geodesics have non-zero angular momentum. Using the orthonormal basis of Section 2.4.1, the expression for P_ϕ, in regions where t is timelike and ϕ is spacelike, reduces to $P_\phi = \sqrt{L}\,\sin\alpha\cos\beta$ so unless $\beta = \pm\pi/2$, $P_\phi = 0 \Rightarrow \alpha = 0$.

In Figure 5.6, seventeen null geodesics in a hypersurface of z = constant leave a point on the cylinder's surface and are plotted in the astronomical rest frame. The dotted geodesics have $\alpha_R = \pi/2$, $\alpha_R = 0$ and $\alpha_R = -\pi/2$. The dotted geodesic going upwards in the diagram has $\alpha_R = 0 \Rightarrow P_\phi = 0$. The radial geodesic has $\alpha_R \simeq -0.578$.

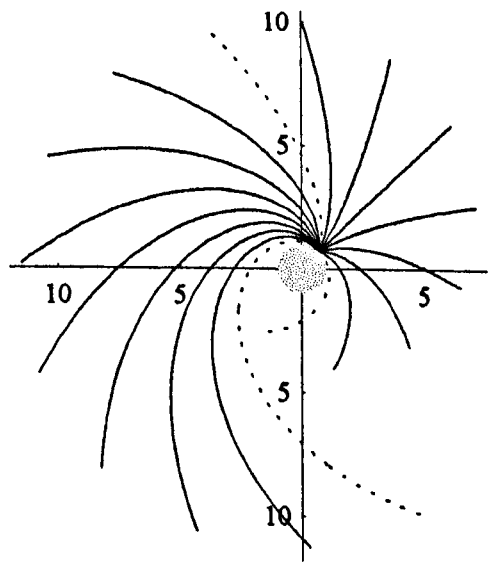

Figure 5.6 Null geodesics in the astronomical rest frame, with $a = 0.49$, $R = 1$.

As we shall see in Chapter 7, the astronomical rest frame has a special relevance in relation to the clock effect in van Stockum spacetime. In fact, in the astronomical rest frame, the clock effect is zero. This is not the case in the locally non-rotating frame described in Section 4.1. Thus the astronomical rest frame has the better claim to be called non-rotating, as noted in Bonnor and Steadman [43].

It was also pointed out by Semerack [47] that the observer in the astronomical rest frame of the van Stockum metric is an example of an 'extremely accelerated observer', a subject which he and others have studied recently, but which is not pursued here.

Van Stockum described the astronomical rest frame as a frame which is not rotating with respect to the fixed stars. Plotting geodesics in this frame can give clearer pictures for case I, especially when several geodesics are shown. Figure 5.7 shows case I null geodesics in the astronomical rest-frame in a hypersurface of z = constant. Since $R = 1$, $aR = 0.19$, 0.29, 0.39 and 0.49 as labelled. All geodesics were plotted for the same range of the affine parameter, except those that hit the dust cylinder.

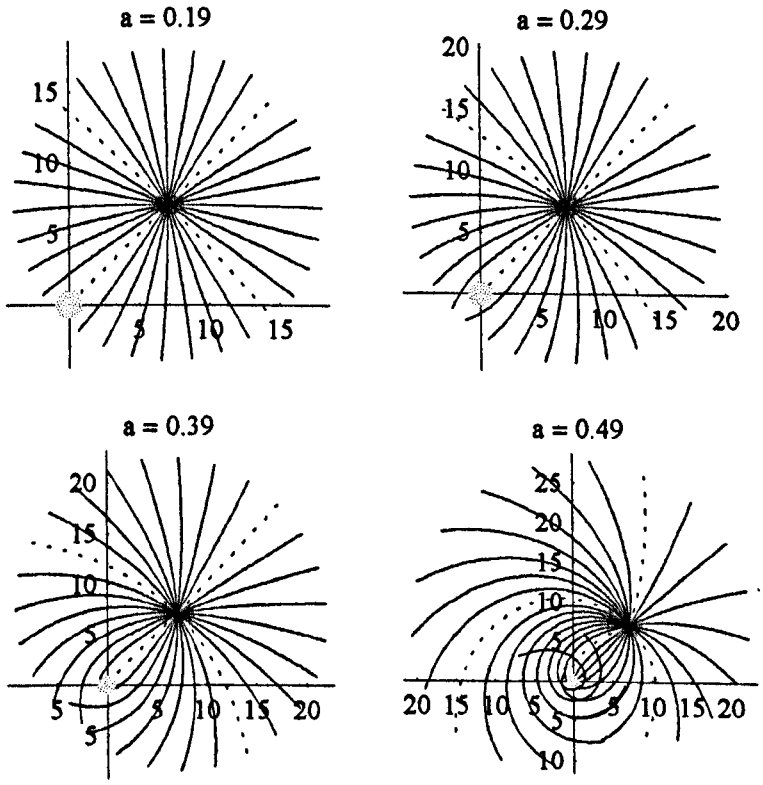

Figure 5.7 Null geodesics in the astronomical rest-frame.

Figure 5.8 shows the same plots as the previous figure but in the co-moving frame. Only the cases $aR = 0.19$ and $aR = 0.49$ are shown, and features of the two cases which are evident in Figure 5.7 are largely overwhelmed by the effect of the rotating reference frame. Plotting more than a few geodesics in the co-moving frame is not usually helpful, often resulting in congested plots.

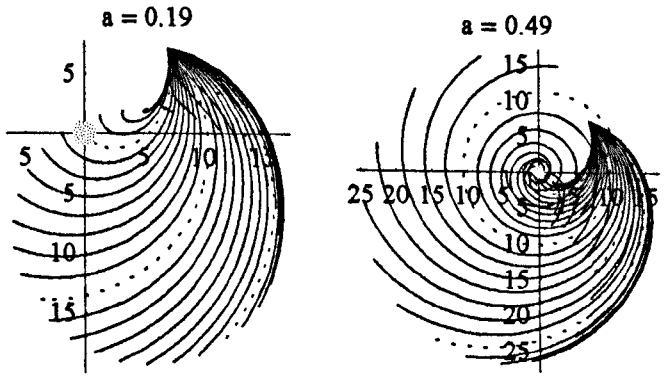

Figure 5.8 Null geodesics in the co-moving frame.

A visual impression of the rotation and tidal effect in the case I van Stockum exterior may be obtained by again using the astronomical rest frame. In Figure 5.9, three test particles in a triangular configuration all have initial speeds $v_0 = 0$. One test particle has $r_0 = 50$ and the other two have $r_0 = 60$. Despite the optical illusion in the diagram, the latter two fall inwards at the same rate. At equal intervals of proper time, the geodesics of the test particles have been connected by straight lines to give an impression of a triangle being swept sideways and stretched radially whilst falling at an increasing speed.

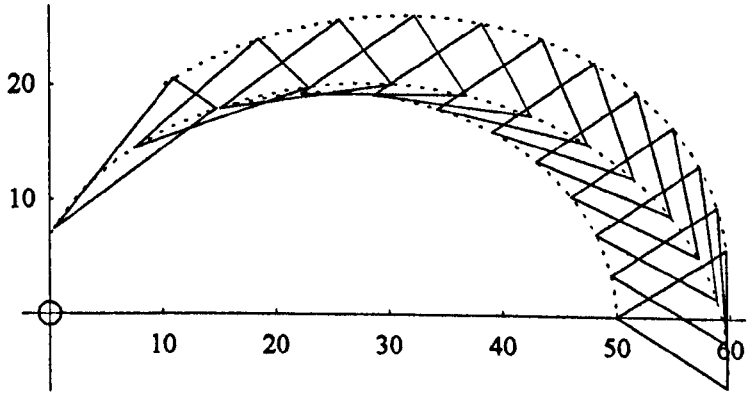

Figure 5.9 A triangular configuration of test particles with $v_0 = 0$ in the astronomical rest frame, with $R = 1$, $a = 0.49$.

5.5 The exterior for $aR > 1$

Since we are restricting attention to metrics with $aR < 1$, it is interesting that Bonnor [5] noted that only for $a^2 R^2 < 1$ do the algebraic invariants of the exterior tend to zero as $r \to \infty$. For $aR = 1$, the invariants are constant and for $a^2 R^2 > 1$ they tend to infinity as $r \to \infty$, suggesting another source, at $r = \infty$, in addition to the central cylinder. It should be noted however, that the exterior is not asymptotically Minkowskian whatever the choice of parameters, a problem shared with the Newtonian version of the infinite cylinder.

~ Chapter 6 ~

Bonnor's rotating dust cloud

6.1 A dust cloud solution

Newtonian mechanics allows the existence of a stationary axially symmetric rotating dust cloud only if it is cylindrically symmetric and infinite in length. Otherwise, the dust cloud would collapse due to a density gradient parallel to the axis of rotation. Remarkably, there are stationary axially symmetric rotating dust cloud solutions in general relativity which are not cylindrically symmetric.

The general solution for stationary axially symmetric dust was given by Winicour [41]. Whilst acknowledging the influence of Winicour, Bonnor took a special solution of van Stockum in developing a rotating dust cloud solution. The van Stockum class of solutions covers rigidly rotating dust only. An outline of Bonnor's solution was shown in Chapter 1, but it is re-written here in more detail, in the notation of Bonnor's paper [40].

Van Stockum's axially symmetric dust metric is

$$ds^2 = \exp(\mu)(dz^2 + dr^2) + (r^2 - n^2)\,d\phi^2 + 2n\,d\phi dt - dt^2, \tag{1}$$

where $0 \le r < \infty$, $-\infty < z < \infty$, $0 \le \phi \le 2\pi$, $-\infty < t < \infty$. Compared with van Stockum, Bonnor used a slightly different but equivalent method for generating solutions, whereby the function n (which differs from the n of van Stockum's solution in the previous sections) is given by

$$n = r\,\xi_{,r}, \tag{2}$$

and $\xi = \xi(r, z)$ is a solution of Laplace's equation

$$\nabla^2 \xi = \xi_{,rr} + \xi_{,zz} + \frac{\xi_{,r}}{r} = 0. \tag{3}$$

The function $\mu = \mu(r, z)$ may then be found from

$$\mu_{,z} = -\frac{n_{,z}\,n_{,r}}{r}, \quad \mu_{,r} = \frac{(n_{,z})^2 - (n_{,r})^2}{2r}. \tag{4}$$

Bonnor found that the simple solution to Laplace's equation given by

$$\xi = \frac{2h}{R}, \quad R^2 = z^2 + r^2, \tag{5}$$

where h is a constant, resulted in a dust cloud whose density tends to zero at spatial infinity. Note that R here is not the same as the R in van Stockum's solution. As $h \to 0$, the metric goes to the Minkowski form. The choice of $\xi = 2h/R$ leads to

$$\mu = \frac{h^2 r^2 (r^2 - 8z^2)}{2R^8}, \quad n = \frac{2hr^2}{R^3}, \tag{6}$$

in the metric equation (1). For comparison, the choice $\xi = ar^2/2 - az^2$, where a is a constant, gives the van Stockum dust cylinder.

The solution describes a cloud of rigidly rotating dust particles moving along circular geodesics in hypersurfaces of z = constant. The dust cloud is at rest with respect to the coordinate frame, its velocity being $u^i = \delta^i_4$. The density of the dust is given by

$$\rho = \frac{\exp(-\mu) h^2 (r^2 + 4z^2)}{2\pi R^8}, \tag{7}$$

so that outside of the singularity at the coordinate origin, $\rho > 0$. The density diminishes rapidly with increasing distance from the origin, tending to zero at spatial infinity.

Bonnor found that on transforming the metric to the locally non-rotating frame (see Section 4.1) and taking $\sqrt{g_{44}}$ as the gravitational potential, in the approximation for large R, the potential contains no mass term. However, attempting to calculate the mass gave a divergent integral. To reconcile these contradictory results, Bonnor speculated that the singularity at $R = 0$ may have infinite negative mass.

6.2 Geodesics in the dust cloud

Since the metric coefficients are functions of both r and z, the geodesic equations, even in the symbolic form used in Section 2.2, are more complicated than those for the van Stockum solution. Writing a general form of the metric as

$$ds^2 = H(z, r)(dz^2 + dr^2) + L(z, r)\, d\phi^2 + 2\, M(z, r)\, d\phi\, dt - F(z, r)\, dt^2, \tag{8}$$

with the ranges of the coordinates as before, enables the geodesic equations to be calculated using *Mathematica* :

$$
\begin{aligned}
\ddot{z} &= \frac{1}{2H}\left((\dot{r}^2-\dot{z}^2)H_{,z}-2\dot{r}\dot{z}H_{,r}+\dot{\phi}^2 L_{,z}+2\dot{t}\dot{\phi}M_{,z}-\dot{t}^2F_{,z}\right),\\
\ddot{r} &= \frac{(\dot{z}^2-\dot{r}^2)H_{,r}-2\dot{r}\dot{z}H_{,z}+\dot{\phi}^2 L_{,r}+2\dot{t}\dot{\phi}M_{,r}-\dot{t}^2F_{,r}}{2H},\\
\ddot{\phi} &= -\frac{1}{r^2}\{\dot{r}[\dot{\phi}(ML_{,r}-LM_{,r})+\dot{t}(LF_{,r}+MM_{,r})]+\\
&\quad \dot{z}[\dot{\phi}(ML_{,z}-LM_{,z})+\dot{t}(LF_{,z}+MM_{,z})]\},\\
\ddot{t} &= \frac{1}{r^2}\{\dot{r}[\dot{t}(MF_{,r}-FM_{,r})-\dot{\phi}(FL_{,r}+MM_{,r})]+\\
&\quad \dot{z}[\dot{t}(MF_{,z}-FM_{,z})-\dot{\phi}(FL_{,z}+MM_{,z})]\}.
\end{aligned}
\tag{9}
$$

Superior dots indicate differentiation with respect to the affine parameter and subscripts denote differentiation with respect to z or r.

6.2.1 Circular geodesics

The presence of circular timelike geodesics may be found by setting the necessary conditions $\dot{r}=\dot{z}=0$ in the geodesic equations. This gives $\ddot{\phi}=\ddot{t}=0$, together with

$$
\ddot{z}=\frac{2\dot{\phi}\dot{t}M_{,z}+\dot{\phi}^2L_{,z}-\dot{t}^2F_{,z}}{2H},\quad \ddot{r}=\frac{2\dot{\phi}\,\dot{t}M_{,r}+\dot{\phi}^2L_{,r}-\dot{t}^2F_{,r}}{2H}. \tag{10}
$$

Since $M=n$, $L=(r^2-n^2)$ and $F=1$, solving $\ddot{z}=0$ and $\ddot{r}=0$ simultaneously, with the function $n=2hr^2/R^3$, gives three solutions,

$$
\dot{\phi}=0,\ \left\{\dot{\phi}=\frac{2hr\dot{t}}{4h^2+r^4},\ z=0\right\},\ r=0. \tag{11}
$$

The first solution clearly describes the dust particles and the second solution shows the presence of additional circular geodesics in the equatorial plane. To find whether these geodesics are timelike, null or spacelike, we can put $dz^2=dr^2=0$ into the metric equation (1) and divide by dt^2 to get

$$
\left(\frac{ds}{dt}\right)^2=(r^2-n^2)\left(\frac{d\phi}{dt}\right)^2+2n\left(\frac{d\phi}{dt}\right)-1. \tag{12}
$$

Since $\dot{\phi} = 0 \Rightarrow d\phi/dt = 0$, the first solution of (11) gives $(ds/dt)^2 = -1$, confirming the timelike geodesics of the dust particles. Substituting $d\phi/dt$ from the second solution, with $z = 0$, gives

$$\left(\frac{ds}{dt}\right)^2 = \frac{r^4(4h^2 - r^4)}{(r^4 + 4h^2)^2}. \tag{13}$$

From the sign of $(ds/dt)^2$, the additional circular geodesics, in the equatorial plane, are timelike where $r > \sqrt{2h}$ and spacelike where $r < \sqrt{2h}$. There is a circular null geodesic at $r = \sqrt{2h}$. The nature and distribution of circular geodesics in the equatorial plane give an indication of the interesting distribution of null geodesics throughout the dust cloud as described in the following section.

6.2.2 The distribution of null geodesics in the dust cloud

From the line element (1) and the dependence of the g_{ik} on z and r, the constants of the motion along any geodesic are given by

$$P_\phi = n\dot{t} + (r^2 - n^2)\dot{\phi}, \quad E = \dot{t} - n\dot{\phi}, \tag{14}$$

where P_ϕ and E are interpreted as angular momentum and energy respectively of photons (or test particles). The superior dot again indicates differentiation with respect to a suitable affine parameter. Thus we may write

$$\dot{\phi} = \frac{P_\phi - nE}{r^2}, \quad \dot{t} = \frac{(r^2 - n^2)E + nP_\phi}{r^2}. \tag{15}$$

For null geodesics we must have $ds^2 = 0$, in which case, from (1) and because $\exp\mu(dr^2 + dz^2) \geq 0$,

$$\dot{t}^2 - 2n\dot{\phi}\dot{t} - (r^2 - n^2)\dot{\phi}^2 \geq 0. \tag{16}$$

Using equations (15) therefore, everywhere along a null geodesic, we have

$$-P_\phi^2 + 2nEP_\phi + (r^2 - n^2)E^2 \geq 0. \tag{17}$$

6.2.3 Null geodesics with $P_\phi \leq 0$

Without loss of generality, the affine parameter may be scaled so that $E = 1$. The simplest case to examine is for null geodesics with $P_\phi = 0$. We must then have $r^2 - n^2 \geq 0$, from (17), so that, using $n = 2hr^2/R^3$ from equations (6),

$$r^2 - \frac{4h^2 r^4}{R^6} \geq 0 \Rightarrow z^2 \geq (2hr)^{2/3} - r^2 . \tag{18}$$

Thus null geodesics having $P_\phi \leq 0$ can exist only outside of the toroidal surface $z^2 = (2hr)^{2/3} - r^2$. Figure 6.1 shows the toroidal surface, with a cut-away section, when $h = 1$.

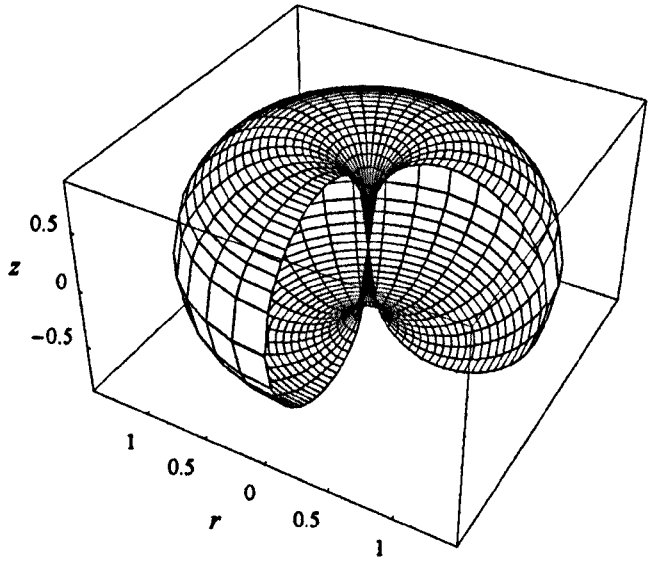

Figure 6.1 Null geodesics having $P_\phi \leq 0$ can exist only outside this surface.

From equations (14), if $r = 0$ and $z \neq 0$ then $P_\phi = 0$ so that geodesics having $P_\phi = 0$ are the only ones that can reach the z-axis. Note that only outside the toroidal surface is the ϕ coordinate spacelike in the rest frame of the dust.

This forbidden region for null geodesics with $P_\phi \leq 0$ is especially interesting in light of the conjecture that the singularity at the origin of coordinates contains negative mass. Are light and test particles repelled by a negative 'gravitational force' associated with the singularity?

6.2.4 Null geodesics generally

To pursue the question of possible repulsion from the central singularity, we shall examine null geodesics with the full range of values of P_ϕ. Using (17) (with $E = 1$) gives

$$-P_\phi^2 + 2n\,P_\phi + (r^2 - n^2) = r^2 - (P_\phi - n)^2 \geq 0, \tag{19}$$

so that

$$(n - r) \leq P_\phi \leq (n + r). \tag{20}$$

Consider a null geodesic with any particular value of P_ϕ. Then any point (r, z) along the geodesic must satisfy (20). Thus the geodesic cannot enter any part of the (r, z) plane for which either $n - r > P_\phi$ or $n + r < P_\phi$. The boundaries between the allowed and forbidden regions in the (r, z) plane are the curves $n - r = P_\phi$ and $n + r = P_\phi$.

To illustrate the extent and nature of the allowed regions for null geodesics with various values of P_ϕ, we can plot the boundaries and colour the forbidden regions. Since $n + r \geq 0$, if $P_\phi < 0$ then there are no points (r, z) such that $n + r < P_\phi$ and there is just one boundary $(n - r = P_\phi)$ and one forbidden region. If $P_\phi > 0$ then there are two boundaries and two forbidden regions.

The allowed regions for a sample of null geodesics with eight different values of P_ϕ are shown as the white areas in Figure 6.2. Forbidden regions wherein $n - r > P_\phi$ are bounded by $n - r = P_\phi$ and are coloured red. Forbidden regions wherein $n + r < P_\phi$ are bounded by $n + r = P_\phi$ and are coloured yellow.

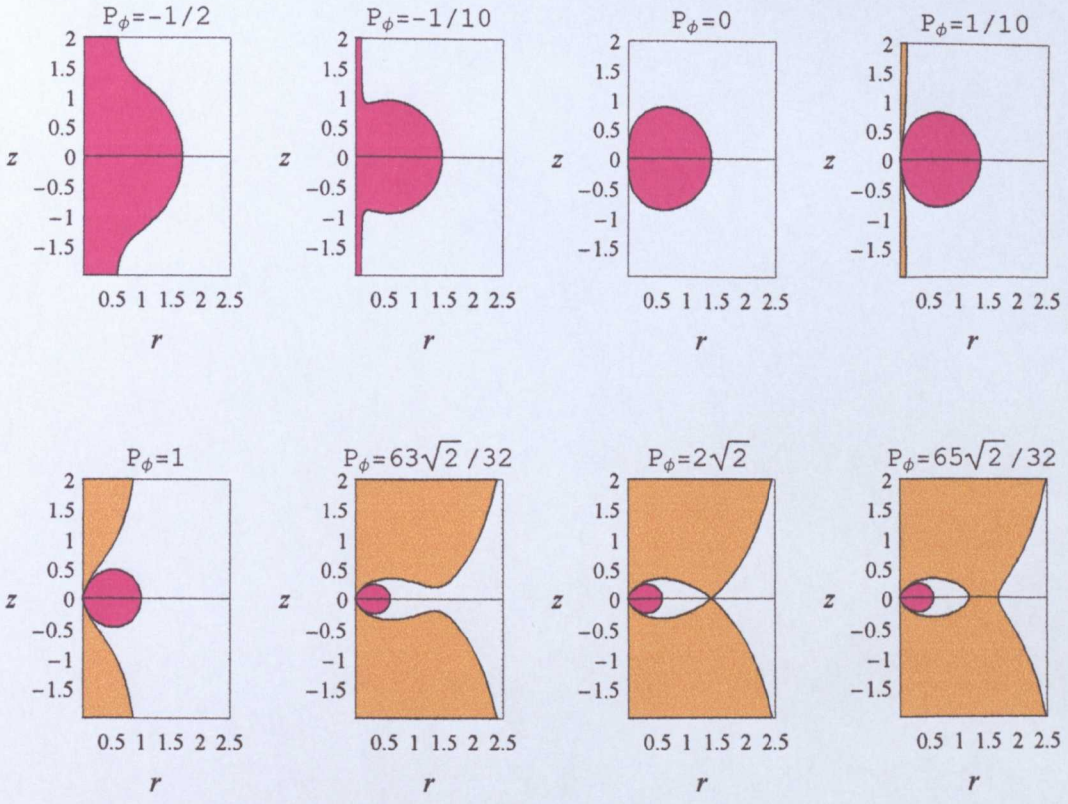

Figure 6.2 Excluded regions (coloured) for null geodesics with P_ϕ as shown. Rotation parameter $h = 1$.

As P_ϕ increases, the red forbidden region shrinks. For $P_\phi > 2\sqrt{2h}$, this region becomes isolated by the yellow forbidden region so that geodesics with $P_\phi > 2\sqrt{2h}$ from the outer region, for example geodesics from spatial infinity, cannot approach the central red region very closely. For $P_\phi > 2\sqrt{2h}$ there are separate inner and outer allowed regions. These features will be examined analytically in the following section.

6.3 Analysing the null geodesic central forbidden region

The isolating of the red forbidden region from incoming null geodesics clearly depends on the disposition of the yellow forbidden region in Figure 6.2. The boundary of the yellow region is given by

$$n + r = \frac{2hr^2}{(r^2 + z^2)^{3/2}} + r = P_\phi . \tag{21}$$

Since both forbidden regions are symmetric about $z = 0$, isolation of the red region implies that the boundary of the yellow region must cross the line $z = 0$. Putting $z = 0$ in (21) and solving for r gives r values where the boundary crosses the line:

$$r = \frac{1}{2}\left(P_\phi - (P_\phi^2 - 8h)^{1/2}\right), \quad r = \frac{1}{2}\left(P_\phi + (P_\phi^2 - 8h)^{1/2}\right). \tag{22}$$

When $P_\phi < 2\sqrt{2h}$ there are no real solutions. When $P_\phi = 2\sqrt{2h}$, $r = \sqrt{2h}$ (twice). When $P_\phi > 2\sqrt{2h}$ there are two distinct real solutions. These results tally with Figure 6.2 and show that there are also two crossings of the line $z = 0$, by the boundaries of the yellow region, for higher values of P_ϕ than those plotted.

The impression given by Figure 6.2, concerning the allowed regions for null geodesics with different values of P_ϕ, is thus supported analytically. The highest value of P_ϕ before the central red region becomes isolated is $P_\phi = 2\sqrt{2h}$ when equations (22) give $r = \sqrt{2h}$, twice. However, as shown in Section 6.2.1, there is a circular null geodesic (having $P_\phi = 2\sqrt{2h}$) at $r = \sqrt{2h}$ in the equatorial plane.

The red forbidden region defined by $n - r = 2\sqrt{2h}$ is significant. As we have just shown, it cannot be entered by null geodesics from the outer allowed regions if they have $P_\phi \geq 2\sqrt{2h}$. But since, as P_ϕ decreases, the red region expands, it is also forbidden to geodesics with $P_\phi < 2\sqrt{2h}$. Thus this region, which cannot be entered by any geodesic from the outer allowed region, is called the central separate zone [48]. An expression for the surface of the zone can be found by putting $n - r = 2\sqrt{2h}$, and solving to get

$$z^2 = \left(\frac{2hr^2}{2\sqrt{2h} + r}\right)^{2/3} - r^2. \tag{23}$$

A plot of the surface of the central separate zone in the (r, z) plane, when $h = 1$, is shown in Figure 6.3.

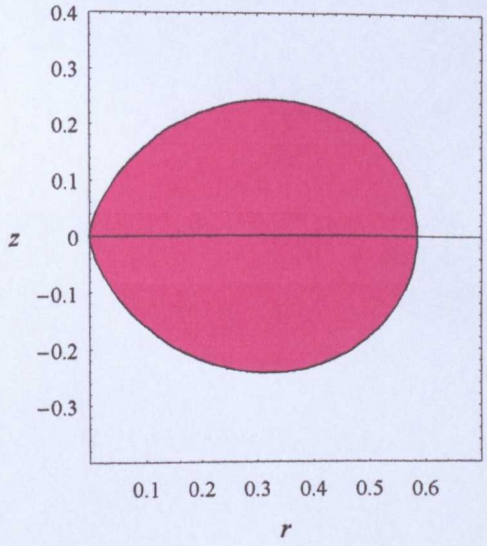

Figure 6.3 The central separate zone at the centre of the dust cloud. It cannot be entered by any null geodesic from the outer allowed region, irrespective of P_ϕ.

No null geodesic with $P_\phi \leq 2\sqrt{2h}$ can exist within the central separate zone. If $P_\phi > 2\sqrt{2h}$ however, the yellow forbidden region isolates the central separate zone from the outer allowed region. Thus any null geodesic originating within the zone is prevented from passing into the outer allowed region. One way of encapsulating the situation is to say that null geodesics from spatial infinity cannot enter the central separate zone and null geodesics from within the zone cannot extend to spatial infinity. In fact, they cannot extend far at all as we shall see in the following section.

6.4 Confinement of null geodesics around a central forbidden region

The allowed region outside of some central forbidden region (whose extent depends on P_ϕ) continues outwards towards spatial infinity for geodesics having $P_\phi < 2\sqrt{2h}$. This is clear from Figure 6.2 and equation (22). However, geodesics close to the central forbidden region and having $P_\phi > 2\sqrt{2h}$ are confined within the inner allowed region. This was seen in the lower right-hand plot in Figure 6.2, and Figure 6.4 shows four more examples. The white regions are where null geodesics, with the given P_ϕ, are confined.

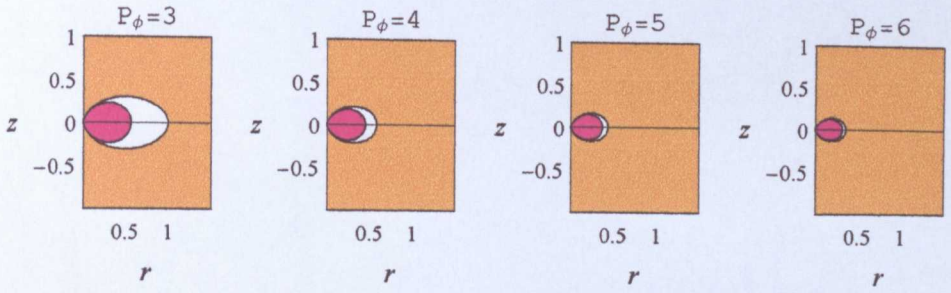

Figure 6.4 Central regions of confinement (white) for null geodesics.

As P_ϕ increases, the bounding surfaces and the space between them decrease. Solving $n - r = P_\phi$ and $n + r = P_\phi$ for z enables the allowed regions for a null geodesic with a given P_ϕ to be specified precisely. Thus the inner allowed region is given by

$$\left(\frac{2hr^2}{P_\phi + r}\right)^{2/3} - r^2 < z^2 < \left(\frac{2hr^2}{P_\phi - r}\right)^{2/3} - r^2, \quad \text{for } P_\phi > 2\sqrt{2h} \text{ and } r \le \frac{1}{2}\left(P_\phi - \sqrt{P_\phi{}^2 - 8h}\right). \tag{24}$$

As $P_\phi \to \infty$, this region shrinks, around the origin, towards zero volume. The outer allowed region is given by

$$z^2 > \left(\frac{2hr^2}{P_\phi - r}\right)^{2/3} - r^2, \text{ for } \left\{P_\phi > 2\sqrt{2h},\ r < P_\phi\right\}, \quad \text{and } -\infty < z < \infty \text{ for } \left\{P_\phi > 2\sqrt{2h},\ r \ge P_\phi\right\}. \tag{25}$$

As an example, Figure 6.5 shows the inner allowed region and part of the outer allowed region for null geodesics with $P_\phi = 3$.

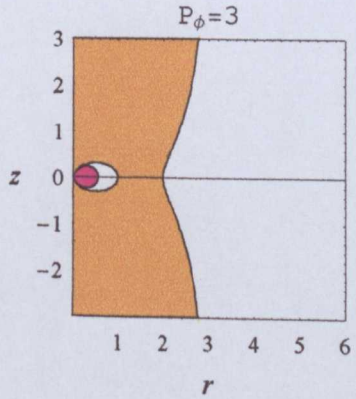

Figure 6.5 Allowed (white) regions for null geodesics with $P_\phi = 3$.

6.5 Geodesics illustrated

This section has diagrams showing the behaviour of some null and timelike geodesics in a dust cloud with the parameter $h = 1$. In the coordinate frame of the diagrams, the dust is at rest. Apart from within the toroidal region shown in Figure 6.1, in this frame, the t coordinate is timelike and the ϕ coordinate is spacelike throughout, so geodesics may be plotted provided that r_0 and z_0 lie outside the toroidal region.

6.5.1 Null geodesics with $P_\phi \approx 2\sqrt{2h}$

The behaviour of null geodesics with $P_\phi \approx 2\sqrt{2h}$, in the equatorial plane of the dust cloud, is very sensitive to initial conditions as shown in the following plots. Note that to five decimal places, $2\sqrt{2} = 2.82843$. In Figure 6.6, a null geodesic with $P_\phi = 2.82844$ is plotted from $r_0 = 5$. It orbits the centre of the dust cloud just outside the circle at r = $\sqrt{2}$ before travelling outwards.

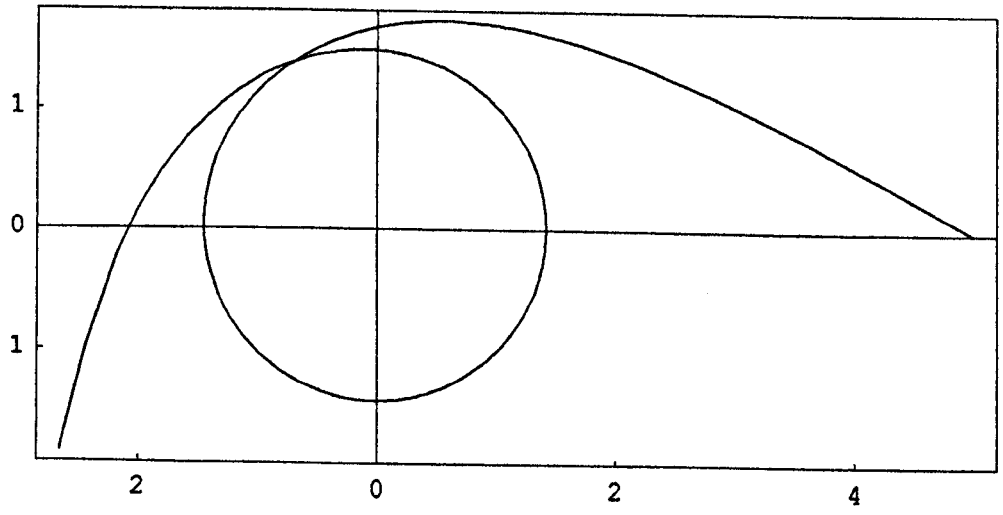

Figure 6.6 A null geodesic, in the equatorial plane, with $r_0 = 5$ and P_ϕ =2.82844.

In Figure 6.7, a null geodesic with $P_\phi = 2.82842$ is plotted from $r_0 = 5$. It first orbits the centre of the dust cloud close to the circle at $r = \sqrt{2}$ and then falls inwards again, before finally travelling outwards.

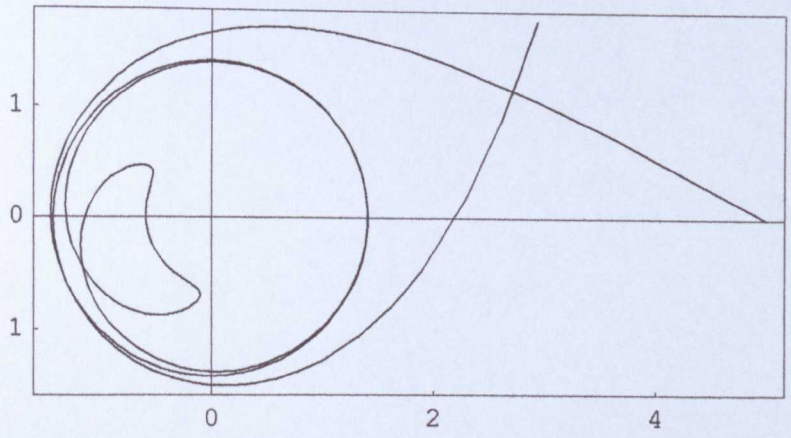

Figure 6.7 A null geodesic, in the equatorial plane, with $r_0 = 5$ and P_ϕ =2.82842.

As well as being remarkably sensitive to initial conditions, the plots in Figures 6.6 and 6.7 are consistent with the circular null geodesic at $r = \sqrt{2}$ having $P_\phi = 2\sqrt{2}h$.

6.5.2 Test particles with initial speeds $v_0 = 0$

Figure 6.8 shows a triangular configuration of test particles in the equatorial plane, similar to that which was 'released' in the van Stockum astronomical rest frame and which was shown in Figure 5.9. The test particles have initial speed $v_0 = 0$ and the geodesics in the figure are plotted in the frame co-rotating with the dust. Note that the geodesic speed of the dust may be found by solving for $\dot{\phi} = 0$ (see orthonormal frame details in Section 2.4.1) to get $v_{\text{dust}} = 2hrR^{-3}$. Remarkably, the test particles fall outwards and the one with the smallest r_0 'overtakes' the others radially; its geodesic is shown blue.

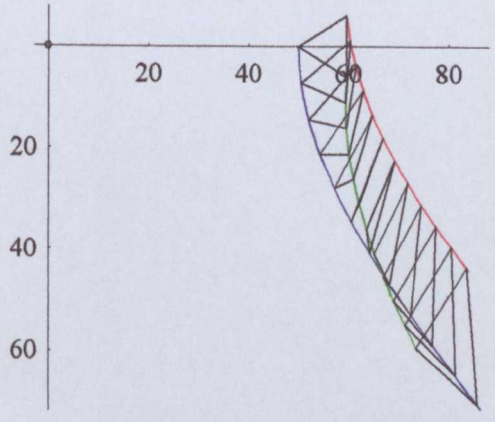

Figure 6.8 A triangular configuration of test particles with v_0=0, z_0=0, $\dot{z}_0$= 0.

In Figure 6.9, the test particles are initially at the same radial coordinates as before, but they start at $z_0 = 10$, not in the equatorial plane. In this three-dimensional plot, the small sphere marks the centre of the dust cloud. The inner test particle (blue plot) overtakes the other two both radially and axially.

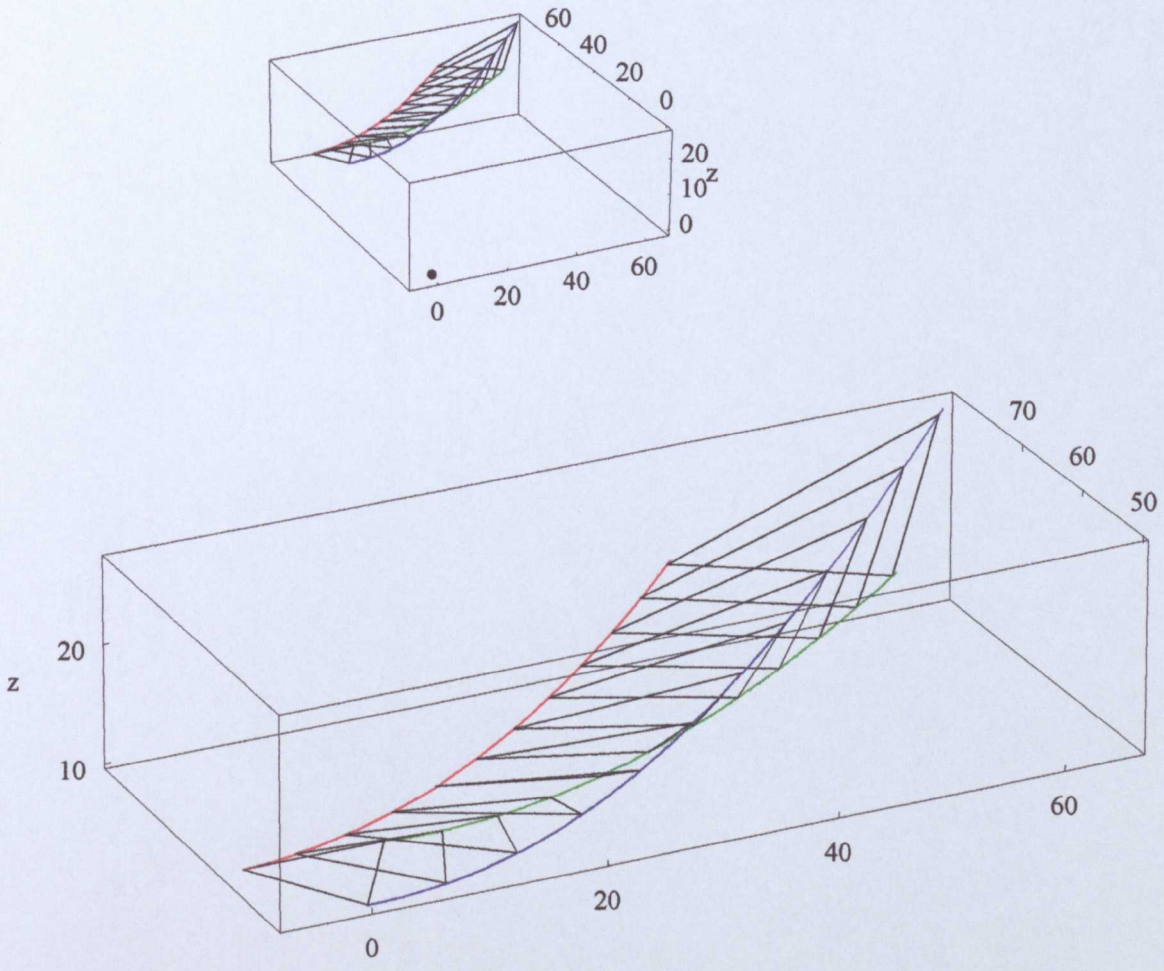

Figure 6.9 The triangular configuration of test particles with v_0=0, $\dot{z}_0$= 0, z_0=10.

The impression of repulsion from the centre of the dust cloud is also given by the behaviour of null geodesics as the following section shows.

6.5.3 Inwards-going null geodesics

In Figure 6.10, thirty-three null geodesics start from the same event in the equatorial plane at $r_0 = 5$ and at slightly different initial angles. Since $\dot{z}_0 = 0$, they remain in the equatorial plane and seem to be repelled from the centre.

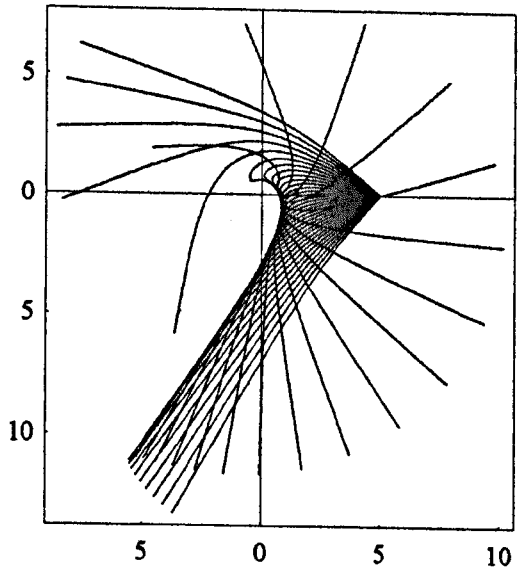

Figure 6.10 Null geodesics from $r_0 = 5$ in the equatorial plane.

Finally, the three-dimensional plots in Figure 6.11 show null geodesics starting with $r_0 = 2$ and $z_0 = 2$. They all have the same $\dot{z}_0 < 0$ such that the central geodesic is initially directed towards the singularity. The toroidal shape depicts the central separate zone which was described by equation (23) although this depiction is rather fanciful since the ϕ coordinate is timelike within the torus of Figure 6.1.

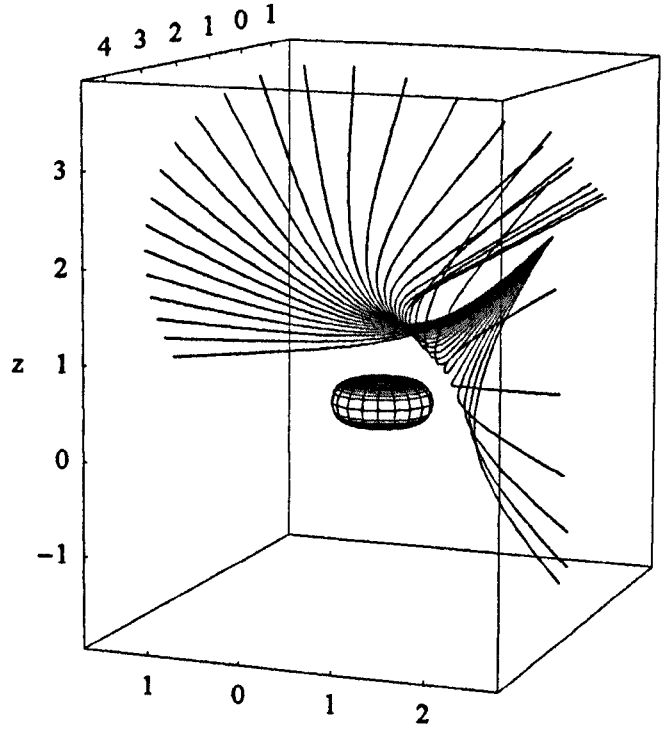

Figure 6.11 Null geodesics from $r_0 = z_0 = 2$.

6.6 Repulsive gravitation

From examining the distribution of null geodesics and plotting both null and timelike geodesics, Bonnor's speculation that the central singularity has negative mass seems to be supported, since negative mass should be a source of repulsive gravitation. As noted in Section 4.1, Abramowicz and coworkers [35-37] developed a method which introduced the concept of acceleration into general relativity as an aid to the understanding of physical phenomena. Although this seems a retrograde step, general relativity having done away with the Newtonian notion of force in gravitation, the scheme has turned out to be very useful. Abramowicz and Lasota have described its early development and some of the consequences in a recent paper [42]. The extension and further application of this work by Prasanna and others is outlined in Appendix 3.

As mentioned in the previous section, the ϕ coordinate is spacelike only outside the toroidal surface of Figure 6.1. Abramowicz's work on the inertial forces uses the angular velocity $\omega = -g_{\phi t}/g_{\phi\phi}$, of the zero angular momentum observer, in formulating the Coriolis and centrifugal forces, so that it is inapplicable in the timelike ϕ region. However, the expression for the gravitational force is derived from a scalar potential and is therefore relevant throughout the dust cloud. Using Abramowicz's formalism, the components of the gravitational acceleration acting on the dust particles in the r and z directions in the rotating dust cloud are given by

$$G^r = \frac{4h^2 r(z^2 - 2r^2)}{R^2(R^6 - 4h^2 r^2)}, \quad G^z = -\frac{12h^2 r^2 z}{R^2(R^6 - 4h^2 r^2)}. \tag{26}$$

The numerator of G^r changes sign where $z = \sqrt{2}r$ and both denominators change sign where $R^6 = 4h^2 r^2$, which also defines the toroidal surface shown in Figure 6.1. The vector and contour plots of G (with $h = 1$), in Figure 6.12, show what is happening. The surface $R^6 = 4h^2 r^2$ is plotted in red.

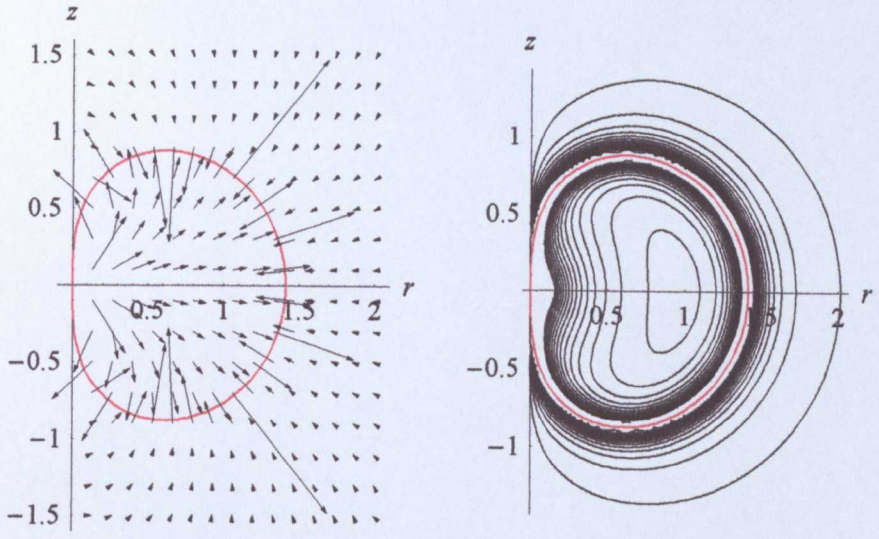

Figure 6.12 Left, vector plot of G.
Right, contour plot of the magnitude of G.

Outside the red line, gravitational acceleration is directed inwards, towards the timelike ϕ region, and is increasing in magnitude, tending to infinity as the line is approached. Inside, the acceleration is directed outwards, again increasing in magnitude, tending to infinity as the line is approached. In the contour plot, the white region around the red line is an artefact of the plotting process. This is the region of maximum acceleration which should have the maximum density of contours. Figure 6.13 shows just the area around the singularity (which is white in Figure 6.12).

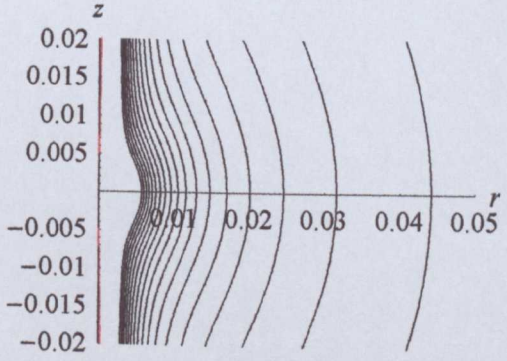

Figure 6.13 Contour plot near the singularity.

If Abramowicz's concept of inertial acceleration in general relativity is valid here, the central singularity must be a source of repulsive gravitation.

~ Chapter 7 ~

The clock effect

7.1 Definition of the clock effect

If a rotating spacetime has circular, timelike geodesics in both directions, the clock effect is defined as the difference in periods of test particles orbiting in either direction. The clock effect depends on the choice of coordinate system in which the periods are measured. For a static spacetime, in non-rotating coordinates the clock effect is zero. For stationary spacetimes, the clock effect may be reduced to zero by a suitable choice of coordinates. Some spacetimes may not admit circular timelike geodesics in both directions, in which case the clock effect is not defined. Examples of the latter are the van Stockum case II and case III exteriors which have circular, timelike geodesics in one direction only.

Tartaglia [49] has shown that the clock effect should be detectable in the solar system, indeed, by clocks orbiting the Earth. Orbits around Jupiter, however, would give more reliable results.

7.2 Formulae for the clock effect

Taking the general form of the cylindrically symmetric metric,

$$ds^2 = H(r)\,(dz^2 + dr^2) + L(r)\,d\phi^2 + 2\,M(r)\,d\phi\,dt - F(r)\,dt^2, \qquad (1)$$

where $-\infty < z < \infty$, $0 \le r < \infty$, $0 \le \phi \le 2\pi$ and $FL + M^2 = r^2$, there are several useful formulae connected with the clock effect and derived in reference [43].

The proper time for the completion of one geodesic orbit is

$$\tau_i = \frac{2\pi s_i}{|\omega_i|}, \qquad (i = 1, 2), \qquad (2)$$

where s_i is defined by

$$s_i^2 = F - 2M\,\omega_i - L\omega_i^2, \tag{3}$$

and ω ($\equiv d\phi/dt$) is given by

$$\omega_i = \frac{\epsilon_i\, p - M'}{L'}, \qquad (\epsilon_1 = +1, \epsilon_2 = -1), \tag{4}$$

$$p = (F'L' + (M')^2)^{1/2} \tag{5}$$

and dashes denote differentiation with respect to r. The clock effect is

$$\Delta\tau = \tau_2 - \tau_1 \tag{6}$$

and it turns out to be convenient to work with the squares of τ_1 and τ_2 in the form

$$\tau_2^2 - \tau_1^2 = 16\pi^2\,\frac{p(F'M - FM')}{(F')^2}. \tag{7}$$

Transformations to rotating coordinate systems (shown barred) are such that

$$\phi = \bar{\phi} + \Omega\bar{t},\ t = \bar{t},\ z = \bar{z},\ r = \bar{r}, \tag{8}$$

and Ω is a constant. The metric coefficients in the transformed system are

$$\bar{L} = L,\ \bar{M} = M + \Omega L,\ \bar{F} = F - 2\Omega M - \Omega^2 L. \tag{9}$$

From equation (7), a non-zero clock effect will be reduced to zero in a rotating coordinate system provided that in the rotating coordinates

$$\bar{F}'\bar{M} - \bar{F}\bar{M}' = \Omega^2(L'M - LM') + \Omega(F'L - FL') + (F'M - FM') = 0. \tag{10}$$

The roots of (10) give Ω for transformation to frames of zero clock effect (ZCE) and the roots are real if

$$(F'L - FL')^2 \geq 4(L'M - LM')(F'M - FM'). \tag{11}$$

This expression can be re-arranged to get

$$(FL + M^2)'^2 \geq 4(FL + M^2)(F'L' + (M')^2). \tag{12}$$

In light of the coordinate condition $FL + M^2 = r^2$ and the definition of p from (5), it follows that the roots are real if

$$p^2 \leq 1. \tag{13}$$

Since Ω in transformation (8) is a constant, if the roots of (10) are r-dependent, the analysis holds only at $r = r_1$ where r_1 is fixed.

7.3 The clock effect in van Stockum spacetime

7.3.1 Dust interior

The van Stockum interior in co-rotating coordinates has

$$L = r^2(1 - a^2 r^2),\ M = ar^2,\ F = 1. \tag{14}$$

Using (3) with (4) and (5) we find that

$$p^2 = 4a^2 r^2,\ s_1{}^2 = 1,\ s_2{}^2 = \frac{(1 - 4a^2 r^2)}{(1 - 2a^2 r^2)^2}, \tag{15}$$

so that the clock effect in the interior is defined only for $ar < 1/2$. Dust cylinders with $aR < 1/2$ are sources for case I spacetimes. Since such cylinders have $p^2 < 1$, they have coordinate frames of ZCE. Furthermore, we find that, in co-rotating coordinates,

$$\tau_1 = \infty,\ \tau_2 = \frac{\pi(1 - 4a^2 r^2)^{1/2}}{a}, \tag{16}$$

and the clock effect for the interior is then infinite.

From (10) and (14), transformation of the interior metric to coordinate systems of ZCE at any particular $r = r_1$ requires

$$\Omega_{ZCE} = \frac{-\left(1 - 2a^2 r_1{}^2 \pm (1 - 4a^2 r_1{}^2)^{1/2}\right)}{2a^3 r_1{}^4.} \tag{17}$$

It might be expected that the locally non-rotating frame (LNRF) would be a frame of ZCE. However, we saw in Section 4.1 that in the LNRF, the angular velocity of the dust is

$$\omega = \frac{a}{1 - a^2 r_1^2}, \tag{18}$$

so that the transformation from the co-rotating frame to the LNRF requires

$$\Omega_{LNRF} = \frac{-a}{1 - a^2 r_1^2} \neq \Omega_{ZCE}. \tag{19}$$

7.3.2 Vacuum exterior

The van Stockum exterior clock effect is defined only in case I. The case I metric coefficients in the rest frame of the dust particles may be written

$$L = \frac{R^2\left((2n+1)^3 y^{2n+1} + (2n-1)^3 y^{1-2n}\right)}{16n},$$

$$M = \frac{aR^2\left((2n+1) y^{2n+1} + (2n-1) y^{1-2n}\right)}{4n}, \tag{20}$$

$$F = \frac{(2n-1) y^{2n+1} + (2n+1) y^{1-2n}}{4n},$$

where

$$y = \frac{r}{R}, \quad n = \frac{1}{2}\sqrt{1-4a^2R^2}\ , \quad \frac{1}{4} > n^2 > 0. \tag{21}$$

Substituting these into Equation (7) gives

$$\tau_2^{\,2} - \tau_1^{\,2} = \frac{256\pi^2 n^2 r R}{(1-4n^2)(y^{2n} - y^{-2n})^2}, \tag{22}$$

which is non-zero for all n in the range.

Using (10), two values of Ω give frames of ZCE. One is indeterminate in the flat space limit and the other is

$$\Omega_{ZCE} = \frac{-4a}{(1+2n)^2}, \tag{23}$$

which is constant. Thus in the transformed frame, and in contrast with the interior, the clock effect is zero for all $r > R$. From equations (9), (20) and (23), the metric coefficients become

$$\bar{L} = L, \ \bar{M} = -\frac{(1-2n)^{3/2} r\left(\frac{r}{R}\right)^{-2n}}{(2n+1)^{3/2}}, \ \bar{F} = \frac{16n\left(\frac{r}{R}\right)^{1-2n}}{(2n+1)^3}, \tag{24}$$

and comparison with Section 5.4 shows that the frame of ZCE is also the astronomical rest frame. The transformation from co-rotating coordinates to the LNRF in case I is given by

$$\Omega_{\mathrm{LNRF}} = \frac{16(1-2n)^{3/2}n}{(2n+1)^{3/2}\left((2n+1)^3\left(\frac{r_1}{R}\right)^{4n}+(2n-1)^3\right)R}, \tag{25}$$

which, as with the interior, differs from Ω_{ZCE} and is valid only at $r = r_1$. This is the justification for saying that the astronomical rest frame has the better claim to be called non-rotating.

~ Chapter 8 ~

Conclusion

Work for this thesis involved the plotting of geodesics and the analysis of interesting features of the plots. The use of a computer to plot geodesics is far from being a new technique but the methods employed here, involving proprietary software and a personal computer, are readily available to any interested researcher.

Whilst Bonnor's remark that "...in the book of exact solutions one finds many whose physical meaning is unknown or only partially understood" still holds true, some progress has been made with two exact solutions, and the technique of geodesic plotting is applicable to many others.

In addition to the elaboration of existing results on interior geodesics in the van Stockum solution, it was shown that, in the case III exterior, all null geodesics originating at the surface of the dust cylinder are radially confined. These results will be of use if ever the solution is found to be applicable to an astrophysical situation.

In Bonnor's dust cloud solution, the existence of a peculiar central toroidal region was demonstrated. This 'central separate zone' cannot be penetrated by inwards-going geodesics and outwards-going geodesics from the region are closely confined to its locality. The dust cloud solution, being asymptotically flat in all directions, may well find a use in astrophysics.

Work on the clock effect is important since it may soon be possible to look for the effect experimentally, giving another test of general relativity in the solar system. Results obtained here, concerning the reference frame for measurements, could have relevance to such tests.

Concerning further research, the rotating dust cloud is a promising subject. With the van Stockum vacuum metric, it shares the phenomenon of the ϕ coordinate being timelike in some regions, in the co-rotating frame. Unlike the van Stockum solution, no convenient coordinate transformation has yet been found to enable the plotting of geodesics starting anywhere in the dust cloud. Dealing with regions in which the rôles of

the ϕ and t coordinates is reversed seems to be a little-researched topic. The central separate zone shares some of the characteristics of both black holes and white holes without being either, but the surface of the zone is not an event horizon. The nature of the central singularity is still uncertain. A clue to the nature of the dust cloud solution may lie in the motion of charged particles in the field of a magnetic dipole (the Störmer effect) [44, 45]. The similarity with the distribution of null geodesics in the dust cloud is remarkable.

~ Appendix 1 ~

Solving geodesic equations with *Mathematica*

This appendix shows how geodesic equations and initial conditions can be written in a form suitable for use by *Mathematica*. An example of a file containing metric functions is 'schwout.m' for the Schwarzschild metric. Such files may contain not only the g_{ik} but the Γ^{l}_{jk}, and components of the Ricci, Riemann, Weyl and Einstein tensors for use elsewhere. These may all be calculated from the metric tensor using *MathTensor* software.

A.1.1 Schwarzschild *Mathematica* expressions

The geodesic equations are re-written so that $\dot{t} \to p$, $\dot{r} \to q$ and $\dot{\phi} \to k$ and then put into a file called 'geo[schwarz-trϕ]' which is in a form suitable for *Mathematica*. The file is bracketed together with the definitions $G = 1$, $M = 1$ and the command to call the file 'schwout.m' which contains the metric functions for the Schwarzschild exterior.

$$\{G = 1,\ M = 1,\ <<\ \text{schwout.m},\ \text{geo[schwarz} - \text{tr}\phi\text{][p\_, q\_, k\_, t\_, r\_, }\phi\text{\_}] :=$$

$$\left\{p,\ q,\ k,\ \frac{2GMpq}{2GMr - r^2},\ \frac{2G^2M^2p^2}{r^3} + k^2 r + \right. \tag{1}$$

$$\left. GM\left(-2k^2 - \frac{p^2}{r^2} + \frac{q^2}{-2GMr + r^2}\right),\ -\frac{2kq}{r}\right\}\};$$

The next expression contains the *Mathematica* routine 'solvelight3A' which will solve the geodesic equations once the initial conditions have been specified. The dashes indicate differentiation with respect to the affine parameter and the precision of the numerical solution may also be specified here. The general expressions for the initial conditions are also defined.

$$\{\{A_0 = \text{Apart}[\text{Metricg}[-4, -4] /. r \to \text{r0}],\ B_0 = \text{Apart}[-\text{Metricg}[-1, -1] /. r \to \text{r0}]\},$$

$$\text{solvelight3A}[x\_,\ b\_:0,\ \{t0\_:0,\ r0\_:0,\ \phi0\_:0\},\ \{\alpha0\_\},\ \text{stop}\_] :=$$

$$\text{Flatten}[\text{Map}[\text{NDSolve}[\#,\ \{t, r, \phi\},\ \{T, 0, \text{stop}\},$$

$$\text{AccuracyGoal} \to 6,\ \text{PrecisionGoal} \to 6,\ \text{WorkingPrecision} \to 16,$$

$$\text{MaxSteps} \to 500]\&,\ \{\text{Join}[\text{MapThread}[\text{Equal},\ \{\{t'[T],\ r''[T],\ \phi''[T]\},$$

$$\text{Take}[\text{geo}[x][t'[T],\ r'[T],\ \phi'[T],\ t[T],\ r[T],\ \phi[T]],\ \{4, 6\}]]],\ \{t[b] == \text{t0},\ r[b] == \text{r0},\ \phi[b] == \phi0,$$

$$t'[b] == \frac{\lambda}{\sqrt{A_0}},\ \phi'[b] == \frac{\lambda v \,\text{Sin}[\alpha0]}{\text{r0}},\ r'[b] == \frac{\lambda v \,\text{Cos}[\alpha0]}{\sqrt{B_0}}\}\}], 1]\};$$

Entering one of the following two lines selects either timelike or null geodesics and resets any initial conditions which may have been entered previously.

$$\{\text{Null geodesic},\ \{\text{r0} =.,\ \alpha0 =.,\ \lambda = 1\}\};$$

$$\{\text{Timelike geodesic},\ \{\text{r0} =.,\ \alpha0 =.,\ \lambda = \frac{1}{\sqrt{1 - v^2}}\}\}; \tag{3}$$

Finally, initial conditions and required length (in terms of the affine parameter) are specified for a particular geodesic, and the equations are solved.

$$\{v = 0.1,\ \text{r0} = 10,\ \alpha0 = \pi/4,\ \text{t0} = 0,\ \phi0 = 0,\ \text{time} = 10,$$
$$\text{sd1} = \text{solvelight3A}[\text{schwarz} - \text{tr}\phi,\ 0,\ \{\text{t0},\ \text{r0},\ \phi0\},\ \{\alpha0\},\ \text{time}]\}; \tag{4}$$

The file containing the data for the geodesic is called 'sd1'. By referring to this file, a simple command to plot radial coordinate r against the parameter T could be:

$$\text{ParametricPlot}[\text{Evaluate}[\{T, r[T]\} /. \text{sd1}],\ \{T,\ 0,\ \text{time}\}]; \tag{5}$$

A.1.2 Kerr *Mathematica* expressions

The geodesic equations for the Kerr metric, in the file called 'geo[kerr-tr$\theta\phi$]', are much lengthier, even when written symbolically. The explicit equations are calculated only when the expression is used, and are not seen on the computer screen.

$$\Big\{M = 1,\ a = 1,\ \text{theta} = \theta,\ \text{phi} = \phi,\ \text{<< kerrout.m, geo[kerr} - \text{tr}\theta\phi\text{][p\_, q\_, j\_, k\_, t\_, r\_, } \theta\text{\_, } \phi\text{\_]} =$$

$$\text{Apart}\Big[\Big\{p,\ q,\ j,\ k,\ (-J[r,\theta]\,(j\,k\,F^{(0,1)}[r,\theta] + j\,p\,J^{(0,1)}[r,\theta] + k\,q\,F^{(1,0)}[r,\theta] + p\,q\,J^{(1,0)}[r,\theta]) +$$

$$F[r,\theta]\,(j\,k\,J^{(0,1)}[r,\theta] + j\,p\,K^{(0,1)}[r,\theta] + k\,q\,J^{(1,0)}[r,\theta] + p\,q\,K^{(1,0)}[r,\theta]))\,/$$

$$(J[r,\theta]^2 - F[r,\theta]\,K[r,\theta]),$$

$$\frac{1}{2\,A[r,\theta]}\,(-2\,j\,q\,A^{(0,1)}[r,\theta] - q^2\,A^{(1,0)}[r,\theta] +$$

$$j^2\,B^{(1,0)}[r,\theta] + k^2\,F^{(1,0)}[r,\theta] + 2\,k\,p\,J^{(1,0)}[r,\theta] + p^2\,K^{(1,0)}[r,\theta]),$$

$$\frac{1}{2\,B[r,\theta]}\,(q^2\,A^{(0,1)}[r,\theta] - j^2\,B^{(0,1)}[r,\theta] +$$

$$k^2\,F^{(0,1)}[r,\theta] + 2\,k\,p\,J^{(0,1)}[r,\theta] + p^2\,K^{(0,1)}[r,\theta] - 2\,j\,q\,B^{(1,0)}[r,\theta]),$$

$$(K[r,\theta]\,(j\,k\,F^{(0,1)}[r,\theta] + j\,p\,J^{(0,1)}[r,\theta] + k\,q\,F^{(1,0)}[r,\theta] + p\,q\,J^{(1,0)}[r,\theta]) -$$

$$J[r,\theta]\,(j\,k\,J^{(0,1)}[r,\theta] + j\,p\,K^{(0,1)}[r,\theta] + k\,q\,J^{(1,0)}[r,\theta] + p\,q\,K^{(1,0)}[r,\theta]))\,/$$

$$(J[r,\theta]^2 - F[r,\theta]\,K[r,\theta])\Big\}\,/.$$

$$\{A[r,\theta] \to \text{Metricg}[-1,-1],\ B[r,\theta] \to \text{Metricg}[-2,-2],$$

$$F[r,\theta] \to \text{Metricg}[-3,-3],\ J[r,\theta] \to \text{Metricg}[-4,-3],\ K[r,\theta] \to \text{Metricg}[-4,-4],$$

$$A^{(1,0)}[r,\theta] \to D[\text{Metricg}[-1,-1], r],\ B^{(1,0)}[r,\theta] \to D[\text{Metricg}[-2,-2], r],$$

$$F^{(1,0)}[r,\theta] \to D[\text{Metricg}[-3,-3], r],\ J^{(1,0)}[r,\theta] \to D[\text{Metricg}[-4,-3], r],$$

$$K^{(1,0)}[r,\theta] \to D[\text{Metricg}[-4,-4], r],\ A^{(0,1)}[r,\theta] \to D[\text{Metricg}[-1,-1], \theta],$$

$$B^{(0,1)}[r,\theta] \to D[\text{Metricg}[-2,-2], \theta],\ F^{(0,1)}[r,\theta] \to D[\text{Metricg}[-3,-3], \theta],$$

$$J^{(0,1)}[r,\theta] \to D[\text{Metricg}[-4,-3], \theta],\ K^{(0,1)}[r,\theta] \to D[\text{Metricg}[-4,-4], \theta]\}\Big]\Big\};$$

The *Mathematica* routine 'solve4' will solve the geodesic equations once the initial conditions have been specified. The general expressions for the initial conditions are defined.

$$\Big\{\{A_0 = \text{Apart}[\text{Metricg}[-1,-1]\,/.\,\{r \to \text{r0},\ \theta \to \theta 0\}],$$

$$B_0 = \text{Apart}[\text{Metricg}[-2,-2]\,/.\,\{r \to \text{r0},\ \theta \to \theta 0\}],$$

$$F_0 = \text{Apart}[\text{Metricg}[-3,-3]\,/.\,\{r \to \text{r0},\ \theta \to \theta 0\}],$$

$$J_0 = \text{Apart}[\text{Metricg}[-4,-3]\,/.\,\{r \to \text{r0},\ \theta \to \theta 0\}],$$

$$K_0 = \text{Apart}[\text{Metricg}[-4,-4]\,/.\,\{r \to \text{r0},\ \theta \to \theta 0\}]\},$$

```
solve4[x_, b_:0, {t0_:0, r0_:0, θ0_:0, φ0_:0}, {α0_, β0_}, stop_] :=
Flatten[(NDSolve[#1, {t, r, θ, φ}, {T, 0, stop}, AccuracyGoal -> 8,
PrecisionGoal -> 8, WorkingPrecision -> 16, MaxSteps → 500]&)/@
{Join[MapThread[Equal, {{t''[T], r''[T], θ''[T], φ''[T]},
Take[geo[x][t'[T], r'[T], θ'[T], φ'[T], t[T], r[T], θ[T], φ[T]], {5, 8}]}],
{t[b] == t0, r[b] == r0, θ[b] == θ0, φ[b] == φ0,
t'[b] == λ Sqrt[F0]/Sqrt[J0^2 - F0 K0], φ'[b] == λ(v Sin[α0] Cos[β0] - J0/Sqrt[J0^2 - F0 K0])/Sqrt[F0],
r'[b] == v λ Cos[α0] Cos[β0]/Sqrt[A0], θ'[b] == -v λ Sin[β0]/Sqrt[B0]}], 1]};
```

A.1.3 van Stockum *Mathematica* expressions

The van Stockum geodesic equations, for a hypersurface of z = constant, in the file called 'geo[vanS-trϕ]'.

```
{{c = 1, a = 1/4, R = 1, n = Sqrt[1 - 4 a^2 R^2]/2, ri = R,
χ = R Cosh[n Log[ri/R]]^2/ri, << vsastout.m, geo[vanS - trφ][p_, j_, k_, t_, r_, φ_] =
Apart[{p, j, k, -(j (L[r] (p F'[r] - k M'[r]) M[r] (k L'[r] +
p M'[r])))/(F[r] L[r] + M[r]^2), -(p^2 F'[r] + j^2 H'[r] - k (k L'[r] + 2 p M'[r]))/(2 H[r]),
-(j (M[r] (-p F'[r] + k M'[r]) + F[r] (k L'[r] + p M'[r])))/(F[r] L[r] + M[r]^2)} /.
{H[r] -> Metricg[-1, -1], L[r] -> Metricg[-3, -3], M[r] -> Metricg[-4, -3],
F[r] -> -Metricg[-4, -4], H'[r] -> D[Metricg[-1, -1], r],
L'[r] -> D[Metricg[-3, -3], r], M'[r] -> D[Metricg[-4, -3], r],
F'[r] -> D[-Metricg[-4, -4], r]}]};
```

(8)

The *Mathematica* routine 'solve3' which will solve the geodesic equations once λ and the initial conditions have been specified.

$$\Big\{\{H_0 = \text{Apart[Metricg[}-1, -1\text{]} /. r \text{ -> r0]}, L_0 = \text{Apart[Metricg[}-3, -3\text{]} /. r \text{ -> r0]},$$

$$M_0 = \text{Apart[Metricg[}-4, -3\text{]} /. r \text{ -> r0]}, F_0 = \text{Apart[}-\text{Metricg[}-4, -4\text{]} /. r \text{ -> r0]}\},$$

$$\text{solve3[x\_, b\_: 0, \{t0\_: 0, r0\_: 0, } \phi\text{0\_: 0\}, \{}\alpha\text{0\_\}, stop\_] :=$$

$$\text{Flatten}\Big[(\text{NDSolve[\#1, } \{t, r, \phi\}, \{T, 0, \text{stop}\}, \text{ AccuracyGoal -> 6,}$$

$$\text{PrecisionGoal -> 6, WorkingPrecision -> 16, MaxSteps} \to 500]\&)/@$$

$$\Big\{\text{Join}\Big[\text{MapThread[Equal,}$$

$$\{t''[T], r''[T], \phi''[T]\}, \text{Take[geo}[x][t'[T], r'[T], \phi'[T], t[T], r[T], \phi[T]], \{4, 6\}]\Big],$$

$$\Big\{t[b] == \text{t0}, r[b] == \text{r0}, \tag{9}$$

$$\phi[b] == \phi\text{0}, t'[b] == \text{tl}\,\lambda\,\frac{\sqrt{L_0}}{\text{r0}\sqrt{\chi}} + \text{sl}\,\lambda\,\frac{v\,\text{Sin}[\alpha\text{0}] - M_0/(\text{r0}\sqrt{\chi})}{\sqrt{-F_0}},$$

$$\phi'[b] == \text{tl}\,\lambda\,\frac{v\,\text{Sin}[\alpha\text{0}] - M_0/(\text{r0}\sqrt{\chi})}{\sqrt{L_0}} + \text{sl}\,\lambda\,\frac{\sqrt{-F_0}}{\text{r0}\sqrt{\chi}},$$

$$r'[b] == \lambda\, v\,\frac{\text{Cos}[\alpha\text{0}]}{\sqrt{H_0}}\Big\}\Big]\Big\}, 1\Big]\Big\};$$

A.1.4 *Mathematica* expressions for the rotating dust cloud

Dust cloud geodesic equations in the file called 'geo[cloud-zrϕt]'.

$$\Big\{h = 1, \text{<< cloudout.m, geo[cloud} - \text{zr}\phi\text{t][p\_, q\_, j\_, k\_, z\_, r\_, } \phi\text{\_, t\_] =}$$

$$\text{Apart}\Big[\Big\{p, q, j, k, \frac{1}{2H[r,z]}(-k^2 F^{(0,1)}[r,z] +$$

$$(-p^2 + q^2) H^{(0,1)}[r,z] + j^2 L^{(0,1)}[r,z] + 2jk M^{(0,1)}[r,z] - 2pq H^{(1,0)}[r,z]),$$

$$\frac{1}{2H[r,z]}(-2pq H^{(0,1)}[r,z] - k^2 F^{(1,0)}[r,z] +$$

$$p^2 H^{(1,0)}[r,z] - q^2 H^{(1,0)}[r,z] + j^2 L^{(1,0)}[r,z] + 2jk M^{(1,0)}[r,z]),$$

$$(M[r,z](kpF^{(0,1)}[r,z] - jpM^{(0,1)}[r,z] + kqF^{(1,0)}[r,z] - jqM^{(1,0)}[r,z]) -$$

$$F[r,z](jpL^{(0,1)}[r,z] + kpM^{(0,1)}[r,z] + jqL^{(1,0)}[r,z] + kqM^{(1,0)}[r,z]))/$$

$$(F[r, z]\,L[r, z] + M[r, z]^2),$$

$$(L[r, z]\,(-k\,p\,F^{(0,1)}[r, z] + j\,p\,M^{(0,1)}[r, z] - k\,q\,F^{(1,0)}[r, z] + j\,q\,M^{(1,0)}[r, z]) -$$

$$M[r, z]\,(j\,p\,L^{(0,1)}[r, z] + k\,p\,M^{(0,1)}[r, z] + j\,q\,L^{(1,0)}[r, z] + k\,q\,M^{(1,0)}[r, z]))/$$

$$(F[r, z]\,L[r, z] + M[r, z]^2)\Big\}/.$$

$$\{H[r, z] \to \text{Metricg}[-1, -1],\ L[r, z] \to \text{Metricg}[-3, -3],$$

$$M[r, z] \to \text{Metricg}[-4, -3],\ F[r, z] \to -\text{Metricg}[-4, -4],$$

$$H^{(1,0)}[r, z] \to D[\text{Metricg}[-1, -1], r],\ L^{(1,0)}[r, z] \to D[\text{Metricg}[-3, -3], r],$$

$$M^{(1,0)}[r, z] \to D[\text{Metricg}[-4, -3], r],\ F^{(1,0)}[r, z] \to D[-\text{Metricg}[-4, -4], r],$$

$$H^{(0,1)}[r, z] \to D[\text{Metricg}[-1, -1], z],\ L^{(0,1)}[r, z] \to D[\text{Metricg}[-3, -3], z],$$

$$M^{(0,1)}[r, z] \to D[\text{Metricg}[-4, -3], z],\ F^{(0,1)}[r, z] \to D[-\text{Metricg}[-4, -4], z]\}\Big]\Big\};$$

The *Mathematica* routine 'solve4' which will solve the geodesic equations once λ and the initial conditions have been specified.

$$\Big\{\{H_0 = \text{Apart}[\text{Metricg}[-1, -1]\,/.\,\{r \to \text{r0}, z \to \text{z0}\}],$$

$$L_0 = \text{Apart}[\text{Metricg}[-3, -3]\,/.\,\{r \to \text{r0}, z \to \text{z0}\}],$$

$$M_0 = \text{Apart}[\text{Metricg}[-4, -3]\,/.\,\{r \to \text{r0}, z \to \text{z0}\}],$$

$$F_0 = \text{Apart}[-\text{Metricg}[-4, -4]\,/.\,\{r \to \text{r0}, z \to \text{z0}\}]\},$$

$$\text{solve4}[\text{x\_}, \text{b\_}: 0, \{\text{z0\_}: 0, \text{r0\_}: 0, \phi 0\_: 0, \text{t0\_}: 0\},$$

$$\{\alpha 0\_, \beta 0\_\}, \text{stop\_}] := \text{Flatten}\Big[(\text{NDSolve}[\#1, \{z, r, \phi, t\},$$

$$\{T, 0, \text{stop}\}, \text{AccuracyGoal} \to 8, \text{PrecisionGoal} \to 8,$$

$$\text{WorkingPrecision} \to 16, \text{MaxSteps} \to 2000]\&)/@ \qquad (11)$$

$$\Big\{\text{Join}\Big[\text{MapThread}[\text{Equal}, \{\{z''[T], r''[T], \phi''[T], t''[T]\},$$

$$\text{Take}[\text{geo}[x][z'[T], r'[T], \phi'[T], t'[T], z[T], r[T], \phi[T], t[T]], \{5, 8\}]\}],$$

$$\Big\{z[b] == \text{z0},\ r[b] == \text{r0},\ \phi[b] == \phi 0,\ t[b] == \text{t0},$$

$$z'[b] == \frac{\nu\lambda\,\text{Sin}[\beta 0]}{\sqrt{H_0}},\ r'[b] == \frac{\nu\lambda\,\text{Cos}[\alpha 0]\,\text{Cos}[\beta 0]}{\sqrt{H_0}},$$

$$\phi'[b] == \frac{\lambda\,(\nu\,\text{Sin}[\alpha 0]\,\text{Cos}[\beta 0] - M_0/\text{r0})}{\sqrt{L_0}},\ t'[b] == \lambda\,\frac{\sqrt{L_0}}{\text{r0}}\Big\}\Big]\Big\},\ 1\Big]\Big\};$$

~ Appendix 2 ~

The electric and magnetic Weyl tensors

In recent years there has been considerable interest in the so-called electric and magnetic parts of the Weyl tensor with view to helping in the interpretation of exact solutions. See, for example, [29,30] for recent papers. This analysis was mentioned in Chapter 5, with regard to the van Stockum metric. We begin with an outline description of the Weyl tensor.

In four dimensions, the Riemann tensor R_{abcd} has twenty independent components. Amongst other symmetry properties,

$$R_{abcd} = -R_{bacd} \text{ and } R_{abcd} = -R_{abdc}, \tag{1}$$

so the trace of the Riemann tensor over the first and second and over the third and fourth indices vanishes. On the other hand, the trace over the first and third or over the second and fourth indices defines the Ricci tensor, for example

$$g^{ac} R_{abcd} = R^{c}{}_{bcd} = R_{bd}. \tag{2}$$

Because of these symmetries, the Riemann tensor may be split into a trace free part and a trace part,

$$R_{abcd} = C_{abcd} + \frac{1}{2}(g_{ac}R_{bd} + g_{bd}R_{ca} - g_{ad}R_{cb} - g_{bc}R_{da}) + \frac{R}{6}(g_{ad}g_{cb} - g_{ac}g_{db}). \tag{3}$$

C_{abcd} is the Weyl tensor and it has all the symmetry properties of the Riemann tensor in addition to being trace free,

$$C^{c}{}_{bcd} = 0. \tag{4}$$

Since the Ricci tensor is given by Einstein's field equations

$$R_{ab} - \frac{1}{2}g_{ab}R = 8\pi T_{ab}, \tag{5}$$

in a vacuum, where $R_{ab} = 0$,

$$C_{abcd} = R_{abcd}. \tag{6}$$

Thus the Weyl tensor is that part of the curvature not determined locally by the matter distribution.

A.2.1 Electric and Magnetic Weyl Tensors, Petrov classification and invariants

The algebraic properties of the Weyl tensor may be used to rank spacetimes according to the Petrov classification. There is an analogy between this scheme and the classification of the electromagnetic field into wave and non-wave types using the invariants of the electromagnetic field tensor. See, for example, Landau and Lifshitz [31]. The analogy is not complete, however, since the Petrov classification gives five types of gravitational field.

The electric and magnetic Weyl tensors are defined [32], for an observer with a timelike velocity vector u, as

$$E_{ac} = C_{abcd}u^b u^d, \quad H_{ac} = \frac{1}{2}\varepsilon_{cdef}C_{ab}^{ef}u^b u^d,$$
$$\text{where } E_{ac} = E_{ca},\ E^a{}_a = 0,\ E_{ac}u^c = 0,\ H_{ac} = H_{ca},\ H^a{}_a = 0, \qquad (7)$$
$$H_{ac}u^c = 0,$$

and ε_{abcd} is the completely alternating unit tensor. Thus the complex Weyl tensor

$$C^*_{abcd} = C_{abcd} + \frac{1}{2}i\varepsilon_{cdef}C_{ab}^{ef}, \qquad (8)$$

may be characterised by

$$-Q_{ac} = C^*_{abcd}u^b u^d = E_{ac} + iH_{ac}, \qquad (9)$$

where

$$Q_{ac} = Q_{ca},\ Q^a{}_a = 0,\ Q_{ac}u^c = 0. \qquad (10)$$

In the frame of the observer, $u^a = (0, 0, 0, 1)$ and Q_{ab} can be written as a three-dimensional tensor $-Q_{\alpha\beta} = C^*_{\alpha 4\beta 4}$, where $\alpha, \beta = (1,2,3)$. The components of $Q_{\alpha\beta}$ form a (3 x 3) symmetric complex matrix $\boldsymbol{Q}$ and hence we have the eigenvector equation

$$\boldsymbol{Q}\boldsymbol{v} = \lambda\boldsymbol{v}. \qquad (11)$$

The number of independent eigenvectors (one, two or three) gives three of the Petrov types, possible degeneracy of the eigenvalues giving the remaining two.

Bonnor [30] considered the two invariants L and M, each formed from the electric and magnetic parts of the Weyl tensor,

$$L = E^{ab}E_{ab} - H^{ab}H_{ab}, \quad M = E^{ab}H_{ab}, \tag{12}$$

remarking on their resemblance to the invariants $\boldsymbol{E}^2 - \boldsymbol{H}^2$ and $\boldsymbol{E}.\boldsymbol{H}$ of electromagnetism.

A.2.2 Electric and Magnetic spacetimes

In vacuum spacetimes, if a timelike unit vector u can be found such that $H_{ab} = 0$ then the spacetime is said to be purely electric. Similarly, if u can be found such that $E_{ab} = 0$, the spacetime is said to be purely magnetic. Note that $E_{ab} + H_{ab} = 0 \Rightarrow$ flat spacetime.

In fluid-dynamic spacetimes, the four-velocity is conventionally chosen for u. There are spacetimes however, where using the four-velocity for u results in mixed spacetimes, ie. $E_{ab} \neq 0$ and $H_{ab} \neq 0$, whereas vectors can be found that make the same spacetimes purely electric in some region. The van Stockum interior and Gödel inhomogeneous metrics are examples of this kind. In other non-vacuum spacetimes, the choice of u is open.

The idea of the scheme is the possibility of being able to associate physical characteristics, for example the presence of gravitational radiation, with different kinds of Weyl tensor in trying to give physical interpretation to solutions of the field equations. For example, Bruni et al [33] suggested that $H_{ab} = 0$ implies absence of gravitational radiation. Bonnor [30] showed that in Petrov type N and type III spacetimes $E^{ab}E_{ab} = H^{ab}H_{ab} > 0$, supporting the existing view that type III spacetimes contain gravitational radiation. However, the attempted association of the electric/magnetic nature of the Weyl tensor with physical characteristics remains problematic. For instance, there are counter-examples [14, 15] to the conjecture that rotation contributes to H_{ab} and there are non-rotating spacetimes that have non-zero H_{ab}.

A.2.3 Electric and Magnetic spacetimes: the van Stockum solution

Calculations with the Weyl tensor are readily carried out using *Mathematica* and *MathTensor* software. For the van Stockum interior in the co-rotating coordinate frame the line element is,

$$ds^2 = \exp(-a^2 r^2)(dz^2 + dr^2) + r^2 (1 - a^2 r^2) d\phi^2 + 2\, a\, r^2\, d\phi\, dt - dt^2. \tag{13}$$

Using the four-velocity

$$u^a = (0, 0, 0, 1), \tag{14}$$

the electric and magnetic parts of the Weyl tensor are given by

$$E_{ab} = \begin{pmatrix} -\frac{2}{3}a^2 & 0 & 0 & 0 \\ 0 & \frac{1}{3}a^2 & 0 & 0 \\ 0 & 0 & \frac{1}{3}a^2 \exp(a^2 r^2) r^2 & 0 \\ 0 & 0 & 0 & 0 \end{pmatrix},$$

$$H_{ab} = \begin{pmatrix} 0 & -a^3 r & 0 & 0 \\ -a^3 r & 0 & 0 & 0 \\ 0 & 0 & 0 & 0 \\ 0 & 0 & 0 & 0 \end{pmatrix} \tag{15}$$

Thus the Weyl tensor is mixed electric and magnetic and the idea of rotation contributing to H_{ab} is supported. However, by putting $u^a = (0, 0, x, y)$, then solving the simultaneous equations

$$\{g_{ab}\, u^a\, u^b = -1,\ H_{ab} = 0\} \tag{16}$$

for x and y, it turns out that the timelike unit vector

$$u^a = \chi\left(0, 0, \sqrt{2}\, a, \frac{1}{\sqrt{2}}\left(1 + 2a^2 r^2 + \sqrt{1 - 4a^2 r^2}\right)\right),$$

$$\text{where } \chi = \left(\sqrt{1 - 4a^2 r^2 + \sqrt{1 - 4a^2 r^2}}\right)^{-1} \tag{17}$$

gives

$$-E_{11} = E_{22} = \frac{1}{6}a^2\left(3\sqrt{1-4a^2r^2}-1\right),$$

$$E_{33} = \frac{a^2\exp(a^2r^2)r^2\left(2a^2r^2+\sqrt{1-4a^2r^2}+1\right)^2}{6\left(1-4a^2r^2+\sqrt{1-4a^2r^2}\right)},$$

$$E_{44} = \frac{2a^4\exp(a^2r^2)r^2}{3\left(1-4a^2r^2+\sqrt{1-4a^2r^2}\right)},$$

$$E_{34} = E_{43} = \frac{a^3\exp(a^2r^2)r^2\left(4a^2r^2+3\sqrt{1-4a^2r^2}-1\right)}{24a^2r^2-6},$$

$$\text{all other } E_{ab} = 0,$$

and

$$H_{ab} = 0. \tag{19}$$

Noting that the vector u in (17) is timelike and of unit length only for $ar < 1/2$, the interior in this case could be classed as electric. This was first shown by Bonnor [30] and is of interest in light of his demonstration [5] that the exterior with $aR < 1/2$ may be rendered 'locally static', albeit only by using a periodic time coordinate in the transformation.

~ Appendix 3 ~

The cumulative drag index

A.3.1 Definition of the drag index

The cumulative drag index is a parameter defined recently by Prasanna [34] and generalised by Prasanna and Iyer [16]. It characterises intrinsic features of stationary axisymmetric spacetimes by considering the forces acting on both co- and counter-orbiting test particles. The index is given by

$$C = \frac{(Cf + Co - G)}{(Cf + Co + G)}, \tag{1}$$

where Cf, Co and G are the centrifugal, Coriolis and gravitational accelerations respectively which act on a test particle in circular orbit in a stationary axisymmetric spacetime. The index is made possible by a covariant definition of inertial forces in general relativity for static spacetimes by Abramowicz et al [35] which they recently extended to general spacetimes [36].

It may seem a retrograde step to re-introduce the concept of force into gravitational theory when general relativity so successfully does away with the idea in favour of the curved spacetime description. However, the work of Abramowitcz and others has led to discoveries concerning centrifugal reversal, reversal of the Rayleigh stability criterion and ellipticity of certain contracting, rotating matter configurations amongst others [37] and may be relevant to some astrophysical situations [16]. Of particular relevance to this thesis is its applicability to both the van Stockum and rotating dust cloud solutions.

The drag index and the component accelerations may be readily calculated, analysed and plotted using *Mathematica* and *MathTensor* software. For the general axisymmetric metric,

$$ds^2 = g_{rr}\,dr^2 + g_{\theta\theta}\,d\theta^2 + g_{\phi\phi}\,d\phi^2 + 2\,g_{\phi t}\,d\phi\,dt + g_{tt}\,dt^2, \tag{2}$$

the components of the individual accelerations are given by

$$G^i = \frac{1}{2}\partial_i \log\left(\frac{g_{\phi t}^2 - g_{tt}\,g_{\phi\phi}}{g_{\phi\phi}}\right),$$

$$Co^i = -A^2(\Omega-\omega)\,g_{\phi\phi}\,\partial_i\left(\frac{g_{\phi t}}{g_{\phi\phi}}\right), \tag{3}$$

$$Cf^i = -\frac{A^2(\Omega-\omega)^2}{2}\,g_{\phi\phi}\,\partial_i \log\left(\frac{g_{\phi\phi}^2}{g_{\phi t}^2 - g_{tt}\,g_{\phi\phi}}\right),$$

where A is the redshift factor, Ω is the angular velocity of the test particle and ω is the angular velocity of the zero angular momentum observer who is thus in a fixed position with respect to the 'gravitational field'. A and ω are defined by

$$A^2 = -\frac{1}{(\Omega^2 g_{\phi\phi} + 2\,g_{\phi t}\,\Omega + g_{tt})},\quad \omega = -\frac{g_{\phi t}}{g_{\phi\phi}}. \tag{4}$$

A.3.2 The van Stockum interior

Since the van Stockum metric is cylindrically symmetric, only the radial components of the accelerations are non-zero. Substituting the metric coefficients into the general expressions gives the following values for the van Stockum interior,

$$C = \frac{2a^2 + 2\Omega a + (4a^4r^4 - 5a^2r^2 + 1)\Omega^2 - 6a^3r^2\Omega}{(a^2r^2-1)\,\Omega\,(2a(ar^2\Omega - 1) - \Omega)}, \tag{5}$$

$$G = \frac{a^2 r}{1 - a^2 r^2},$$

$$Co = -\frac{2a^3r^3(\omega-\Omega)}{(a^2r^2-1)(a^2\Omega^2r^4 - 2ar^2\Omega - r^2\Omega^2 + 1)}, \tag{6}$$

$$Cf = \frac{r(3a^2r^2-1)(\omega-\Omega)^2}{a^2\Omega^2r^4 - 2ar^2\Omega - r^2\Omega^2 + 1}.$$

It is clear from G and Co that the gravitational and Coriolis accelerations are infinite at $ar = 1$ which is another constraint on the interior metric indicating that we must have $ar < 1$. From the numerator of Cf we can see that there is an orbit of zero centrifugal force at $r = (a\sqrt{3})^{-1}$ and this is the radial coordinate at which the Weyl tensor is zero, as

described in Section 4.1.

The index C 'blows up' at $ar = 1$, as it does for test particles with

$$\Omega = 0, \quad \Omega = \frac{2a}{2a^2 r^2 - 1}. \tag{7}$$

This is because $(Cf + Co + G) = 0$ for those values of Ω, thus the test particles must be following circular geodesics. $\Omega = 0$ shows the angular momentum of the dust particles consituting the cylinder - the particles are at rest in the co-moving frame. The other value of Ω turns out to describe counter-rotating geodesics in agreement with the findings of Section 4.3.1, but here the results were found without having to solve the geodesic equations.

Plotting the drag index confirms these results. Since Ω is the angular velocity of test particles, it make sense to restrict the range of Ω so that it does not exceed the value for light. The speed of light may be obtained from the metric for the interior,

$$ds^2 = \exp(-a^2 r^2)(dz^2 + dr^2) + r^2 (1 - a^2 r^2) d\phi^2 + 2\ a\ r^2 d\phi\ dt - dt^2, \tag{8}$$

by setting $dz = dr = 0$ then solving for $ds^2 = 0$ to get $d\phi/dt$ for light moving tangentially to circular orbits. This gives

$$\left(\frac{d\phi}{dt}\right)_1 = \frac{1}{ar^2 + r}, \quad \left(\frac{d\phi}{dt}\right)_2 = \frac{1}{ar^2 - r}. \tag{9}$$

Putting $a = 1$ and $r = 1/4$ gives a plot where the infinities show the dust particle geodesic with $\Omega = 0$ and a test particle geodesic with $\Omega = -16/7$.

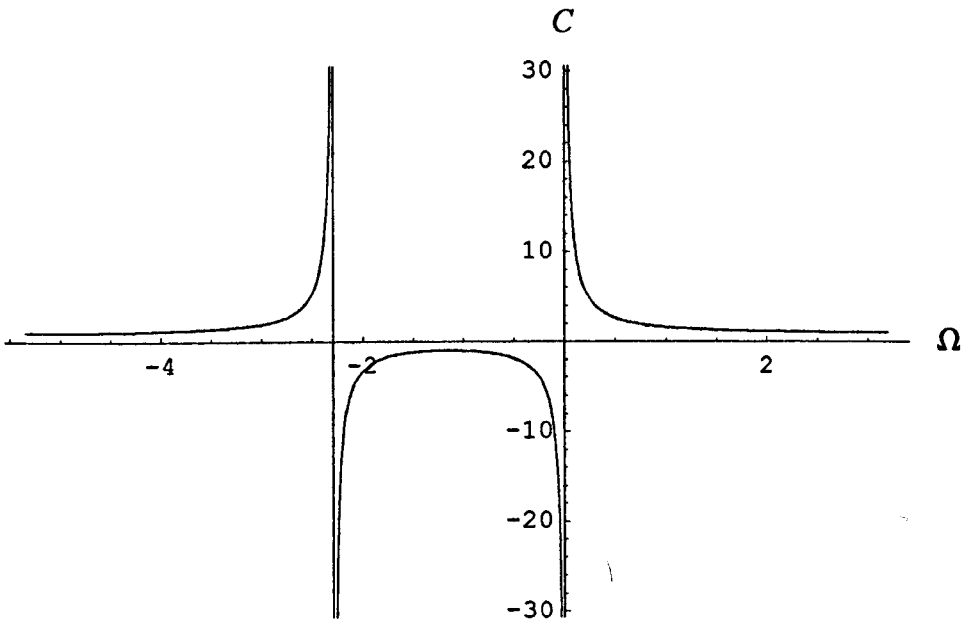

Figure A3.1 The index with $a = 1$ at $r = 1/4$.

With $a = 1$ and $r = 10/21$ the plot shows the dust particle geodesic with $\Omega = 0$ and a test particle geodesic with $\Omega = -882/241$, which is approaching the velocity of light.

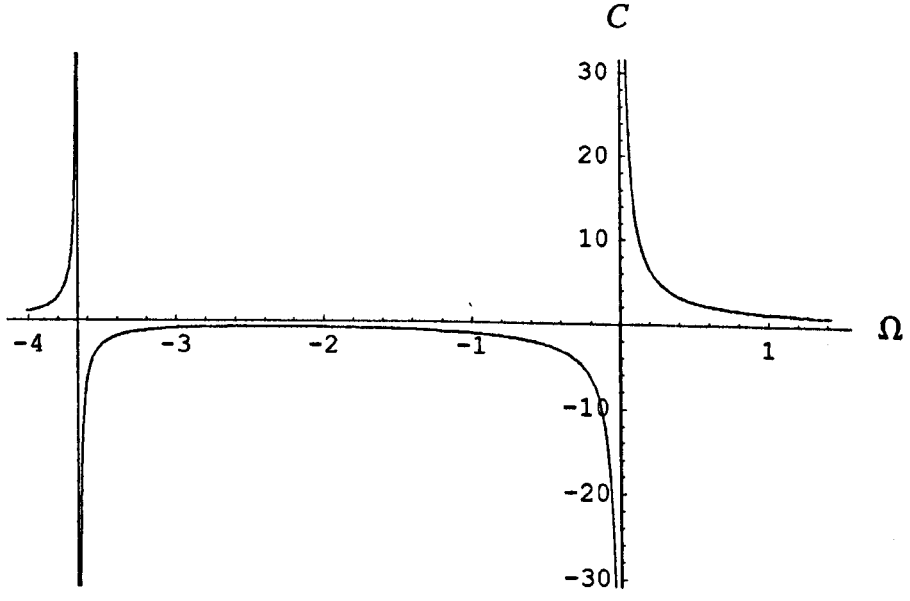

Figure A3.2 The index with $a = 1$ at $r = 10/21$.

With $a = 1$ and $r = 3/4$ the plot shows only the dust particle geodesic with $\Omega = 0$. The other circular geodesic is spacelike.

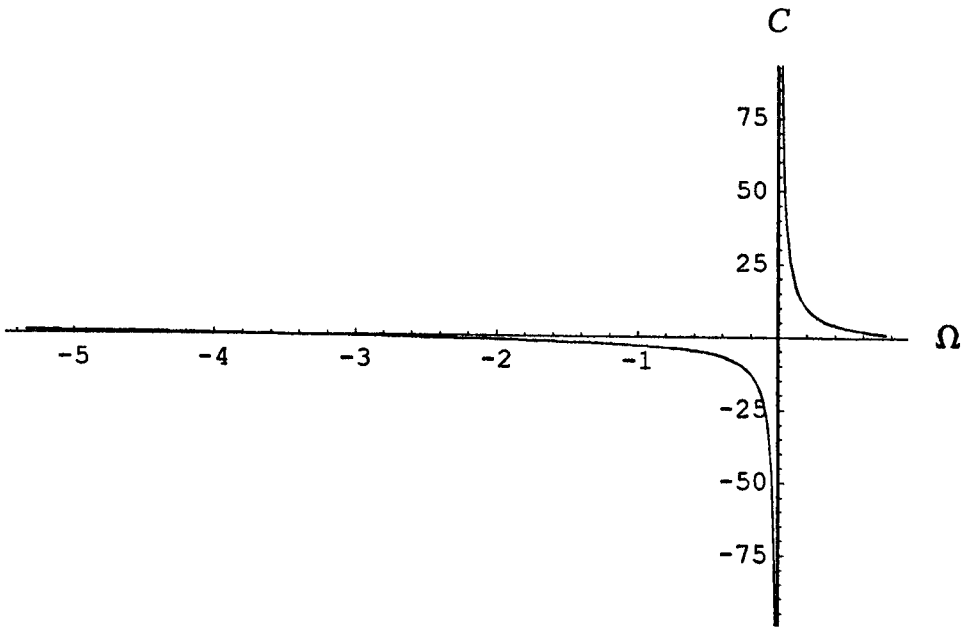

Figure A3.3 The index with $a = 1$ at $r = 3/4$.

A.3.3 Bonnor's dust cloud

Substituting the metric coefficients into the general expressions of Section A.3.1 gives the following values for circular orbits in the dust cloud metric, the superscripts r and z indicating the directions of the accelerations

$$G^r = \frac{4h^2 r(z^2 - 2r^2)}{R^2(R^6 - 4h^2 r^2)}, \quad G^z = -\frac{12h^2 r^2 z}{R^2(R^6 - 4h^2 r^2)}, \tag{10}$$

$$Co^r = \frac{2hr^3 R(3R^6 + 4h^2(r^2 - 2z^2))(\omega - \Omega)}{(R^6 - 4h^2 r^2)(R^6 + 4hr^2 \Omega R^3 + r^2(4h^2 r^2 - R^6)\Omega^2)},$$

$$Co^z = \frac{6hr^2 R(R^6 + 4h^2 r^2) z(\omega - \Omega)}{(R^6 - 4h^2 r^2)(R^6 + 4hr^2 \Omega R^3 + r^2(4h^2 r^2 - R^6)\Omega^2)}, \tag{11}$$

$$Cf^r = -\frac{r(R^8 + 12h^2 r^2(r^2 - z^2))(\omega - \Omega)^2}{R^8 + 4hr^2 \Omega R^5 + r^2(4h^2 r^2 - R^6)\Omega^2 R^2},$$

$$Cf^z = -\frac{24h^2 r^4 z(\omega - \Omega)^2}{R^8 + 4hr^2 \Omega R^5 + r^2(4h^2 r^2 - R^6)\Omega^2 R^2}. \tag{12}$$

There does not seem to be any constraint on the value of h, whereas the van Stockum equations did constrain the value of ar. The denominators of both components of the gravitational and Coriolis accelerations are multiplied by the term $(R^6 - 4h^2 r^2)$. From

Section 6.2.3 however, $R^6 = 4h^2r^2$ defines the surface within which null geodesics must have $P_\phi > 0$. Therefore as this surface is approached, the gravitational and coriolis accelerations on orbiting test particles tend to infinite values. It appears that within the surface the gravitational acceleration is directed outwards. The validity of (11) and (12) for the other forces within the surface is uncertain since ϕ is timelike there.

By putting $\Omega = 0$ and substituting ω from (4) we can examine the accelerations acting on the dust particles. These are

$$G^r = \frac{4h^2r(z^2-2r^2)}{R^2(R^6-4h^2r^2)},\quad G^z = -\frac{12h^2r^2z}{R^2(R^6-4h^2r^2)}, \tag{13}$$

$$Co^r = \frac{4h^2r^3(3R^6+4h^2(r^2-2z^2))}{R^2(R^6-4h^2r^2)^2},\quad Co^z = \frac{12h^2r^2(R^6+4h^2r^2)z}{R^2(R^6-4h^2r^2)^2}, \tag{14}$$

$$Cf^r = -\frac{4h^2r(R^8+12h^2(r^4-r^2z^2))}{R^2(R^6-4h^2r^2)^2},\quad Cf^z = -\frac{96h^4r^4z}{R^2(R^6-4h^2r^2)^2}. \tag{15}$$

Clearly, all these expressions 'blow up' on the toroidal surface $R^6 = 4h^2r^2$. However, it is easy to check that

$$G^r + Co^r + Cf^r = G^z + Co^z + Cf^z = 0, \tag{16}$$

as expected for the dust particles which are on geodesic orbits.

~ References ~

[1] Lanczos K, *Zeitschrift für Physik* **21**, 73 (1924).
Lanczos K, *Gen. Rel. Grav.* **29**, 363 (1997). (English translation).

[2] Opher R, Santos N O, Wang A, *J. Math.Phys.* **37**, 1982 (1996)

[3] van Stockum W J, *Proc. R. Soc. Edinburgh* **57**, 135 (1937).

[4] Lewis T, *Proc. R. Soc. London, A* **136**, 176 (1932).

[5] Bonnor W B, *J. Phys. A* **13**, 2121 (1980).

[6] Wolfram S, *The Mathematica Book*, 3rd ed.
(Wolfram Media/Cambridge University Press, 1996)

[7] *MathTensor*, A system for doing tensor analysis by computer.
(MathTensor Inc. 1994).

[8] Bardeen J M, *Astrophys. J.* **162**, 71 (1970)

[9] Tipler F J, *Phys. Rev. D* **9**, 2203 (1974)

[10] Carter B, *Phys Rev.* **174**, 1559 (1968)

[11] *Gravitation: An introduction to current research*, ed. Witten L, Wiley, 1962.

[12] Frehland E, *Commun. Math. Phys.* **23**, 127 (1971)

[13] Bonnor W B, *Class. Quantum Grav.* **12**, 1483 (1995).

[14] Collins C B, *J. Math. Phys.* **25**, 995 (1984).

[15] Sklavenites D, *J. Math. Phys.* **26**, 2279 (1985).

[16] Prasanna A R, Iyer S, *Phys. Letts. A.* **233**, 17 (1997).

[17] Chandrasekhar S, *The Mathematical Theory of Black Holes.* OUP, (1983).

[18] Hawking S W & Ellis G F R, *The large scale structure of space-time.*
CUP, (1993).

[19] Rindler W, Phys.Lett. A 233 (1997) 25.

[20] Gray A, *Modern Differential Geometry of Curves and Surfaces.* CRC Press.

[21] Islam J N, *Rotating fields in general relativity.* CUP, (1985).

[22] Einstein A, *Cosmological considerations on the general theory of relativity.*
English translation in *The Principle of Relativity*, Dover, (1952).

[23] Pais A, *'Subtle is the Lord...'*, OUP, (1982).

[24] Weyl H, *Ann. Physik.* **54**, 117 (1917)

[25] Levi Civita T, *R. Acc. Lincei*, **28**, 101 (1919)

[26] da Silva M F A, Herrera L, Paiva F M, Santos N O,
Gen. Rel. Grav. **27**, 859, (1995).

[27] da Silva M F A, Herrera L, Paiva F M, Santos N O,
Class. Quantum Grav. **12**, 111, (1995).

[28] MacCallum M A H, Santos N O, *Class. Quantum Grav.* **15**, 1627 (1998).

[29] McIntosh C B G, Arianrhod R, Wade S, Hoenselaers C A,
Class. Quantum Grav. **11**, 1555 (1994).

[30] Bonnor W B, *Class. Quantum Grav.* **12**, 499 (1995).

[31] Landau L D, Lifschitz E M, *The Classical Theory of Fields*, Pergamon, (1983).

[32] Kramer D, Stephani H, MacCallum M A H, Herlt E,
Exact Solutions of Einstein's Field Equations. CUP.

[33] Bruni M, Matarrese S, Pantano O, *Astrophys. J.* **445**, 958 (1995).

[34] Prasanna A R, *Class. Quantum Grav.* **14**, 227 (1997).
[35] Abramovicz M A, Carter B, Lasota J P, *Gen. Rel. Grav.* **20**, 1173 (1988).
[36] Abramovicz M A, Nurowski P, Wex N, *Class. Quantum Grav.* **10**, L183 (1993).
[37] Abramowicz M A, in *The Renaissance of General Relativity and Cosmology*, edited by Ellis G, Lanza A, Miller J, CUP, (1993).
[38] Steadman B R, *Class. Quantum Grav.* **15**, 1357 (1998).
[39] Bonnor W B, *Gen. Rel. Grav.* **24**, 551, (1992).
[40] Bonnor W B, *J. Phys. A* **10**, 1673 (1977).
[41] Winicour J, *J. Math.Phys.* **16**, 1805 (1975)
[42] Abramovicz M A, Lasota J P, *Class. Quantum Grav.* **14**, A23 (1997).
[43] Bonnor W B, Steadman B R, *Class. Quantum Grav.* **16**, 1853 (1999).
[44] Sandoval-Vallarta S M, *Theory of the geomagnetic effect of cosmic radiation.* Handbuch der Physik, XLVI/I, p88.
[45] José J V, Saletan E J, *Classical Dynamics.* CUP, (1998).
[46] Image of M87, copyright Space Telescope Science Institute, Baltimore.
[47] Semerak O, *Class. Quantum Grav.* **16**, 3769 (1999).
[48] Steadman B R, *Class. Quantum Grav.* **16**, 3685 (1999).
[49] Tartaglia A, *Class. Quantum Grav.* **17**, 783 (2000).